

# 2023

## ANNUAL REPORT

### HP-HT Laboratory

EXPERIMENTAL VOLCANOLOGY  
AND GEOPHYSICS

### LNTS

NEW TECHNOLOGIES and Instruments  
Laboratory

### ROMA 1 Section

Istituto Nazionale di Geofisica e Vulcanologia  
Via di Vigna Murata 605 | 00143 Rome Italy  
Phone +39-0651860437 | Fax +39-0651860507  
[www.ingv.it](http://www.ingv.it)



Follow us on



HPHTlab - Science, Technology & Engineering



HPHTlab (@hphtlab) | Twitter

## CONTENTS

<b>1 </b> ABSTRACT	5
<b>2 </b> PERSONNEL	9
<b>3 </b> INSTRUMENTS and FACILITIES	13
<b>4 </b> LABORATORY ACTIVITIES	17
<b>5 </b> RESEARCH PROJECTS	23
<b>6 </b> PARTNER LABORATORIES	27
<b>7 </b> PARTNER INSTITUTIONS	29
<b>8 </b> RESEARCH ACTIVITY and RESULTS	31
<b>9 </b> SEMINARS and TEACHING	99
<b>10 </b> VISITING SCIENTISTS	103
<b>11 </b> MEETINGS, WORKSHOP and SYMPOSIA	107
<b>12 </b> PUBLICATIONS	115



C H A P T E R O N E

# ABSTRACT



This report summarizes the facilities, activities, collaborations, scientific and technological products of the High Pressure High Temperature Laboratory of Experimental Volcanology and Geophysics (HPHT Lab) and of the Laboratory of New Technologies (LNTS) updated to the year 2023. The two laboratories are an active part of all the three main Departments of INGV: Earthquake, Volcano and Environment. Research activities were framed within 17 nationally- and internationally-funded research projects (two more than in 2022) and involved 18 access proposals. In collaboration with Italian and foreigner universities, the Laboratories hosted 6 Master students and 9 PhD students. Scientific production for 2023 amounts to 26 publications. 9 visiting scientists accessed the Laboratories through successful Trans-National Access proposals.

Beside the four EU-funded projects that are continuing, (IMPROVE - Innovative Multi-disciplinary European Research training network on VolcanoEs; SYN FEAR - Fault activation and Earthquake Rupture; and EXCITE-Electron and X-ray microscopy Community for structural and chemical Imaging Techniques for Earth materials, and ENDGAME - Experiments, Numerical moDelling and field observations of basaltic maGmA fragmentation), the Piano Nazionale di Ripresa e Resilienza - Next Generation Europe Program: Monitoring Earth's Evolution and Tectonics Project MEET brought a strong improvement to the Laboratory personnel and facilities, and even stronger improvements are planned for the next years. At national level, a new PRIN project involving the Laboratories has been funded.

Great additions strengthened the Laboratories fleet of drones for remote sensing of terrain: i) a new thermal infrared camera-equipped drone allows detecting and tracking ground temperature anomalies and their evolution; ii) a LIDAR-equipped drone complements and enhances the current photogrammetry capability to perform digital ground reconstruction; and iii) the simultaneous imaging by two drones is a novel tool to stereoscopically reconstruct explosive activity at active volcanoes. The LNTS developed several prototypes of advanced devices, including an automated ash sampler and a seismically-generated infrasound detector.

Finally, we are delighted and proud of the many students, media and authorities that visited us in 2023, also during the 20th anniversary Open Day of the Laboratories.





C H A P T E R T W O  
PERSONNEL

## HPHT LABORATORY

**Piergiorgio Scarlato** | Senior Researcher,  
Responsible of the HP-HT Laboratory

**Stefano Aretusini** | Contract Researcher  
**Emanuela Bagnato** | Researcher  
**Riccardo Civico** | Researcher  
**Chiara Cornelio** | Contract Researcher  
**Gianfilippo De Astis** | Senior Researcher  
**Elisabetta Del Bello** | Researcher  
**Fabrizio Di Fiore** | Contract Researcher  
**Giuseppe La Spina** | Researcher  
**Valeria Misiti** | Technologist  
**Manuela Nazzari** | Researcher  
**Francesco Pennacchia** | Contract Technician  
**Alessio Pontesilli** | Contract Researcher  
**Giacomo Pozzi** | Contract Researcher  
**Tullio Ricci** | Researcher  
**Roberta Ruggeri** | Contract Researcher  
**Elena Spagnuolo** | Researcher  
**Laura Spina** | Researcher  
**Jacopo Taddeucci** | Senior Researcher  
**Giancarlo Tamburello** | Researcher

## LABORATORY OF NEW TECHNOLOGIES

**Giuseppe Di Stefano** | Senior Technologist  
Responsible of the Laboratory of New Technologies

**Alessandro Iarocci** | Engineer Technologist  
**Massimo Mari** | Technician  
**Francesco Pongetti** | Engineer Technician  
**Marcello Silvestri** | Technician  
**Giuseppe Spinelli** | Engineer Technologist  
**Massimiliano Vallocchia** | Engineer Technician  
**Giovanni Romeo** | Associated

## **ASSOCIATED RESEARCHERS**

**Cristiano Collettini** | Sapienza Università di Roma, Italy | **Full Professor in Structural Geology**

**Frances M. Deegan** | Uppsala University, Sweden | **Researcher**

**Giancarlo Della Ventura** | Università di Roma Tre | **Full Professor in Mineralogy**

**Giulio Di Toro** | Università degli Studi di Padova | **Full Professor in Structural Geology**

**Silvio Mollo** | Sapienza Università di Roma, Italy | **Associate Professor of Petrology**



C H A P T E R T H R E E

# INSTRUMENTS and FACILITIES

## HPHT LABORATORY

- **Multiple press 840 ton** | Voggenreiter
- **Piston cylinder - 3/4" and 1" pressure plates** | Voggenreiter
- **Multianvil - Walker type 6/8** | Voggenreiter
- **Quick Press - Piston Cylinder 3/4" and 1" pressure plates** | Depth of the Earth
- **Bi-Tri-Axial Press (BRAVA)** | RMP - INGV
- **Low to High Velocity Apparatus (SHIVA)** | RMP - INGV
- **Electron microprobe equipped with 5 WDS and 1 EDS** | JEOL JXA-8200
- **Field Emission Scanning Electron Microscope equipped with EDS and BSE detectors**  
JEOL JSM-6500F
- **Auto Carbon coater** | JEOL JEC-530
- **Fine coater** | JEOL JFC-2300HR
- **High and low temperature furnaces** | Lenton
- **Impedance analyser** | Solartron SI1260
- **Digital oscilloscope** | Tektronix DPO4032
- **Wave generator** | Agilent 33250A
- **H-Frame presses 10 ton** | Enerpac
- **Uniaxial testing machine with double load cell (15 and 250 kN) and LVDT controller** | Tecnotest
- **Precision balance** | Sartorius
- **Optical and stereo microscopes** | Leica DMRXP and Euromex
- **Ultra-high velocity, intensified, gated digital camera** | Cordin 204-2
- **Stereomicroscopes** | Leica MZ 9.5
- **Semiautomatic polisher** | Buehler Minimet 1000
- **Power Supply** | Agilent 6575A
- **Helium Picnometer** | AccuPyc II 1340
- **Permeameter with double intensifier** | Rock Physics
- **Rheometer MCR 301 Physica** | Anton Paar
- **Vertical Furnace RHTV 120-300/18** | Nabertherm
- **High Temperature Furnace LHT 04/18** | Nabertherm
- **Cecchi data acquisition system** | Applied Seismology
- **Rock drilling, cutting, and grinding equipment for samples preparation**
- **Thermal High speed camera** | FLIR SC 645
- **Welder PUK U3** | Lampert
- **Laser line generator** | Edmund optics
- **Precision test sieves** | Endecotts
- **Laser MGL-III, 532nm 200mW, PSU-III-LED/Unit** | Changchun New Industries
- **Multi-Wavelength Analyser LUMiReader® PSA with Particle sizing according to ISO 13317**
- **2 Polarized Free-field Microphones 40AN 1/2", Low Frequency (0.5Hz - 20kHz)** | G.R.A.S.
- **Ext. Polarized Pressure Microphone 46DP-1 1/8", High Frequency (6.5Hz -140kHz)** | G.R.A.S.

- **Vacuometro Pirani PVG-500**
- **Petrographic microscope ECLIPSE E-50i POL** | Nikon
- **Drying oven UF 75** | Memmert
- **4K digital camcorders** | Sony
- **High Speed digital camcorder** | NAC Memrecam - HX6
- **Shock-tube apparatus (Jet-Buster)** | INGV
- **High speed digital camcorders** | NAC 512 SC, Optronis CR600x2, NAC HX6, NAC HX3
- **Laser range finder** | Vectronix VECTOR 21
- **Time Lapse Camera with 24-70 lens** | Brinno TLC200 Pro
- **Precision Syringe Pumps** | ISCO
- **Ash dispersal/settling apparatus (Ash-Buster)** | INGV
- **Drone Matrice 300 RTK** | DJI
- **Drone Mavic 2 Pro** | DJI
- **Drone Phantom 4 RTK** | DJI
- **Drone Mini 2** | DJI
- **Dual UV cameras 340 UVGE** | Thorlabs
- **Laboratory sieve shaker Octagon 200** | Endecotts
- **Optical Profilometer Modus6ZS-3D** | DeltaPIX
- **Triaxial ICP accelerometer** | PCB Plezotronics
- **Two high frequency ICP pressure sensors** | PCB Plezotronics
- **Three ceramic shear ICP accelerometers** | PCB Plezotronics
- **Two 4-channel ICP sensor signal conditioners** | PCB Piezotronics
- **MEERA biaxial direct shear apparatus**
- **High-temperature, vacuum, inert, and reactive gas furnace**
- **Microdriller for experimental glasses** | ARNOLD 561/01
- **Mortar grinder for experimental glasses** | PULVERISETTE 23 FRITSCH
- **SKO-D XL Orbital Shaker** | SKO
- **Centrifuge Neya 8 Basic** | NEYA
- **DANTE** | Carbolite Gero – Verder Scientific
- **SKATE (Setup for the Kinematic Acquisition of Explosive Eruptions)** | INGV/T.E.E.S.
- **FBG interrogator DM-8120 (SENTEA)**

## LABORATORY OF NEW TECHNOLOGIES

- **Analog Oscilloscope** | HP
- **Analog Oscilloscope** | Iwatsu SS5710
- **Analog Oscilloscope** | Tektronix TDS220
- **Analog Oscilloscope** | Tektronix
- **Oscilloscope** | HP54201

- **Oscilloscope** | HP54602b
- **Power supply** | Elind HL series
- **Power supply** | Elind 6TD20
- **Power supply** | DC DF1731SB
- **Signal generator** | HP8656A
- **Function generator** | HP3325A
- **Multimeter** | HP3478A
- **Milling machine for printed circuit boards** | T-Tech
- **Logic state analyzer** | HP16500A
- **Soldering-reworking station** | JBC advanced AM6500
- **Oscilloscope portable** | Scopemeter FLUKE 199C
- **Oscilloscope portable** | Scopemeter FLUKE 192
- **Oscilloscope** | Tektronix DPO4000
- **Oscilloscope** | Tektronix MSO4034
- **Calibrator** | FLUKE 5700 (series II)
- **Function generator** | HP33120
- **Function generator** | AGILENT 33250 A
- **PXI Industrial computer with I/O boards** | National Instruments
- **Universal counter** | HP53131A
- **Waveform generator** | Agilent 33210 A
- **Oscilloscope W wave surfer** | LeCroy 44MXs-A
- **Drone Phantom 3 pro with termination system**
- **Power supply (4 items)** | RSPRO 3005D
- **Spectrum Analyzer** | Rohde&Swartz FPC1500, 3GHz

## MACHINE SHOP

- **Lathe** | Grazioli Fortuna
- **Small lathe** | Ceriani
- **Small milling machine** | Schaublin
- **Cutting machine** | Ercoletta
- **Bending machine** | Ercoletta
- **Drill press** | Serrmac
- **Small drill press** | Webo
- **Bandsaw** | Femi
- **Extractor hood** | Filcar
- **Inverter welding machine** | Tecnica
- **TIG welding machine** | Cebora
- **Miter saw**
- **Numerically controlled milling machine**

C H A P T E R F O U R

# LABORATORY ACTIVITIES

## EXPERIMENTAL LABORATORY

### Quick press | Piston cylinder

Experiments were conducted to study phase relations and volatile concentration in magmas at ambient (0.1 MPa), low (150 MPa) to moderate (400 MPa) pressures.

In particular experimental phase relations and volatile concentration in magmas from the Hunga volcano (Hunga Ha'apai, Hunga Tonga), in the framework of the PhD thesis of Enrico Califano (Sapienza University, Otago University), a collaboration involving A. Pontesilli, P. Scarlato, S. Mollo, Marco Brenna (University of Otago).

Experiments aimed at determining volatile diffusion in magmas were also conducted at 0.1 MPa.

### BRAVA

BRAVA performed 70 experiments during 2023 including: room pressure friction experiments (double-direct and double-direct configuration) with and without temperature control (up to 100°C in wet conditions), and in-vessel experiments up to 35 MPa of confining pressure.

We worked on the following topics:

1. Systematic characterisation of the frictional properties (friction, healing, and rate and state) gouges composed of ternary mixtures of calcite, quartz, and muscovite. R. Ruggieri, G. Pozzi in collaboration with C. Collettini (La Sapienza University of Rome) and ENI researchers.
2. Frictional properties and imaging of frictional instabilities in montmorillonite clay to unveil the nucleation processes in shallow subduction zones. G. Volpe (PhD candidate at La Sapienza University of Rome) in collaboration with G. Pozzi, J. Taddeucci, C. Collettini, and C. Marone (La Sapienza University of Rome).
3. Frictional properties of bitumen-rich limestones. R. Ruggieri and G. Pozzi, in collaboration with C. Collettini and C. Marone (La Sapienza University of Rome).
4. Characterisation of the frictional properties and permeability of hydrothermally altered rocks of the Tolfa-Allumiere lithocap. B. Marchesini (Post-doc at La Sapienza University of Rome) in collaboration with G. Pozzi.
5. Investigation of the frictional and chemical healing processes of cements deformed in simple shear conditions. G. Volpe (PhD candidate, La Sapienza University of Rome) in collaboration with G. Pozzi.
6. Study of the friction of representative rocks hosting the seismicity of the Northern and Central Apennines. Master thesis of F. Clivet (student at La Sapienza University of Rome), supervised by C. Doglioni and G. Pozzi

G. Pozzi worked on the implementation of a new sample holder and heating apparatus to perform shear experiments at room pressure and temperatures up to 100 °C at water-saturated conditions.

### Slow to High Velocity Apparatus (SHIVA)

SHIVA performed 17 experiments (s1989-s2006) during 2023 including: fault gouge and bare rock experiments under fluid pressure confinement, stress and pore pressure stepping.

We worked on the following topics:

1. Experimental reactivation of the Vajont landslide by pore fluid pressure increase. S. Aretusini (INGV-HPHT) collaborating with G. Di Toro and L. Sanavia (University of Padova). Bachelor thesis of N. Cavaliere (University of Padova).
2. Experimental reactivation of the Bedretto granite by pore fluid pressure increase. S. Aretusini, E. Spagnuolo, C. Cornelio, G. Pozzi (INGV-HPHT) collaborating with FEAR team.
3. Experimental deformation of bituminous dolostones from Monte Camicia. S. Aretusini, E. Spagnuolo, C. Cornelio (INGV-HPHT) collaborating with M. Chinello, E. Spagnuolo, T. Tesei, G. Di Toro (University of Padova) in the framework of M. Chinello Phd Thesis.

S. Aretusini and E. Spagnuolo (INGV) worked on the implementation of Fiber Bragg Grating technology for strain and temperature measurements.

S. Aretusini and M. Sbarra (INGV) developed a prototype of a data repository allowing the management and storage of experimental data and metadata.

Cornelio C. and Spagnuolo E. developed models for the parameterization of frictional laws, for dynamic propagation along 2D fractures and for deformation of poroelastic media in the presence of multiple faults.

## ANALOG MODELING LABORATORY

The shock tube system performed dozens of experiments exploring the effect of different geometries of the analogue conduit, solid-particle shape and content and the rheology of the analogue magma. Collected data include high-speed video and acoustic and accelerometric signals from subsonic to supersonic analogue jets.

In the framework of the Marie-Curie ENDGAME Project, we are advancing the development of a novel large 2D shock-tube apparatus integrating Schlieren shadow photography, to explore fragmentation phenomena in bubble and particle-bearing analogue fluids.

Additionally, within the objectives of Pianeta Dinamico VT-DYNAMO Project we implemented a novel setup, devoted to the investigation of the role of conduit permeable caps in generating seismic tremor and LP signals. To perform an ample database of experiments with this novel device and discuss the obtained results, we hosted two colleagues from University of Alaska Fairbanks: Kyungmin Kim (September to December 2023, PhD student) and Tarsilo Girona (2-7 December 2023, associate professor). 23 experimental conditions (exploring the role of conduit cap permeability, pore structure, cap geometry, gas flux) were investigated in up to 263 experimental runs.

## MICROANALYTICAL LABORATORY

FE-SEM and EMP performed 180 days of analysis in the frame of the following 18 research proposals and of 4 EXCITE TNA projects (described in chapter 10' Visiting Scientists'). Analysed samples included natural rocks, minerals, experimental products.

### PROPOSALS

- 1. Magma-carbonate interaction under dynamic conditions: experimental insights on crystallization kinetics, element partitioning and multiphase rheology**  
G. Giuliani – P. Scarlato | Sapienza University of Rome - INGV Roma1
- 2. Characterization of Vulcano-La Fossa rocks**  
G. De Astis | INGV Roma 1
- 3. MAGIC-Research project PNRA**  
A. Di Roberto | INGV PI
- 4. Understanding the Ordinary to forecast the extraordinary: An integrated approach for studying and interpreting the explosive activity at Stromboli volcano**  
P. Scarlato – M. Nazzari | INGV Roma 1
- 5. The a.d. 79 eruption of Vesuvius: timescales and dynamics of magmatic processes**  
M.A. Di Vito – M. Nazzari | INGV OV - INGV Roma1
- 6. Fabric evolution of gouge-bearing faults during multiple seismic slip velocity pulses**  
C. Cornelio | INGV Roma 1
- 7. Tephrochronological study of the lacustrine succession of the maar of Castiglione (Central Italy) and evaluation of the possible impact on the climate of the explosive eruptions of the perithyrrenic volcanoes**  
A. Di Roberto | INGV PI
- 8. Coupled Thermo-Hydro-Mechanical-Chemical processes controlling earthquakes and landslides**  
Aretusini | INGV Roma 1
- 9. Characterising the proximal pyroclastic deposits in Central Anatolia to complete the recent explosive volcanic history, synchronise sedimentary records, and better assess volcanic hazards in Turkey**  
I. Sunyè Puchol – M. Nazzari | Sapienza University of Rome - INGV Roma1
- 10. Experimental characterization of friction and permeability properties of fault gouge**  
R. Ruggieri | INGV Roma 1

11. **Mirror-like faults in radiolarites**  
T. Tesei – G. Pozzi | University of Padova - INGV Roma 1
12. **Analyses of tephra products from the recent eruption of Cumbre Vieja volcano**  
J. Taddeucci | INGV Roma 1
13. **The depth-to-surface dynamics of silicic peralkaline magmas from Pantelleria Island**  
C. Magri – F. Di Fiore F. Di Fiore | University of Roma Tre - INGV Roma1
14. **3ESSE – Shallow Subduction Seismicity**  
G. Volpe – G. Pozzi | INGV Roma 1
15. **Short-term Magma-Carbonate Interaction at various P-T-t conditions**  
M. Knüver – V. Misiti | University of Bari - INGV Roma1
16. **Textural characterization of mafic lava flows: new insights on the emplacement dynamics and solidification path of lava flows from rheological modeling**  
F. Di Fiore | INGV Roma1
17. **Petrography of historical concretes and ornamental stones of Chieti's Roman Thermal Baths**  
G. Iezzi – M. Nazzari | University of Chieti - INGV Roma1
18. **Constraining cooling-decompression paths of alkaline basaltic magmas at Mt. Etna and Stromboli**  
P. Moschini | INGV Roma 1

## **FIELD DATA ACQUISITION OF VOLCANIC ACTIVITY**

### **FaMoUS (Fast Multiparametric Setup) & SKATE (Setup for the Kinematic Acquisition of Explosive Eruptions)**

The new field system SKATE developed within the framework of the Departmental project UNO to improve our capabilities to investigate active volcanic phenomena, became operational during 2023, replacing the old one for the acquisition of imaging/acoustic data on active volcanoes. Some further implementations, like a new zoom lens and the implementation of solar panel, further increased the performance of the system. As for the previous year, the UNO field multiparametric experiments took place in May and October, the first one coinciding with the first Dynamo (Pianeta Dinamico project) field experiment. In July, the group participated in the ETNA field experiment organized by the ITN project IMPROVE. The field data acquired this year are reported below

Visible High Speed cameras/acoustic data (SKATE): i) from 4 to 6 days of continuous recording at Stromboli during the periods 20-25 May and 11-17 October, and at Etna in the period 25-31 July

Infrared Camera (FLIR Sc655)/ UV Camera: the two cameras worked in tandem recording about 4 to 7 hours per day of the volcanic activity from the 270 m. elevation Sciara observation point of Stromboli in the periods 20-25 May and 11-17 October.

### **Unmanned Aircraft Systems (UASs)**

We performed UAS surveys at Rotokawa geothermal area - New Zealand (February), Solfiorata di Pomezia (March), Stromboli (May and October), Cumbre Vieja - La Palma (June), and Vulcano (December). The main applications were photogrammetry (RGB and IR), Lidar, and observation of volcanic activity (RGB and IR) while the derived products were DEMs (DSMs and DTMs) and related elaborations, orthophotos, HR videos and photos. Surface topography was characterised using Structure from Motion (SfM) photogrammetry and lidar surveys, which allowed us to produce very high resolution (10-50 cm/pixel) Digital Surface Models (DSMs), Digital Terrain Models (DTMs), and orthophotomosaics and detect elevation, volumetric, and areal variations. Main results from Stromboli surveys have been promptly published on the INGV surveillance bulletins for Stromboli and on «INGVvulcani» social media.

C H A P T E R F I V E

# RESEARCH PROJECTS

1. **Piano Nazionale di Riprese e Resilienza - Next Generation Europe Program: Monitoring Earth's Evolution and Tectonics Project MEET** | WP 3 Integrated Laboratories for the Geosciences and the Environment ILGE | **WP leaders P. Scarlato - F. Funicello**
2. **MIUR Progetto PRIN 2017** | Scales of solidification in magmas: applications to volcanic eruptions, silicate melts, glasses, glass- ceramics | **P.I. M. Carroll**
3. **MIUR Progetto PRIN 2022** | PROVES: an integrated PetRO-Volcanological monitoring approach applied to Mt. Etna and Stromboli - 2022N4FBAA | **P.I. M. Masotta**
4. **MIUR PON** | GRINT | **P.I. G. Puglisi**
5. **European research project** | EXCITE 'Electron and X-ray microscopy Community for structural and chemical Imaging Techniques for Earth materials' | **P.I. V. Cnudde**
6. **European research project** | Marie Skłodowska-Curie European Training Network IMPROVE, Innovative Multi-disciplinary European Research training network on VolcanoEs | **P.I. P. Papale**
7. **INGV "Ricerca libera" Project** | Magma dynamics triggering the 3 July and 28 August 2019 paroxysms at Stromboli volcano: A comparative approach based on the ascent rates, timescales and P-T-H<sub>2</sub>O paths of magma | **P.I. P. Scarlato**
8. **INGV "Ricerca libera" Project** | FRAMMENTI, FRAGmentation of Mafic Magmas: ExteNt and TIming | **P.I. J. Taddeucci**
9. **INGV "Ricerca libera" Project** | ROUGHER, expeRimental Observations aboUt irReGular cHannel gEometRies | **P.I. L. Spina**
10. **INGV Departmental Strategic Projects** | UNO - UNderstanding the Ordinary to forecast the extraordinary: An integrated approach for studying and interpreting the explosive activity at Stromboli volcano | **P.I. P. Scarlato**
11. **ASI-INAF Project** | "Esopianeti" | **P.I. G. De Astis**
12. **ERC Syn Fear** | Fault activation and Earthquake Rupture | **P.I. D. Giardini, F. Amman, M. Cocco, S. Wiemer**
13. **Marie Skłodowska-Curie Individual Fellowship** | "Experiments, Numerical moDelling and field observations of basaltic maGmA fragMEntation (ENDGAME)" | **P.I. J. Taddeucci, G. La Spina**

14. **INGV “Pianeta Dinamico” Project** | DYNAMO DYNAmics of eruptive phenoMena at basaltic vOlcanoes | P.I. L. Zuccarello
15. **INGV “Pianeta Dinamico” Project** | CAVEAT | P.I. M. Palano
16. **IRGIE** Inventario delle Risorse Geotermiche delle Isole Eolie. stima del potenziale e proposte di utilizzo | P.I. M. Procesi
17. **INGV “Pianeta Dinamico” Project** | Sibilla | P.I. A. Pignatelli



C H A P T E R S I X

PARTNER  
LABORATORIES

1. **Planetary Environmental Facilities** | Aarhus University | Denmark
2. **Experimental & Physical Volcanology** | Ludwig Maximilians Universitat | Germany
3. **Dipartimento di Scienze** | Università di Roma Tre | Italy
4. **Geoscience Department** | Utrecht University | Netherlands
5. **Institute of Geochemistry and Petrology** | ETH Zurich | Switzerland
6. **Dipartimento di Scienze Biologiche, Geologiche e Ambientali** | Università di Catania | Italy
7. **Dipartimento di Fisica e Scienze della Terra** | Università di Ferrara | Italy
8. **Petro-Volcanology Research Group (PVRG)** | Department of Physics and Geology  
Università di Perugia | Italy
9. **School of Earth and Environmental Sciences** | University of Queensland | Australia
10. **Department of Geology** | University of Otago | New Zealand
11. **Dipartimento di Geoscienze** | Università di Padova | Italy
12. **LEMUR | EPFL** | Lausanne | Switzerland
13. **Rock Mechanics Laboratory** | Durham University | UK
14. **Jackson School of Geosciences** | Texas University of Austin | USA
15. **The Rocks Physics and Mechanics Laboratory (RPML)** | ETH | Switzerland
16. **Rock Mechanics Laboratory** | UCL Earth Sciences | UK
17. **Laboratoire Aleas géologiques et Dynamique sédimentaire** | IFREMER | France
18. **RMP LAB** | ETH | Switzerland
19. **Geotechnical lab** | RWTH Aachen University | Germany

C H A P T E R S E V E N

# PARTNER INSTITUTIONS

1. **Ludwig Maximilians Universitat Munchen** | Munich | Germany
2. **Department of Geology and Geophysics, SOEST** | University of Hawaii | USA
3. **Department of Physics and Astronomy** | Aarhus University | Denmark
4. **HVO Hawaiian volcano observatory** | USGS | USA
5. **School of Earth and Environmental Sciences** | University of Queensland | Australia
6. **Department of Geology** | University of Otago | New Zealand.
7. **Department of Earth Science** | University of Durham | UK
8. **Instituto Volcanologico de Canarias INVOLCAN** | Spain
9. **Dipartimento di Geoscienze** | Università degli Studi di Padova | Italy
10. **Dipartimento di Scienze della Terra** | La Sapienza Università di Roma | Italy
11. **Departamento Tecnología Electrónica** | Universidad Carlos III Madrid | Spain
12. **Natural History Museum** | Volcano Petrology Group | UK
13. **University of Alaska Fairbanks** | USA

C H A P T E R E I G H T

RESEARCH  
ACTIVITY  
and RESULTS



## 8.1 PETROLOGY, MINERALOGY, VOLCANOLOGY

### CASCADING VOLCANIC PROCESSES IN ACIGÖL CALDERA: IMPLICATIONS FOR MULTI-HAZARDS IN THE CAPPADOCIAN REGION (CENTRAL ANATOLIA)

Sunyé-Puchol I., Bolós X., Özsoy R., Akkas E., Tavazzani L., Nazzari M., Bachmann O., Scarlato P., Mollo S.

In the last few decades Acigöl caldera have been the focus of several volcanological studies to better characterise this long-lived magmatic system of the Central Anatolian Volcanic Province (Turkey), which was the source of the last two Cappadocian ignimbrites during the middle Pleistocene. Some of these studies have been focused on these Neogene-to-Quaternary widespread ignimbrites, others on more recent, late Pleistocene tephra cones, rhyolitic maars and intra-crater lava domes. Although it is well-known that Acigöl has had several large explosive eruptions during the last ~25 ka, no detailed tephrostratigraphic studies have been done to improve our knowledge on the caldera volcanic history, and to better evaluate the hazards in a potential future eruption. For this reason, in this investigation we have analysed the volcanic deposits of Acigöl to better understand the geological processes occurred in this caldera during the last 200 ka (Fig. 1). The results of this volcanological study suggest that in Acigöl caldera numerous natural processes can be activated contemporaneously as a cascading effect and therefore, multi-hazards can be triggered simultaneously. Volcano-stratigraphic relationships exposed in two long and continuous outcrops, together with original glass chemical data and published geochronological ages, suggest that monogenetic explosive eruptions within the caldera can trigger energetic debris avalanches, and at the same time, might be a precursor signal of a larger caldera-forming ignimbrite eruption. Thus, considering that 1) Acigöl had at least eight monogenetic eruptions in the last thousands of years; 2) the melted material potentially available below the caldera; and 3) the increment in seismicity along the Central Anatolian Volcanic Province, the volcanic multi-hazards that this active magmatic system can induce in case of a future eruption, must be taken into consideration. And above all, a future caldera-forming ignimbrite eruption in Cappadocia should not be excluded.

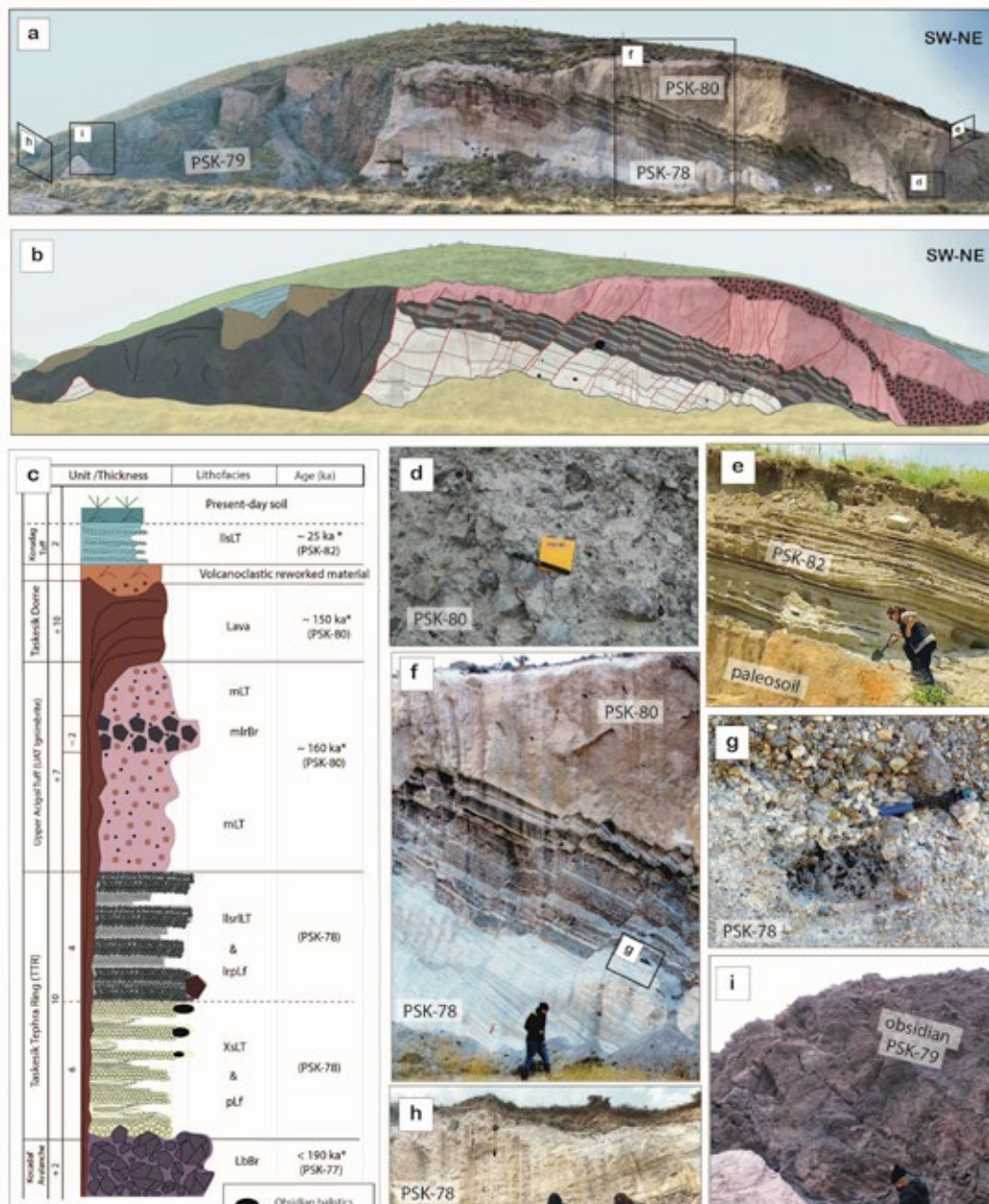
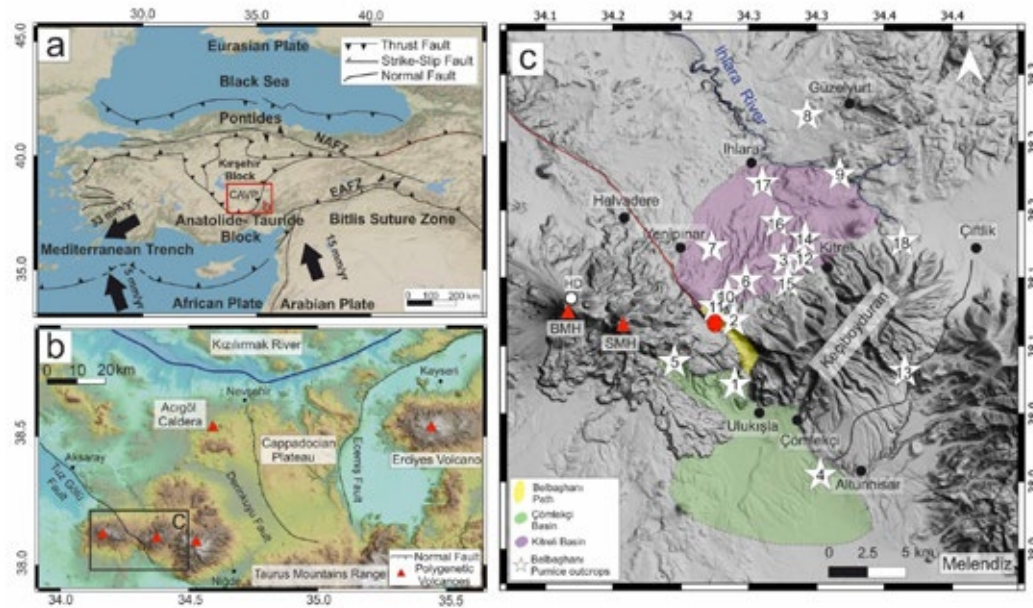


**Figure 1**  
 Taskesik site: **a)** Panoramic view of the outcrop; and **b)** sketch to highlight the main Acigol volcanic units and its relationships exposed in this quarry. **c)** Composite stratigraphic column of the Acigol products (lithofacies nomenclature based in Branney and Kokelaar, 2002; LbBr = Lava blocks Breccia; XsLT = crosstratified Lapilli Tuff; llslrLT = parallel stratified, rich-in-lithics, Lapilli Tuff; plf = pumice lapilli fall; lrplf = lithic-rich, pumice lapilli fall; mIrbR = massive lithic rich Breccia; mLT = massive Lapilli Tuff; llslT = parallel stratified Lapilli Tuff. **d)** Detail of the coignimbritic lithic lag breccia within the UAT ignimbrite. **f)** Zoom-in to see the faults affecting the pyroclastic deposits and the continuous contact between the upper part of the Taskesik tephra ring (TTR) and the bottom of the UAT ignimbrite. **h)** Contact between the debris avalanche deposit below the TTR (no discontinuity). **e)** Korudag tuff above a paleosoil developed atop of the UAT ignimbrite. **g)** Detail of an obsidian lithic ballistic within the TTR. **i)** Discordant contact between the TTR and the obsidian dike.

## RECONSTRUCTING THE BELBAŞHANI PUMICE PLINIAN ERUPTION: TEPHROSTRATIGRAPHY, ERUPTION SOURCE PARAMETERS, AND IMPLICATIONS FOR VOLCANIC HAZARD ASSESSMENT AT HASANDAĞ VOLCANO (CENTRAL ANATOLIA, TURKEY)

Özsoy R., Sunyé-Puchol I., Pedrazzi D., Akkaş E., Costa A., Massaro S., Tavazzani L., Nazzari M., Bachmann O., Scarlato P., Miggins D.P., Kaya S., Mollo S.

Hasandağ volcano, which recently has undergone an increase in fumarolic activity and local seismicity, produced multiple large explosive eruptions during the last million years (Fig. 1). One of these is the Belbaşhani Pumice, a Plinian eruption occurred at  $\sim 417 \pm 20.5$  ka ( $40\text{Ar}/39\text{Ar}$ ). The eruption was characterised by a column of 18-29 km height with a  $\sim 2$  km<sup>3</sup> of bulk volume pumice fallout deposits that corresponds to a Volcanic Explosive Index (VEI) of 5. Here, we present a complete volcanological study including stratigraphy, glass chemistry and morphology, geochronology, and estimation of physical parameters aimed to characterise the Belbaşhani Pumice eruption. We also assess and quantify the uncertainties associated with volume and column height estimations. According to isomaps, we found that the Belbaşhani Pumice plume had the main dispersal axis towards the NNE, accumulating a pumice layer up to  $\sim 17$  m in proximal deposits, and up to 2 m in medial-distal at  $\sim 20$  km from the vent. Both isopach and isopleth maps indicate that the volcanic source of Belbaşhani Pumice eruption could be at the intersection of the Tuz Gölü fault and Ulukışla caldera, situated on the Hasandağ volcanic complex. The glass compositional evolution is comparable with that from other pyroclastic deposits of Hasandağ and the presence of highly vesicular glass shards confirms that the Plinian eruption was primarily magmatic. Our reconstruction of the Belbaşhani Pumice eruption represents a step forward for a better hazard assessment in Central Anatolia, useful to characterise a potential future Plinian eruption at Hasandağ. Furthermore, our chemical and geochronologic data sets could improve future tephrochronological correlations in order to synchronise paleoenvironmental and paleoclimatic registers, as well as archaeological sites.



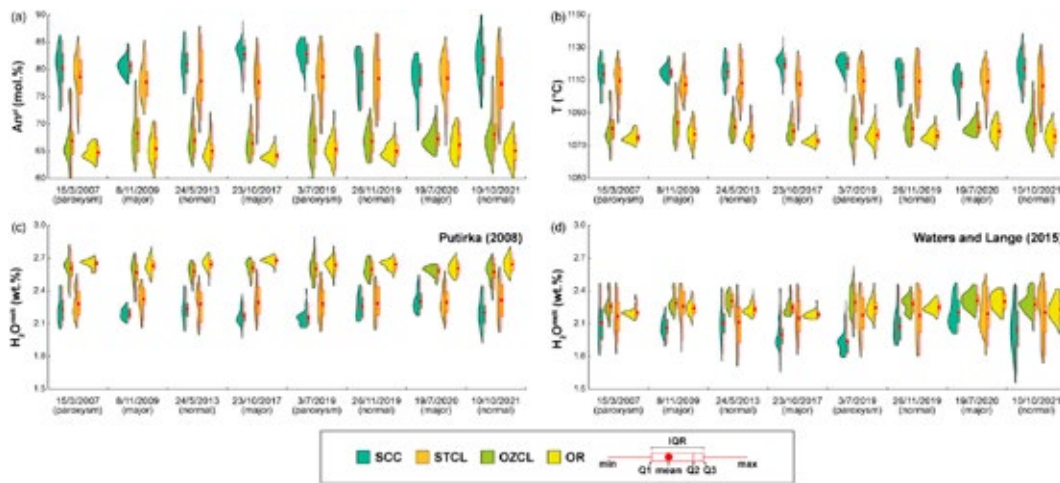
**Figure 1**

Fig. 1. **a)** Geographical and structural map of the Anatolian microplate and adjacent regions, showing the main structural features, continental blocks and location of the Central Anatolian Volcanic Province (CAVP; red frame in the overview map). Large black arrows indicate the motion of the neighbour tectonic plates. Small black arrows indicate the direction of major strike-slip fault systems in Anatolia (NAFZ: North Anatolian Fault Zone; EAFZ: East Anatolian Fault Zone). **b)** map of the CAVP showing the major volcanic centres (red triangles) and tectonic lineaments (black lines), including the three volcanoes present in the study area within the Nigde Volcanic Complex (NVC), such as Hasandag, Keçiöbydüran, and Melendiz (east to west). **c)** Digital elevation model (DEM) of the study area showing the location of the Belbashi pumice exposures (white stars). BMH, Big Hasandag. SMH, Small Hasandag. Black line between Keçiöbydüran and Melendiz volcanoes denotes the Altunhisar-Çiftlik road. Red line delineates the Tuz Gölü Fault Zone. Red circle indicates the volcanic vent. Black circles indicate the towns. White circles correspond to the locations of the Pumice Fallout dated by Schmitt et al. (2014).

## **A REVIEW OF PLAGIOCLASE GROWTH RATE AND COMPOSITIONAL EVOLUTION IN MAFIC ALKALINE MAGMAS: GUIDELINES FOR THERMOMETRY, HYGROMETRY, AND TIMESCALES OF MAGMA DYNAMICS AT STROMBOLI AND MT. ETNA**

Moschini P., Mollo S., Pontesilli A., Nazzari M., Petrone C.M., Fanara S., Vona A., Gaeta M., Romano C., Scarlato P.

Mafic alkaline magmas, such as those feeding the persistent eruptive activity of Stromboli and Mt. Etna volcanoes in Italy, are dominated by the crystallization of plagioclase via cooling and degassing phenomena related to the dynamics of shallow crustal reservoirs and eruptive conduits. Because plagioclase textures and compositions are extremely sensitive to the changes of intensive variables in subvolcanic plumbing systems, the phenomenological variability of erupted crystals preserves detailed evidence of complex growth histories. From this point of view, we reappraise the textural maturation and compositional complexity of plagioclase by allying thermodynamic and kinetic principles to natural and experimental observations, with the purpose of drawing up guidelines for reconstructing magma dynamics in mafic alkaline volcanic settings. A multifaceted statistical method is adopted to parameterize the decay of crystal growth rate with increasing crystallization time, as relaxation kinetics prevails over melt supersaturation effects. This model parameterization is combined with the textural analysis of natural plagioclase crystals to quantify the residence time of phenocrysts in equilibrium with magmas at Stromboli and Mt. Etna and/or the timescale of rapid microlite growth during disequilibrium ascent of magmas within the conduit. The role played by temperature and melt-water content on plagioclase components and major cation substitution mechanisms is also evaluated under both isobaric-isothermal and decompression conditions. The emerging paradigm is that the influence of dissolved water on anorthite-albite exchange between plagioclase and melt is overwhelmingly mitigated by changes in temperature. As a corollary, anorthite and albite melt activities are almost fully encapsulated in the variation of anhydrous melt components as the crystallization of plagioclase proceeds during magma cooling. Following this line of reasoning, we propose an integrated modeling approach to decipher complex zoning patterns in natural plagioclase phenocrysts from mafic alkaline eruptions. Key findings from our re-assessment of equilibrium, thermometric, and hygrometric models indicate that temperature and dissolved water can be iteratively estimated for different plagioclase textural patterns if crystals are sufficiently strongly zoned and probability-based criteria are applied to determine the maximum probability distribution from kernel density analysis (Fig. 1).



**Figure 1**

Violin plots and box plots for anorthite in plagioclase phenocrysts from 2007 to 2021 eruptions at Stromboli (a), temperature predicted from this study (b), and melt-water content predicted by the hygrometers of Putirka (2008) (c) and Waters and Lange (2015) (d). A kernel density estimation is used to visualize the underlying probability density function of each set of data in violin plots, whereas the statistical dispersion of data is illustrated by the box plot. The width of the box represents the interquartile range (IQR) extending from the first quartile (25<sup>th</sup> percentile Q1) to the third quartile (75<sup>th</sup> percentile Q3) and whiskers go from each quartile to the minimum or maximum. SCC, subrounded corroded cores. STCL, sieve-textured concentric layers. OZCL, oscillatory-zoned concentric layers. OR, overgrowth rims.

## **PLAGIOCLASE CRYSTAL SIZE DISTRIBUTION PARAMETERIZATION: A TOOL FOR TRACKING MAGMA DYNAMICS AT STROMBOLI**

Schiavon B., Mollo S., Pontesilli A., Del Bello E., Nazzari M., Scarlato P.

In this study we parameterize the textural attributes of plagioclase phenocrysts and microlites from nineteen pyroclasts ejected during mild to violent explosions at Stromboli over a timespan of ~18 years, from 2003 to 2021. By allying kinetic and crystal size distribution principles, we document that the morphological stability of large-sized, euhedral phenocrysts is superimposed on an internal textural heterogeneity due to growth-dissolution phenomena associated with the input rate of hot, H<sub>2</sub>O-rich recharge magmas rising from depth. As a result, the volumetric plagioclase proportion, dominant size, and number of phenocrysts per unit volume decrease from mild to violent explosions responding to a more efficient magma mixing process via sustained injections of mafic magmas into the shallow reservoir. On the other hand, the crystallization of anhedral plagioclase microlites is controlled by fast growth kinetics taking place in the uppermost part of the conduit during magma acceleration towards the surface. Under such highly dynamic crystallization conditions, the microlite number density closely depends on the increase of melt liquidus temperature via magma decompression and water exsolution. This mutualism allows to model the degassing rate and ascent velocity of magma under open-conduit flow regimes for the different eruptive styles, thereby supporting the idea that violent explosions at Stromboli are driven by sustained influxes of recharge magmas favoring strong acceleration (~12–27 m/s), decompression (~0.25–0.49 MPa/s), and water exsolution (~0.005–0.01 wt%/s) before magma discharge at the vent (Fig. 1).

**Schematic illustration of  
magma dynamics  
driving violent explosion**

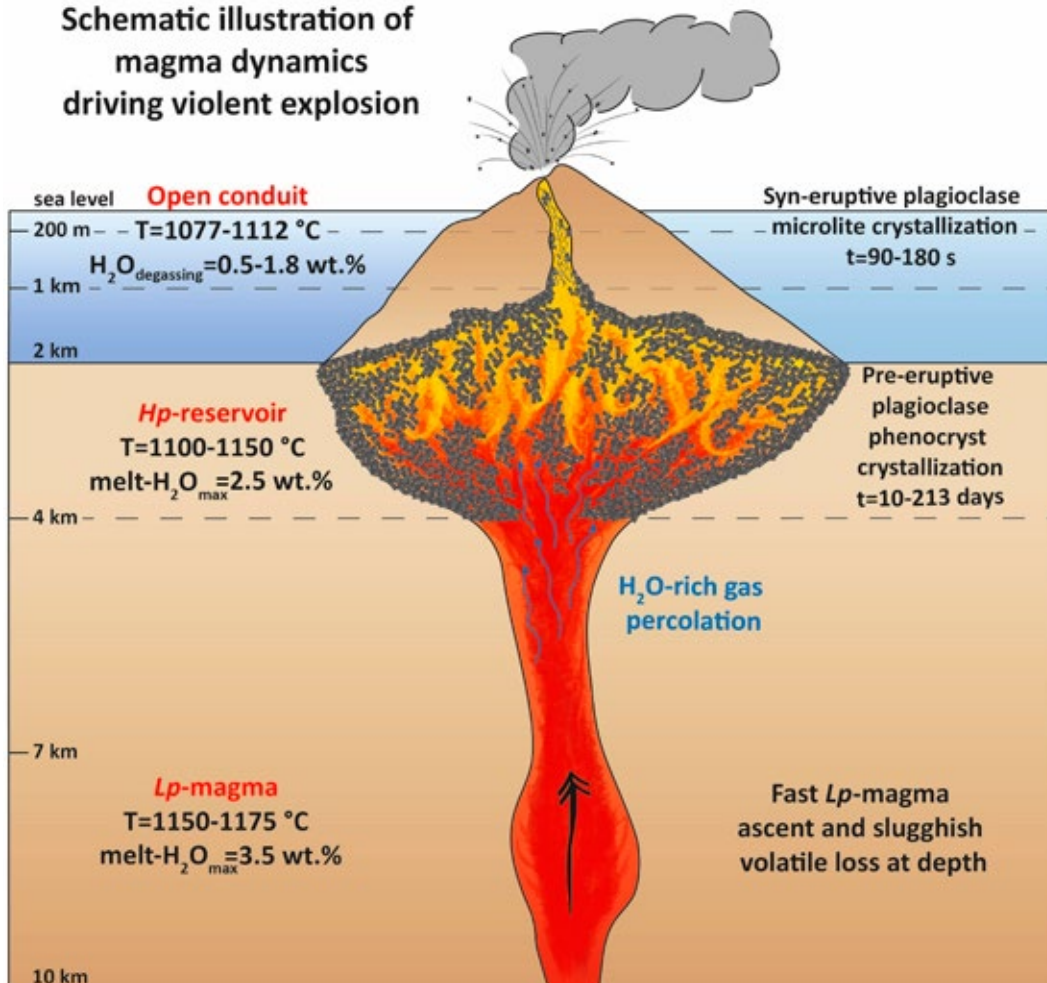


**Figure 1**  
Schematic illustration of magma dynamics driving major/paroxysm (violent) explosions at Stromboli. Pre- and syn-eruptive crystallization conditions of plagioclase phenocrysts and microlites, as well as magma residence times and ascent timescales.

## KINETIC PARTITIONING OF TRACE CATIONS BETWEEN ZONED CLINOPYROXENE AND A VARIABLY COOLED-DECOMPRESSED ALKALI BASALT: THERMODYNAMIC CONSIDERATIONS ON LATTICE STRAIN AND ELECTROSTATIC ENERGIES OF SUBSTITUTION

Mollo S., Moschini P., Ubide T., MacDonald A., Vetere F., Nazzari M., Misiti V., Miyajima N., Melai C., Di Genova D., Vona A., Di Fiore F., Romano C.

We present kinetic partitioning data for trace cations measured in zoned clinopyroxene crystals obtained from a variably cooled and decompressed olivine basalt erupted at Mt. Etna volcano in Italy. Supersaturation effects and compositional heterogeneities at the interface melt lead to the development of sector zoning, concentric zoning, and patchy zoning in clinopyroxene crystals. Apparent partition coefficients between compositionally different growth layers and adjacent melts for isovalent groups of trace elements are tested for internal consistency on the thermodynamic basis of lattice strain and electrostatic energies of substitutions. The excess energy of partitioning for trace cations in zoned crystals accounts for a kinetic incorporation control leading to large enthalpic effects through distortion of the lattice and changes in the electrostatic forces. Polyhedral sectors, skeletal forms, and overgrowth zones have partition coefficients settled by the number of charge-balanced and -imbalanced configurations taking place in the lattice site as a function of aluminium in tetrahedral coordination, and crystal structural changes produced by heterovalent cation substitutions (Fig. 1). In an energetically unstable macroscopic system ruled by cooling and decompression, thermodynamic requirements for the crystallochemical control of partition coefficient encompass the attainment of local equilibrium at the crystal-melt interface via the establishment of small-volume reaction kinetics. The requisite of local interface equilibrium is however susceptible to the anisotropic growth velocity of each specific clinopyroxene surface, thereby giving reason to different energetic properties of the crystallographic site. This axiomatic control requires that transition metal cations partition also in consideration of electronic effects related to the crystal field stabilization energy. The overriding implication is that  $D_i$  values for trace cations having different size, charge, and electronic configuration serve as sensitive probes of the different crystal growth mechanisms, surface incorporation sites, and arrangements of atoms at the lattice-scale. In this perspective, fractional crystallization modeling of 2011–2013 bulk rock data from lava fountains indicates that the compositional evolution of magmas erupted at Mt. Etna cannot be described by a unique equilibrium value of partition coefficient for a given clinopyroxene-melt interface. The leverage of interface kinetics is distinctively dominant along the subvolcanic plumbing system, thereby requiring that values of partition coefficient differ for structurally and compositionally distinct zones in clinopyroxene phenocrysts. To successfully interpret the trace element signature of Etnean magmas, the archetypal constancy of partition coefficient at bulk thermodynamic equilibrium must be in some measure reappraised in favor of the establishment of a local interface equilibrium upon highly dynamic crystallization and growth conditions.

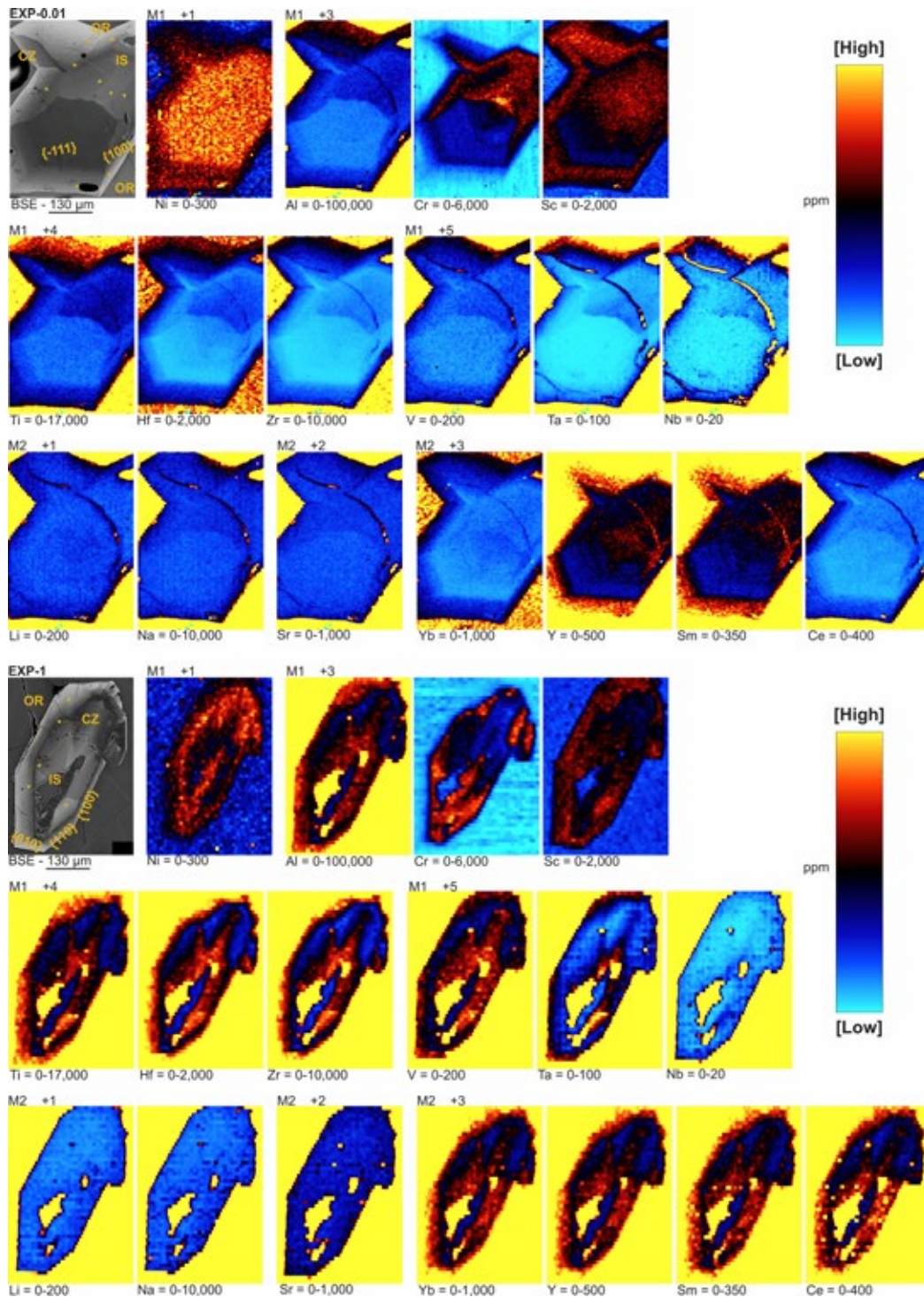


**Figure 1**

Laser ablation inductively coupled plasma mass spectrometry maps for clinopyroxene crystals from slow (EXP-0.01) and fast (EXP-1) decompression experiments. Major (Al), minor (Na and Ti) and trace cations (TE, REE + Y, HFSE, LILE, and Sc) are arranged according to their ionic radius, charge, and host crystallographic site. TE, transition elements. REE, rare earth elements. HFSE, high field strength elements. LILE, large ion lithophile elements.

## MAGMA DIFFERENTIATION IN DYNAMIC MUSH DOMAINS FROM THE PERSPECTIVE OF MULTIVARIATE STATISTICS: OPEN- VS CLOSED-SYSTEM EVOLUTION

Pontesilli A., Di Fiore F., Scarlato P., Ellis B., Del Bello E., Andronico D., Taddeucci J., Brenna M., Nazzari M., Bachmann O., Mollo S.

Open-conduit conditions characterize several of the most hazardous and active volcanic systems of basaltic composition worldwide, persistently refilled by magmatic inputs. Eruptive products with similar bulk compositions, chemically buffered by continual mafic inputs, exhibit nevertheless heterogeneous glass compositions in response to variable magma mixing, crystallization, and differentiation processes within different parts of the plumbing system. In this study we document how multivariate statistics and magma differentiation modeling based on a large data set of glass compositions can be combined to constrain magma differentiation and plumbing system dynamics. Major and trace elements of matrix glasses erupted at Stromboli volcano (Italy) over the last twenty years provide a benchmark against which to test our integrated petrological approach. Principal component analysis, K-means cluster analysis, and kernel density estimation reveal that trace elements define a multivariate space (Fig. 1) whose eigenvectors are more readily interpretable in terms of petrological processes than major elements, leading to improved clustering solutions. Comparison between open- and closed-system differentiation models outlines that steady state magma compositions at constantly replenished and erupting magmatic systems approximate simple fractional crystallization trends, due to short magma residence times. Open-system magma dynamics imply lower crystallinities pervade the magmatic storage than those associated with closed-system scenarios, allowing efficient crystal-melt separation toward the top of the reservoir, where eruptible melts continuously supply the ordinary activity at the volcano. Conversely, a mush-like environment constitutes the bottom of the reservoir, in which poorly evolved magmas result from mixing events between mush residual melts and primitive magmas injected from deeper crustal levels.

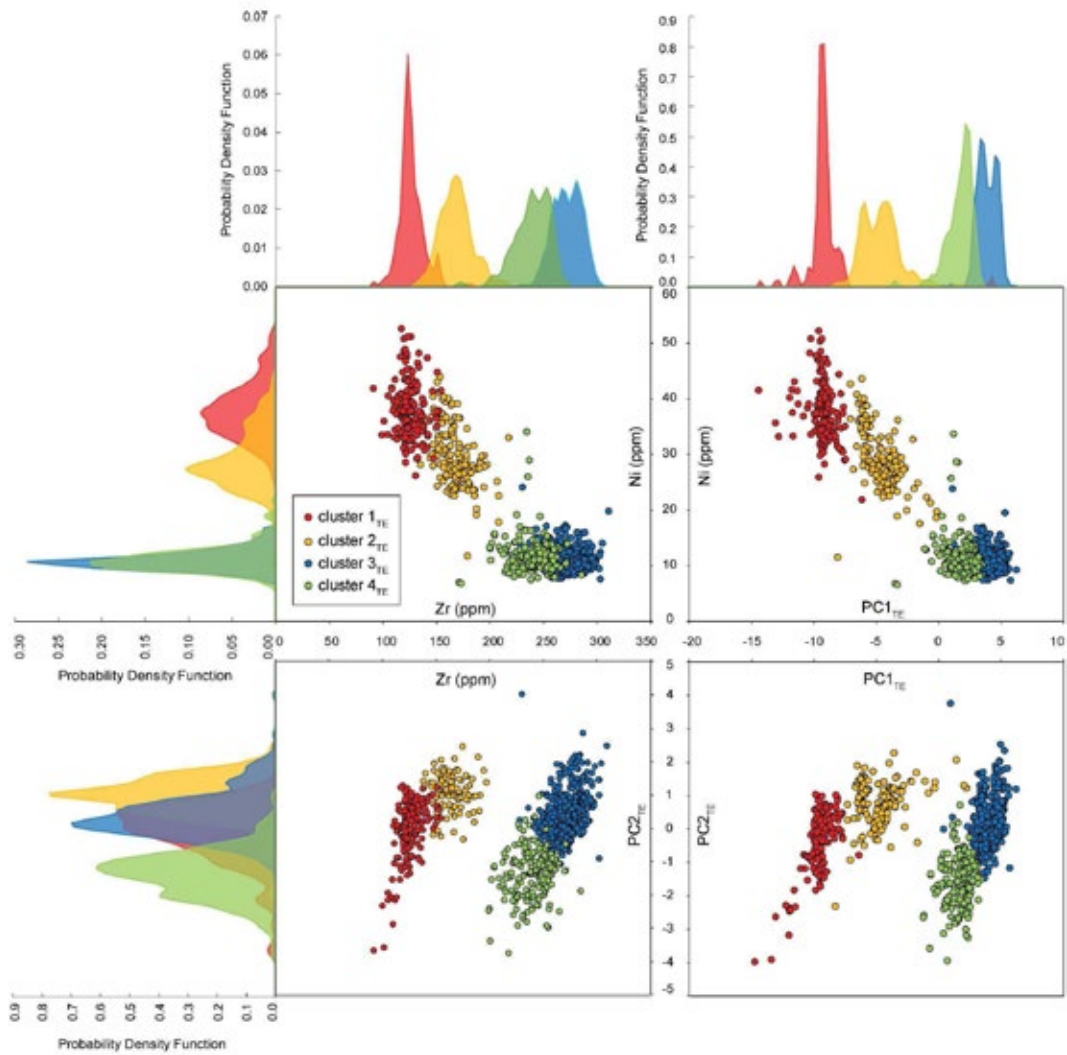


**Figure 1**  
 Bivariate plots of Ni against Zr (in ppm) and principal component scores based on trace elements (i.e., PC1<sub>TE</sub> and PC2<sub>TE</sub>) integrated with kernel density estimates for each cluster.

## THE A.D. 79 ERUPTION OF MT. VESUVIUS: TIMESCALES AND DYNAMICS OF MAGMATIC PROCESSES

Pelullo C., Romano P., Arienzo I., Doronzo D., Nazzari M., Sparice D., Rizzo LA., Di Vito MA.

The A.D. 79 Pompei eruption (Vesuvio, South Italy), is one of the first well-documented and most studied Plinian eruptions occurred in the last two millennia. In order to investigate magma chamber processes, we performed a detailed characterization of clinopyroxene zoning pattern by acquiring major elements concentration (Si, Ti, Al, Fe, Mg, Mn, Ca, Na). The data were collected at the HP-HT Laboratory of Experimental Volcanology and Geophysics of the Istituto Nazionale di Geofisica e Vulcanologia in Rome (Italy), using a Jeol-JXA8200 electron microprobe equipped with five wavelength dispersive spectrometers. Clinopyroxenes are diopsidic and Fe-diopsidic ( $Wo_{53-45}En_{49-17}Fs_{30-6}$ ; Fig. 1a) in composition and show normal, reverse and multiple zoning patterns; several crystal cores are characterized by patchy zoning. We analyzed 35 crystals, acquiring major elements composition along core-to-rim profiles. Mg# [Molar  $Mg^{2+}/(Mg^{2+} + Fe_{tot}) * 100$ ] of clinopyroxenes ranges between 91 and 52. Chemical zoning records changes in magma composition and crystallization conditions. 63% of crystals are normally zoned, 14% are reverse zoned while 23% present a complex zoning pattern. Some elements (e.g., Mg, Fe and Al) allow to identify five chemically different populations (ME0 to ME4, Fig. 1b) in the clinopyroxene zoning pattern, which can be related to distinct crystallization conditions. We used clinopyroxene, whole rock and glass (melt inclusions and matrix glasses) compositions to calculate the magma temperature which show a good linear correlation with the Mg# of clinopyroxene across the detected populations (Fig. 1b). The relationship among the compositional populations in the clinopyroxene zoning pattern (Fig. 1c) tracks the sequential growth of crystals in different magmatic environments, reflecting crystallization at different temperatures. The diffusion modelling applied with rim specific temperature at the clinopyroxene zoning pattern yield crystals residence times at the different magmatic environments from c. 5 months to c. 36 years with 88% of the crystals recording less than 10 years (Fig. 1d-e). The zoning pattern of clinopyroxene crystals from the A.D. 79 Pompei eruption reflects the interaction between a high-T mafic (high Mg#, low  $Al_2O_3$ ) magma (in equilibrium with ME0/ME1 clinopyroxenes) and a low-T evolved (low Mg#, high  $Al_2O_3$ ) magma (in equilibrium with ME3/ME4 clinopyroxenes) that also caused the formation of intermediate compositions (ME2/ME3) mostly at the crystal rims. The duration of such a process is in the order of a few years and refers to the pre-eruptive events, that is the building of the magmatic reservoir feeding the A.D. 79 eruption.

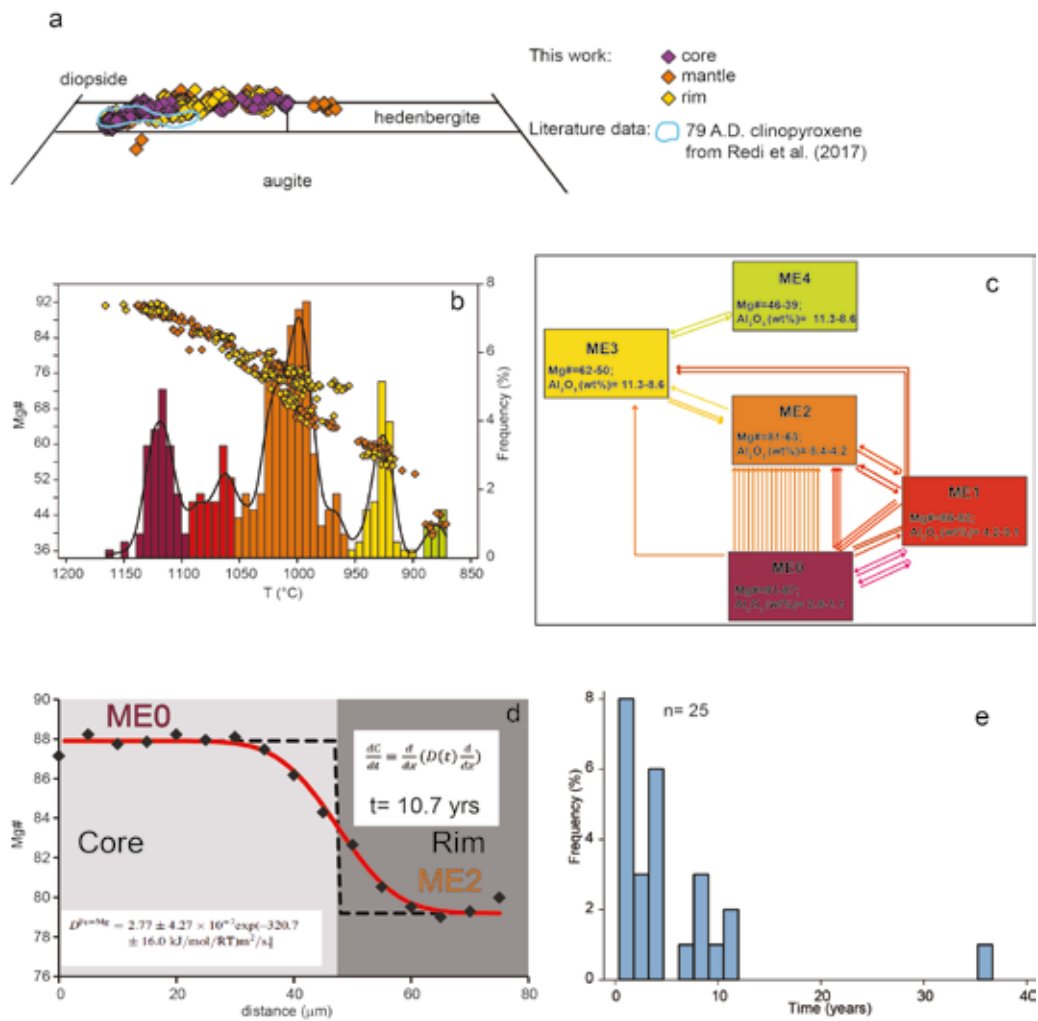


**Figure 1**  
**a)** clinopyroxenes classification diagram of the analyzed core-to-rim profiles; **b)** T (°C) vs clinopyroxene Mg# variation diagram and histogram of the calculated T values showing different compositional populations; **c)** system analysis of the clinopyroxene zoning pattern with each line indicating the core to rim composition; **d)** diffusion modeling applied to a A.D. 79 clinopyroxene crystal; **e)** histogram of the timescales calculated from all the 25 crystals suitable for diffusion modeling.

## ASH-LEACHATES' UPDATE IN STUDYING ERUPTIVE DYNAMICS AT STROMBOLI VOLCANO

Bagnato E., Cinti D., Andronico D., Scarlato P.

Fine-grained ash erupted from active volcanoes and transported through volcanic plumes can adsorb, and therefore rapidly scavenge, volatile elements such as sulphur and halogens, in the form of soluble salts adhering to ash surfaces. The analysis of such water-soluble surface materials, by leaching experiments ('ash leachates'), may represent an important additional tool to detect (and potentially forecast) changes in the activity state of the volcano, as for example evidencing the arrival of S-rich magmas into the shallow system before a more explosive event. The relationship between the chemical composition of water-soluble components and the state of activity of Stromboli allowed obtaining marked temporal variations in the composition of the ash-leachate.

In the last year, ash leachates dataset at Stromboli volcano has been intensively enriched by improving ash sampling frequency, thanks to both automatic ash collector and volunteers' activity in the island, within the UNO project's objectives. In detail, from November 2022 to October 2023, fifty new fresh ash samples have been collected during different types of activity, from ordinary to major explosions, lava flows and pyroclastic flows due to lava fronts collapses. While we aimed at measuring the chemical composition of ash leachates and evaluating its temporal variations in relation with the plume chemistry, often it has not been possible to associate ash leachate data (in terms of molar S/Cl and S/F time series) with the gaseous phase abundances (by FTIR data), due to both logistic and meteorological issues. Nevertheless, data analysis demonstrated that S/Cl and S/F molar ratios in ash leachates agree well with the Stromboli's bulk gas signature, while Cl/F ratios fall within the typical volcanic arc gas range (1.9 – 160; Fig. 1a, b).

This suggests a prevalent volcanogenic origin of S, Cl and F, confirming that the adsorption of plume acidic gases onto volcanic ash is among the key controlling factors on ash leachates composition. Besides, we found that ash leachates S:Cl:F proportions are highly variable in time (Fig. 1c), reflecting changes in the eruptive style of the volcano as well as plume variation around its time-averaged composition (2019-2023). In particular, S/F and S/Cl molar ratios in ash-leachates increased significantly during the most vigorous episodes, including the July 2019 paroxysm, concurring well with a greater volume of volatiles within the plume and the finest nature of the emitted ash. Further increases in ash leachates' molar ratios were observed during explosive and lava flow events occurred during 2021-2023 (Fig. 1c). As expected, once the events ended, the molar ratios decreased back to the mean values reported for ordinary activity. Similar trends have also been observed previously at other volcanoes worldwide, such as in 1974 Fuego eruption (S/Cl ratios > 4), 1982 El Chichón eruption (S/Cl ratios ~ 9) and 1982 Galunggung eruption (S/Cl ratios of ~ 7-8). Finally, most of Stromboli's ash leachates fall close to the composition of Anhydrite and Halite minerals, as confirmed by the strong Na-Cl and Ca-SO<sub>4</sub> correlations found in the extracted solutions. These trends manifested mainly during major eruption/paroxysm, pyroclastic flow and/or lava flow episodes (like those occurred in October and December 2022, respectively). These results indicate that the higher the availability of acidic gases (SO<sub>2g</sub> and HCl<sub>g</sub>) in the volcanic plume, the more favourable the extraction of cations from dissolving ash fragments, followed by precipitation of CaSO<sub>4s</sub> and NaCl<sub>s</sub> on ash surfaces.

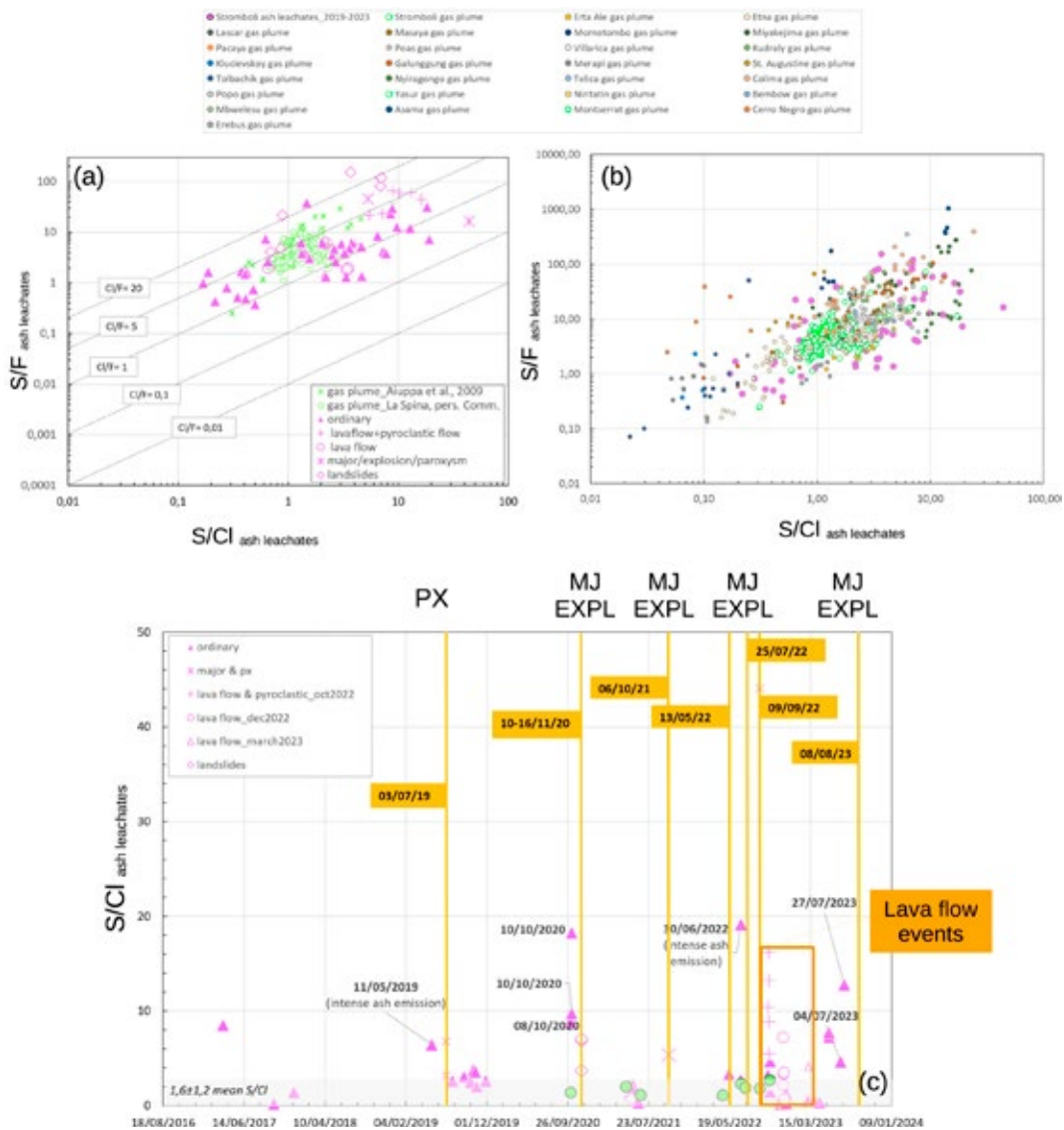


**Figure 1**  
**a)** S/Cl variation with S/F molar ratio for leachate solutions from Stromboli 2019–2022 eruptions. Green circles indicate Stromboli's plume chemical composition (personal communication by Aiuppa, 2010 and La Spina). The dashed diagonal lines represent Cl/F ratios of 0.01, 0.1, 1, 5, and 20; **b)** S/Cl and S/F variation in Stromboli's ash leachates compared with gas plume chemistry from arc volcanism worldwide; **c)** Time series of S/Cl molar ratios in Stromboli's ash leachates from different volcanic activity since 2017 to date. The averaged S/Cl molar ratio for ordinary activity is also reported (grey area). The orange box groups data from the 2022–2023 lava flow events. PX: paroxysm; MJ EXPL: major explosions.

## LABORATORY SETUP FOR INVESTIGATING GAS-DRIVEN VOLCANIC TREMOR AND LONG PERIOD SEISMICITY

Kim K., Spina L., Taddeucci J., Pennacchia F., Cornelio C., Spagnuolo E., Girona T.

Volcanic tremor and long-period (LP) events are seismic signals linked to magmatic/hydrothermal fluid processes. Previous studies suggest that the accumulation of gas beneath permeable caps within the shallow volcanic conduit leads to spontaneous pressure oscillations that can produce volcanic tremor and LP events. To test this hypothesis and investigate the role of permeable cap physical and geometrical properties we built a novel experimental setup at the HP-HT laboratory.

The setup is schematized in Figure 1 and comprises: 1) a lower conduit section, i.e. a vertically-arranged cylindrical Plexiglass pipe (4 cm internal diameter, ca. 90 cm length) filled with air and water at different proportion; 2) an upper conduit section, made up of a cylindrical Plexiglass pipe featuring different types of permeable caps; 3) two connection units, at the base and bottom of the upper conduit section, working also as pressure sensor-holder.

We injected compressed air by using a set of flux-meters (Cryotek Eng;  $10^{-3}$ -1.2 l/s) into the lower conduit section at the base of the pipe and monitored pressure oscillations beneath the permeable cap and at the conduit vent by using flush-mounted PCB Piezotronic ICP® Pressure Sensors (sensitivity: 25 mV/psi, measurement range: 200 psi).

Additionally, we characterized the elastic radiation at the conduit vent by using a PCB Piezotronics monoaxial accelerometer (sensitivity: 0.1 V/g in the band 0.5–10,000 Hz) located along the conduit wall and a microphone PCB Piezotronic microphone (sensitivity: 50 mV/Pa in the band 7–10,000 Hz ( $\pm 1$  dB), and  $\pm 2$  dB in the band 3.75–20,000 Hz) or alternatively a GRAS 40 AN microphone (frequency: 0.5 Hz–20 KHz sensitivity: 50 mV/Pa) above the vent.

Two series of experiments were performed to explore the role of pore arrangements, permeability and thickness of the permeable cap:

i) by varying the number and diameter of straight pores carved in a gypsum matrix of variable length; ii) by using foam rubbers with different densities (18 up to 75 kg/m<sup>3</sup>). To determine the permeability of the foam rubber samples we performed measurements at different confining pressure by using the PERMIE device.

Preliminary results show that gas flow through the water without a permeable cap generates low-frequency pressure oscillation ( $< 1$ -5 Hz) in the free air above, which is likely related to bubble bursts. When a permeable cap is present, pressure oscillations in the 2-150 Hz frequency band appear in the air pocket beneath the cap, suggesting resonance due to gas accumulation. Different characteristics of the porous media, as mentioned above, generate distinct waveform features, including different vibrations and acoustic signals. For example, gas flow through straight capillary pores exhibits periodic peaks in microphone records, indicating that permeable gas flow may control periodic volcanic outgassing. Our study offers a laboratory approach to unveil the seismoacoustic signals linked to gas circulation within porous media and serves as a reference for explaining volcano monitoring signals in natural settings.

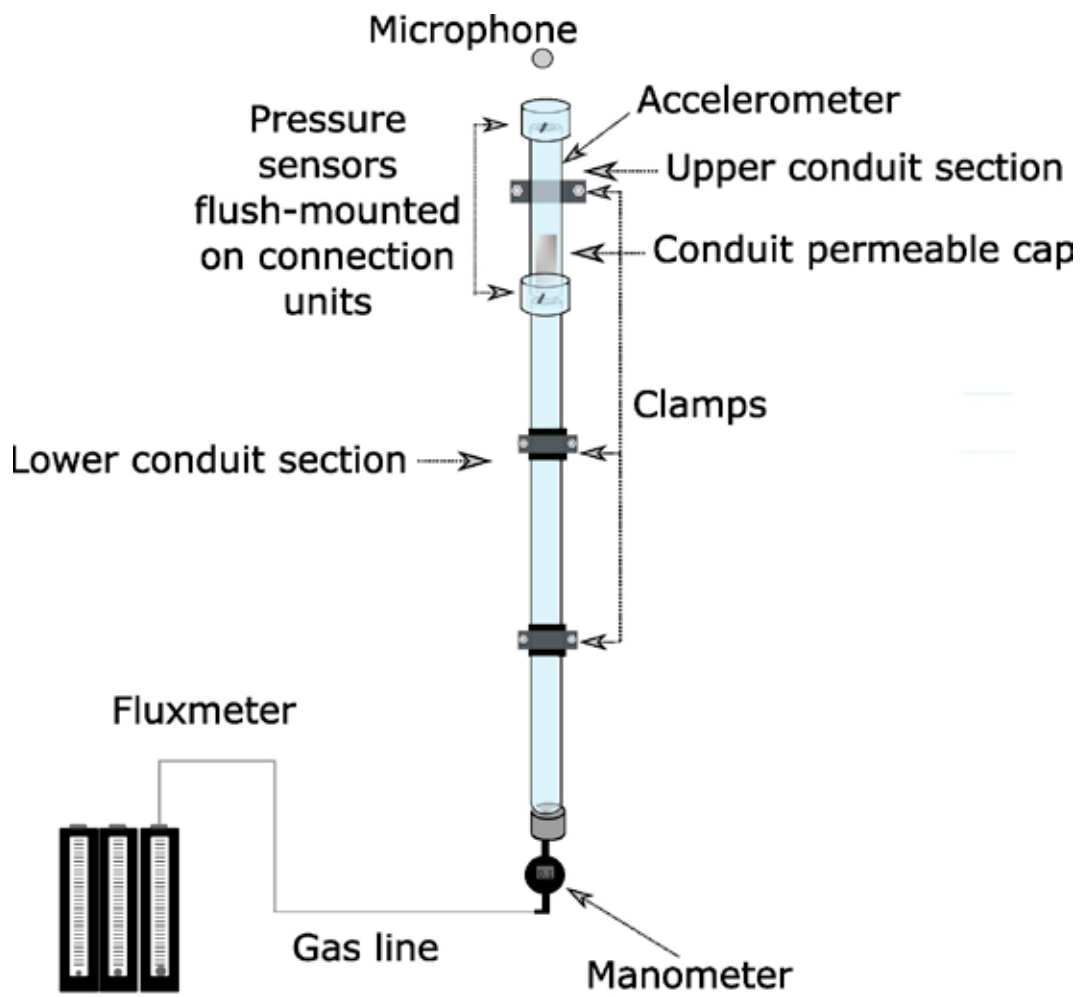


Figure 1  
Simplified sketch of the experimental setup.

## THE DEPTH-TO-SURFACE DYNAMICS OF SILICIC PERALKALINE MAGMAS FROM PANTELLERIA ISLAND

Magri C., Romano C., Vona A., Frontoni A., Di Fiore F.

The cases in which a magma with a defined chemical composition can discriminate eruptions of different styles are not rare. An example are the peralkaline magmas from Pantelleria island called pantellerites, i.e. rhyolitic and trachytic magmas with an agpaitic index  $[(\text{Na}_2\text{O} + \text{K}_2\text{O})/\text{Al}_2\text{O}_3]$  generally higher than 1.75. These magmas, although chemically acidic, have generated both large eruptions, typical of acidic magmas, and smaller eruptions typical of basic magmas.

The aim of this study is to understand the mechanisms that allows the fragmentation of these low viscosity magmas and that can cause the shift between large-scale explosive and mild effusive eruptions. In order to do this, we propose to use textural observations made on juvenile products, together with viscosity measurements and observations of the glass structure by Raman spectroscopy, for three different eruptions from Pantelleria Island expressive of different eruptive styles.

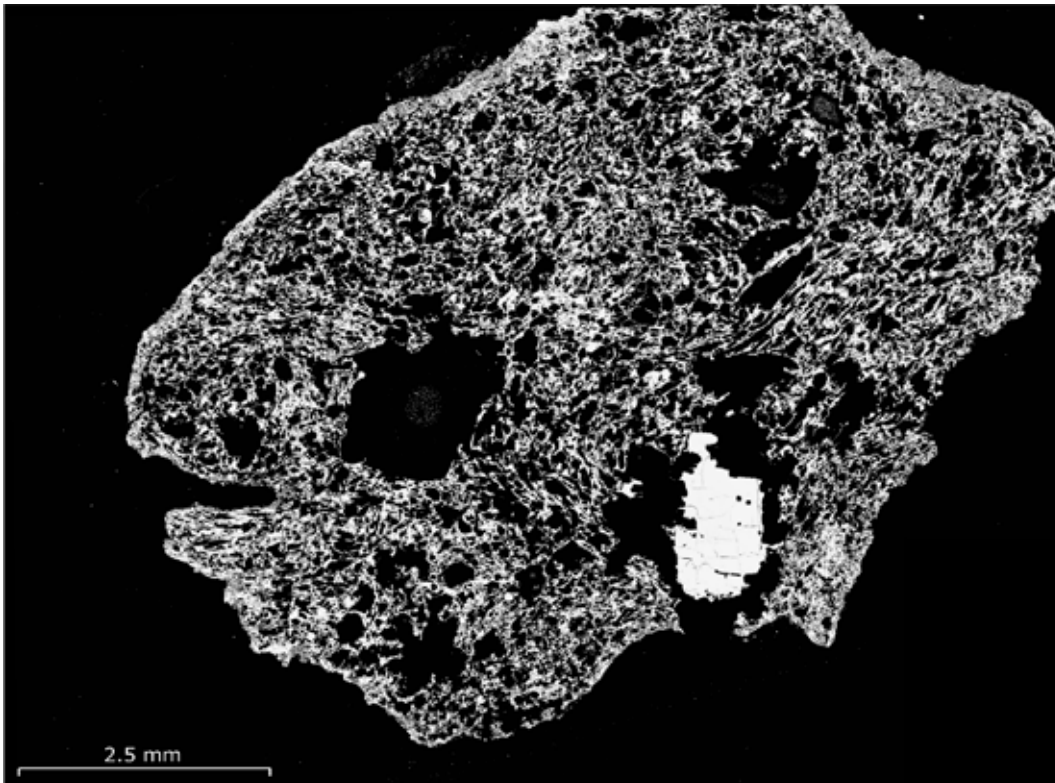


**Figure 1**  
SEM image of pumice from Cuddia Mida eruption (Pantelleria Island, Italy; 9.7 ka).

## EXPERIMENTAL INSIGHTS ON THE SHEAR-INDUCED CRYSTALLIZATION OF A PHONOTEPHRITE MAGMA

Di Fiore F., Vona A., Mollo S., Nazzari M. Giordano G., Romano C.

In active volcanic environments, magmas that ascend within the conduit and erupt at the surface as lava flows experience physico-chemical perturbations related to temperature changes and variable degrees of deformation. We have conducted experimental investigations to examine the concurrent effects of undercooling and stirring on the crystallization kinetics of a leucite-bearing phonotephrite from Somma-Vesuvius (Italy).

Two sets of undercooling experiments have been carried out within the same temperature range of 1300-1150 °C. The first set involved classical static undercooling (SU) experiments with no stirring applied to the melt, while the second set involved dynamic undercooling (DU) experiments with a shear strain rate of 1 s<sup>-1</sup> applied. By comparing SU and DU results with previous data from literature obtained using the same experimental approach, we observe that the degree of crystallization and the textural evolution of leucite and clinopyroxene progress upon the effect of melt stirring by shortening the incubation time.

As a result, the solidification process is markedly enhanced in DU experiments, accompanied by a substantial increase in the crystal nucleation density and growth rate. Thermorheological modeling indicates that stirring-induced crystallization increases the melt viscosity by a factor of ~1.5-4.5 depending on the system temperature. At a given temperature, mass transport can therefore produce higher crystallinity and higher viscosity magmatic suspensions than static crystallization conditions. We document that if subsequent cooling occurs, the existing crystal cargo in such suspensions may promote the onset of non-Newtonian rheological response, causing a transition from homogeneous viscous flow to shear localization and magma/lava rupture.

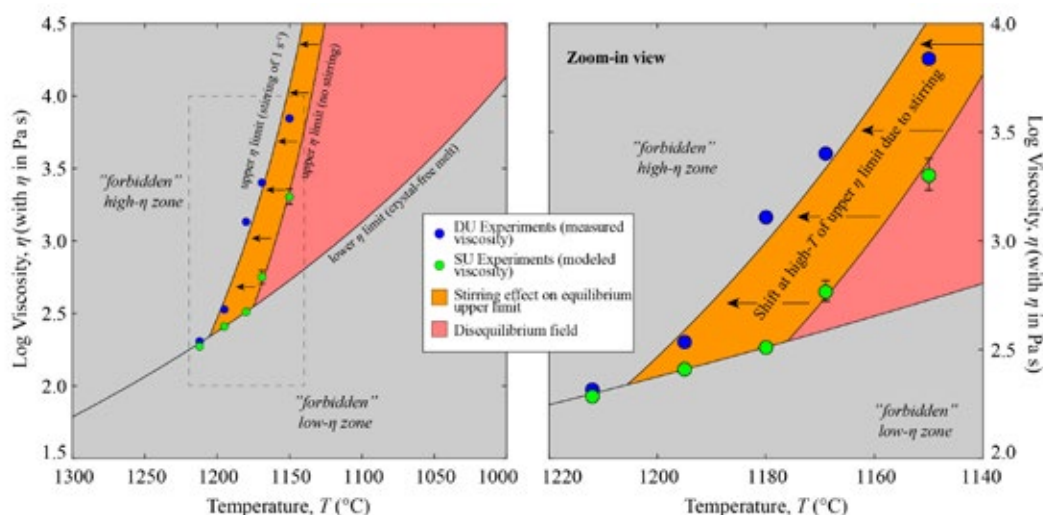


Figure 1

Viscosity-temperature regime diagram of a phonotephrite magma. The zoom-in view on the right side of the diagram shows the upper  $\eta$  limit area to better appreciate the shift at higher T due to the effect of stirring on melt crystallization.

## COMPREHENSIVE ANALYSIS OF STROMBOLIAN EXPLOSION PARAMETERS USING HIGH-FREQUENCY, THERMAL, UV, VISUAL, AND ACOUSTIC TIME SERIES DATA

Del Bello E., Bagnato E., Spina L., Tamburello G., Ricci T., Taddeucci J., Scarlato P., Andronico D., Pennacchia F.

Stromboli volcano provides a unique opportunity to investigate dynamic volcanic processes by employing a variety of techniques, including thermal, UV and visible imagery, and acoustic signals. These combined methods allow for the frequent monitoring of volcanic phenomena, offering valuable insights into rapid processes like Strombolian explosions and enabling the quantification of several parameters, such as gas and pyroclasts flow rates, explosion characteristics, and energy output.

During three specific periods, May 2019, October 2020 and May 2021, we conducted comprehensive, high-frequency, multi-parameter measurements. Daily, we collected 2-5 hours of continuous time series data, including UV, thermal infrared, visible imagery, and acoustic information. UV images measured SO<sub>2</sub> emissions perpendicular to the plume's path, thermal analysis tracked temperature changes during explosions, and combined with visual data to monitor plume and pyroclast ejection speeds, and acoustic signals were assessed for spectral properties related to eruptive styles.

Wavelet analysis of select events provided insights into volcanic jet behaviour. Integrating and analysing these datasets allowed us to identify various active degassing patterns at the summit vents and distinguish between observed activity styles.

Notably, a correlation between thermal and SO<sub>2</sub> signals was observed, particularly at the start of each explosion. In some cases, we determined the mean masses and fluxes specific to individual explosions. The high data acquisition rate enabled us to derive more precise quantitative eruption parameters compared to traditional low-frequency methods, further validated through independent estimation techniques.

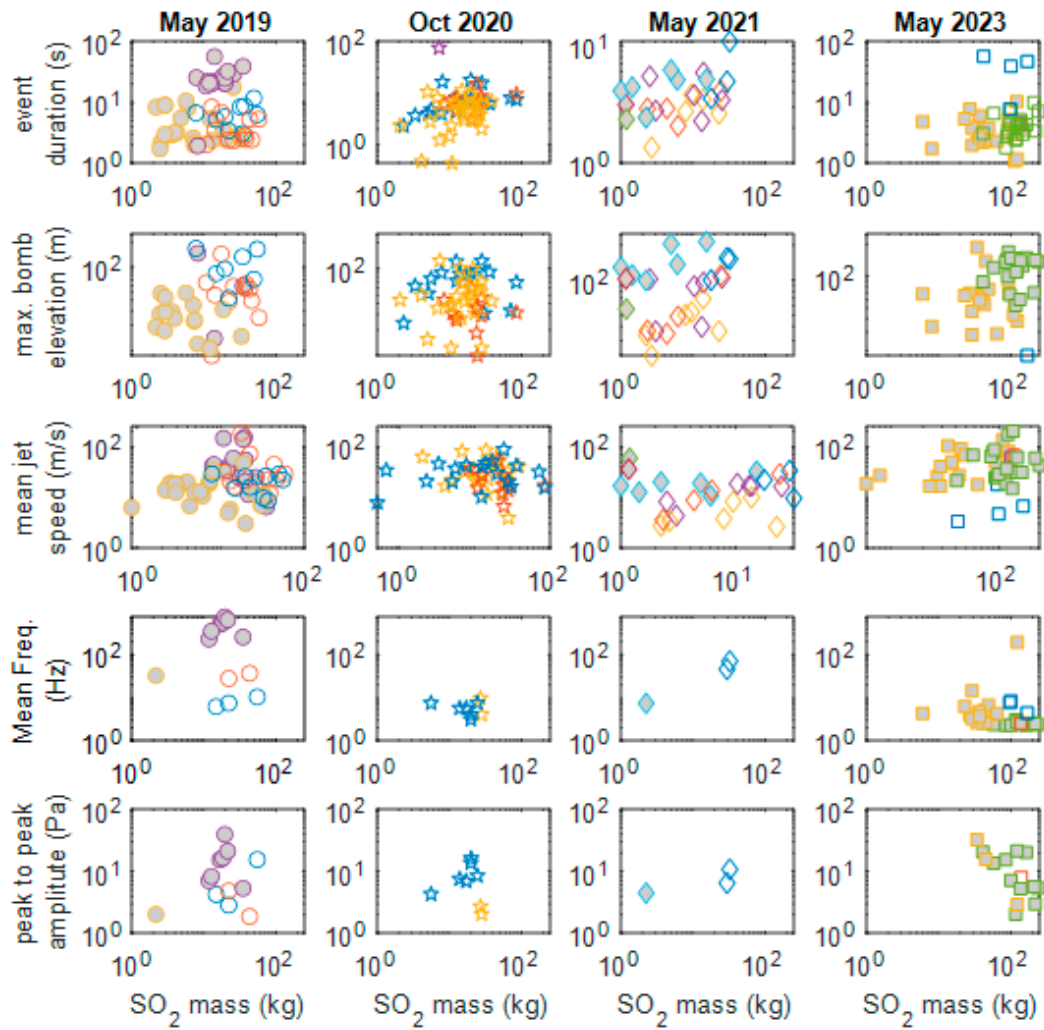


**Figure 1**  
 Comparison between explosive SO<sub>2</sub> masses, acoustic parameters (mean frequency and peak to peak amplitude) and thermally retrieved parameters (max thermal elevation of bombs, duration of explosions, mean jet speed at exit), for the explosive events in different periods of activity at Stromboli. The different colors of symbols represent the different active vents in the SW sector (filled symbols), and in the NE sector (blank symbols), respectively.

## PETROGRAPHY OF HISTORICAL CONCRETES: THE ROMAN THERMAL BATHS OF CHIETI (TEATE MARRUCINORUM)

Casarin A., Nazzari M., Giaccio F., Pierigè M.I., Iezzi G., Masciotta M.G., Scarlato P., Brando G., Criber E., Tuteri R.

The characterisation of geomaterials (natural rocks) and their artificial analogues (concretes, mortars, types of cement, bricks, ceramics, etc.) used in ancient times is crucial to reconstruct their provenance and production techniques and establish their preservation. The exceptional durability of numerous Roman archaeological sites can be attributed to the remarkable properties of the mortars and concretes employed. Roman mortars and concretes are composite materials made of a binder (aerial or hydraulic) mixed with fine- or coarse-grained aggregates, respectively. Differentiation of types of aggregates (lithic fragments, crushed ceramics, volcanic ash, etc.) enabled the optimisation of formulations to increase the mechanical performance of mortars and concretes and adapt them to variable uses. Mineralogical, chemical, and textural analyses can allow us to reconstruct these processes from the types of raw materials used in recipes adopted by ancient craftsmen.

Here, the Roman Thermal Baths (1<sup>st</sup>-2<sup>nd</sup> century AD) in Chieti (Abruzzo, Italy, fig.1a), the ancient Teate Marrucinorum, were supplied by a cistern complex adjacent to the site (fig.1b). Three horizontal cores were extracted from these walls; they were cored coaxially with the ground to expose the outermost to innermost layers of them (fig.1c). Seven thin sections were prepared from these samples, at varying positions (three from sample MCGL-CLS-1, two from MCGL-CLS-2, and two from MCGL-CLS-3). A high-resolution scanner (HRS, fig.1d) was employed to scan mesoscopic samples and thin sections. These latter were also imaged with transmission optical microscopy (TOM) and scanning electron microscopy under back-scatter mode (BS-SEM) to obtain digital images (fig.1e); the thin sections were also used to characterise the micro-chemical features of the various phases contained in the different portions of these Roman concretes.

The digital images were used to quantify the textures, i.e. sizes, shapes, perimeters, areas, etc. of phases (voids, crystalline and non-crystalline) hosted in the various materials contained in these concretes. Then, the micro-chemical attributes of solid phases were also carried out to constrain their similarities and differences. These two complementary characterisations elucidate the type of mix utilised for the cistern walls, including whether an aerial or hydraulic binder was employed, as well as the types of aggregates and binders used and their provenance.

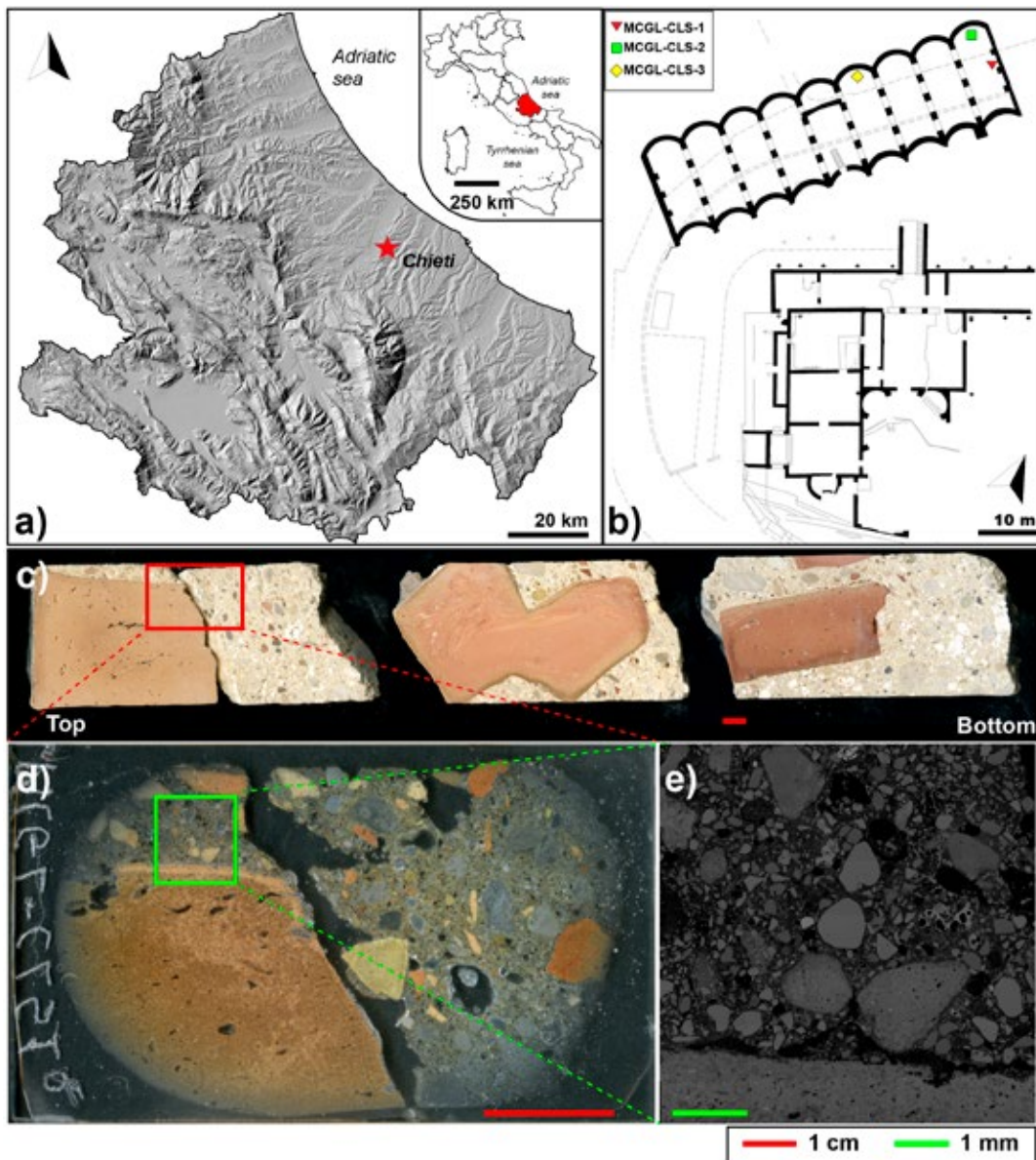


**Figure 1**

**a)** Geographical position of the Abruzzo region (Italy), with the location of the city of Chieti as red star (DEM from Tinitaly, Tarquini et al 2023); **b)** samples position in the cisterns complex near the Roman Thermal Baths; **c)** core sample MCGL-CLS-1. The red box represents the position of thin section MCGL-CLS-1-a; **d)** High-resolution scan of MCGL-CLS-1-a thin section. The green box is the area acquired as a BSE-SEM puzzle of sequential micrographs; **e)** BSE-SEM acquisition was obtained at the HP-HT lab of INGV of Rome.

## **CHARACTERISATION OF ERUPTIVE PRODUCTS FROM GLACIAL/SUB-GLACIAL ERUPTIONS IN THE MOUNT MELBOURNE AREA (NORTHERN VICTORIA LAND, ANTARCTICA)**

Rocchi I., Di Roberto A., Giacomoni P.P., Rocchi S.

In the frame of the PNRA project, several expeditions in Antarctica sampled a wealth of volcanic products during the field seasons 2005-2006, 2011-2012 and 2014-2015.

The last project, which started in 2018, focussed on the MAGma-ICe interaction (MAGIC), with the objective to reconstruct the ice cover evolution and the effects of variable ice load on the eruptibility and composition of magma. Several data concerning the tephra chemical composition and their relations with different volcanoes and eruptions have already been published. However, there was no data available concerning the chemical composition of glassy products formed by interacting with the ice cover.

For this reason, in this study two types of samples were analysed: hyaloclastites (a volcanoclastic deposit formed by the explosive interaction between magma and water) and lapilli tuffs.

The samples were prepared and preliminarily selected at INGV, Pisa, using a scanning electron microscope equipped with an energy-dispersive system (SEM-EDS). Then, they were analysed for their chemical content using the electron microprobe provided by the INGV, Roma.

The EPMA analyses were performed with the main objective to achieve a good overview of all the different types of samples and to select the most representative ones to perform further chemical analyses (LA-ICP-MS). Moreover, the comparison with the tephra chemical composition from the literature has highlighted some possibly interesting correlation between our samples (proximal) and the distal tephra. The results show a general homogeneity of the analyses performed in each sample (Fig. 1). However, some sites present very interesting results, as they include chemical composition that varies along a probable trend of evolution.

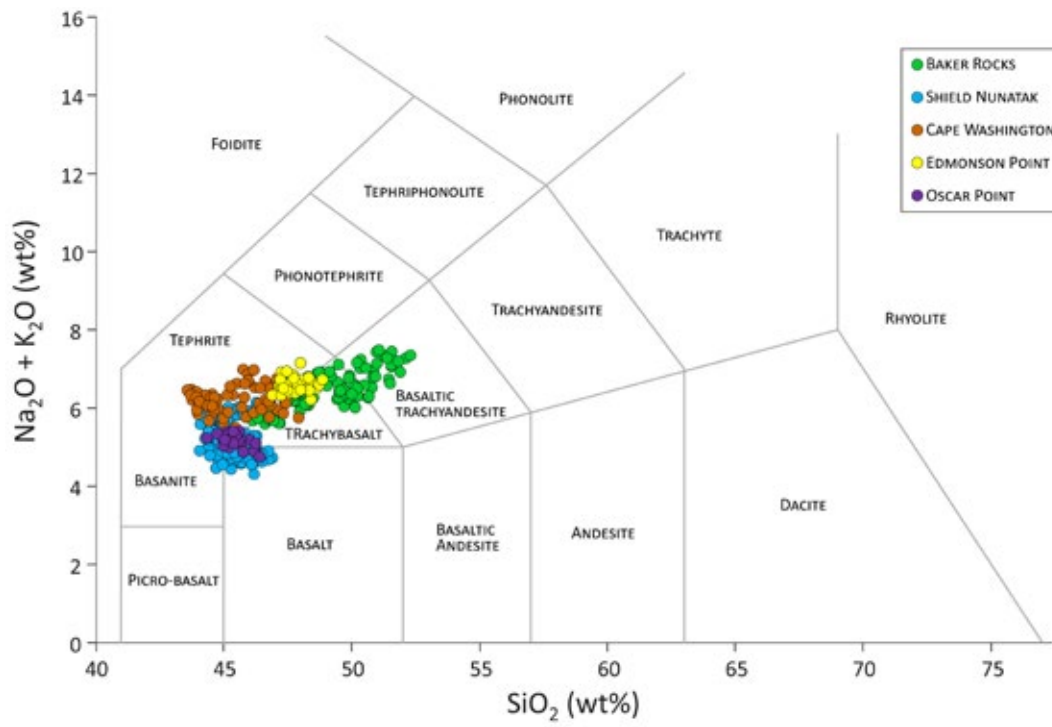


Figure 1  
 EPMA-WDS results of some representative samples reported on the TAS diagram.

## **TEPHROCHRONOLOGICAL STUDY OF THE LACUSTRINE SUCCESSION OF THE CASTIGLIONE MAAR (CENTRAL ITALY) AND EVALUATION OF THE POSSIBLE IMPACT ON THE CLIMATE OF THE EXPLOSIVE ERUPTIONS OF THE PERI-THYRRENIC VOLCANOES**

Di Roberto A., Scateni B., Re G.

The research activity was part of the multidisciplinary project AMUSED: A MULTidisciplinary Study of past global climatE changes from continental and marine archives in the Mediterranean region (Environment Department Project-INGV). The project aims to reconstruct climate variability in the central Mediterranean region during the middle-late Quaternary, with a specific focus on the Holocene. The carried-out activity involves the tephrochronological study of a succession of continental sediments sampled in the Castiglione maar (Central Italy), located 20 km east of Rome along the ancient Via Prenestina. Here, two parallel 120 m-long cores and one 15-m long core were drilled. Additionally, two 12 m-long and 3 m-long cores at the edge of the basin were performed. We studied the composite sequence resulting from the two main boreholes.

In the past 20 years, tephrochronology, which uses volcanic ash (tephra) as a time marker, has proven to provide high temporal and stratigraphic resolution information crucial for dating, correlation, and synchronization of archaeological, geological, paleoecological, and paleoclimatic records. Tephra deposits almost synchronously over large areas, forming a level with an almost identical geological age in all identified sites (isochronous). The age of the eruption that produced the tephra can be determined through various methods, including the dating of minerals contained in the tephra (e.g., potassium feldspar) using methods such as  $^{40}\text{Ar}/^{39}\text{Ar}$  and K/Ar.

Tephrochronology can complement or sometimes replace classic dating methods with time limitations, such as the  $^{14}\text{C}$  method, which is applicable for materials no older than approximately 50,000 years. The study of tephra also provides important information from a volcanological perspective. By studying the physical characteristics, mineralogy, and chemical composition of the tephra, it is possible to identify the volcanic source and the eruption that produced the tephra.

Tephrochronological studies provide information on the eruptive frequency of a given volcano, eruptive dynamics, or the geochemical evolution of the source. Due to its geodynamic structure and the abundance of active volcanoes, the Mediterranean area has always been considered an ideal area for the development and application of tephrochronology. The intense explosive activity of the peri-Thyrrenic volcanoes and the Hellenic arc has produced numerous tephra levels that are interspersed in continental and marine sedimentary sequences.

As part of the project, the major-element glass compositions were determined for 55 tephra layers bearing fresh volcanic glass at INGV HPHT Laboratory in Rome, using a JEOL JXA 8200 electron microprobe (EPMA) equipped with five wavelength-dispersive spectrometers.

The major elements glass compositions of tephra from the Castiglione maar sequence were compared with literature data, including the composition of proximal pyroclastic deposits erupted during the explosive activity of volcanoes from central Italy and the composition of tephra markers identified in other records of central Italy such as the Fucino basin, the Lago Grande di Monticchio, and marine sediment cores from the Tyrrhenian Sea. For most of the studied tephra, the volcanic source was identified; these resulted in the Colli Albani, (Albano maar last two eruptive cycles), Sabatini, Vico, Ischia, Latera-Vulsini and Roccamonfina volcanic complexes. Some tephra layers remain undetermined, although their general geochemical affinity indicates the aforementioned volcanoes of central Italy as the most probable source.

## SHOCK-TUBE EXPERIMENTS AND HIGH-SPEED SCHLIEREN SHADOW PHOTOGRAPHY

La Spina G., Spina L., Pennacchia F., Scarlato P., Taddeucci J.

During explosive volcanic eruptions the sudden release of gas and pyroclast mixtures produces jet flows and acoustic waves which propagate into the atmosphere. Jet dynamics and acoustic signals are strongly affected by the processes occurring within the conduit, and thus their study can be used to infer magma dynamics below the vent. However, the influence of gas-pyroclast flow within the conduit on jet behavior remains still poorly understood.

To better understand the correlation of the jet flow dynamics, acoustic signals and conduit dynamics we employed a novel apparatus combining a shock-tube system together with a high-speed Schlieren shadow photography and acoustic sensors. The shock-tube consists of a high-pressure reservoir connected with a cylindrical tube through a diaphragm pulse valve which allows a fast release of pressurized gas into the ambient pressure tube (Fig 1a). The Schlieren shadow photography is deployed using a parabolic mirror (primary parabolic mirror of 400 mm diameter with focal length of 1800 mm, Fig. 1a). The pointwise light source necessary for the Schlieren technique is obtained with a Fiber optic illuminator (150 W, model OL-2, Fig. 1b). During decompression experiments, images are collected using a high-speed camera (NAC MEMRECAM HX-3, Fig. 1b) acquiring data at 30,000-50,000 fps. Acoustic signals are recorded at 200 KHz using two microphones, a PCB Piezotronic microphone (sensitivity:  $\pm 1$  dB in the band 7–10,000 Hz, and  $\pm 2$  dB in the band 3.75–20,000 Hz) and a GRAS 46 DP-1 microphone (frequency: 6.5 up to 140 KHz; sensitivity 0.9 mV/Pa) above the vent (Fig. 1a). Experiments were performed at different conditions, varying the pressure within the reservoir, the length and diameter of the cylindrical tube. We performed experiments with pressured gas only and adding particles with different volumes (~0.1-0.3 mm in diameter) and shapes (spherical and discs), distilled water, or various amounts of viscous analogue materials.

Preliminary results show a strong correlation of acoustic waves and characteristics and jet flow dynamics with the volume and type of materials (particles, water, or analogue material) inserted in the shock tube (Fig. 1c,d). Further analyses and experiments will be fundamental to better correlate observations at active volcanoes with conduit dynamics below the vent, but preliminary results suggest that this will be achievable.

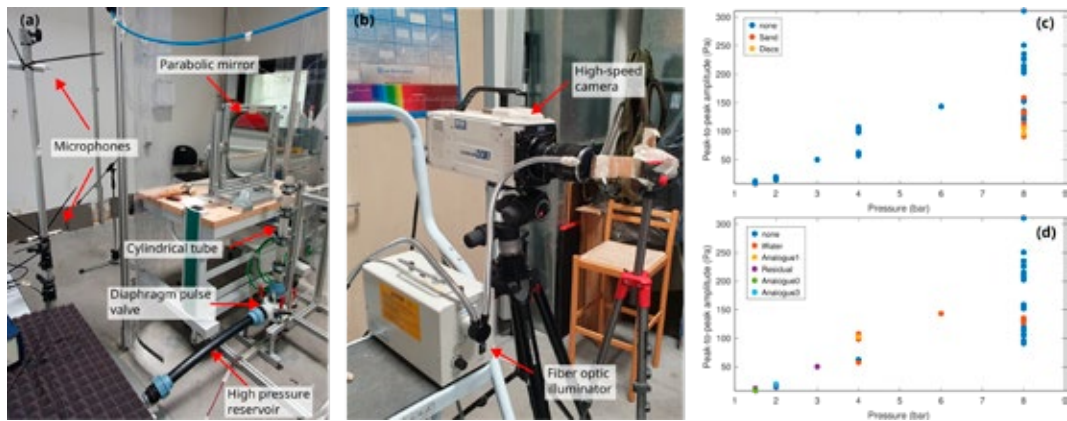


**Figure 1**  
**(a-b)** Shock tube apparatus in combination with the setup for the Schlieren shadow photography. **(c-d)** Preliminary results obtained performing experiments with different materials (pressurized gas only, particles, water, and analogues materials).

## THE ANALYSIS OF MUDSTONE IN ARCHAEOOMETRY

Xanthopoulou V., Nazzari M., Iliopoulos I.

Excite TNA project ID: EXCITE\_C3\_2023\_50- CERMUD

Mudstones are detrital fine-grained sediments including terrigenous and carbonate mud (micrite), silt and siltstone, as well as deep-sea ooze and sapropel. Mudstone provenance studies help us to infer about source-to-sink transport pathways and achieve a better understanding of the source mineralogy of the sedimentary deposit before any alteration has influenced it during burial diagenesis. Moreover, exploring differences in origin might help explain why mudstones with similar diagenetic paths may have different final compositions. Given their abundance in various geological environments worldwide as well as their compositional similarity to the ceramic paste prepared for most of the pottery manufacture it is not surprising that mudstone is one of the most commonly used inert material employed by the very first potters as temper, ie. as an inclusion purposefully added in the ceramic paste for improving their performance characteristics. In Greece for example, and focusing specifically on the northern Peloponnese, mudstone ceramic fabrics are widespread in prehistoric pottery. Ancient Helike, Pheneos, Ancient Corinth and Argolida to name a few, are well known case studies wherein likewise ceramic assemblages have been thoroughly studied.

The present research aims to explore the potentiality of the mudstone temper as a compositional and technological “marker” of coeval pottery productions and unveil intra- and inter-regional technological choices of the ancient potters and trace provenance issues. Under this framework, at a first step a thorough compositional characterization of local geological outcrops of mudstone is expected to offer a detailed inspection of their intra- and inter-deposit compositional variability in the study area. Several chemical indices have been proposed to quantify weathering effects. The most popular is the chemical index of alteration (CIA) defined as  $[Al_2O_3 / (Al_2O_3 + CaO^* + K_2O + Na_2O)] \times 100$  where  $CaO^*$  is  $CaO$  exclusive of that present in carbonates and the values are in molar proportions to emphasize mineralogical relationships. High CIA values, greater than 90%, indicate extensive alteration of feldspar to clay and consequently intense weathering. Furthermore, since oxide ratios can be used for exploring differences between the samples, different proportions of alumina can give significant evidence about mudstone weathering. That can be achieved by defining the ratio of the Index of Compositional Variability (ICV):  $(Fe_2O_3 + K_2O + Na_2O + CaO + MgO + MnO + TiO_2) / Al_2O_3$ . Non-clay minerals have lower  $Al_2O_3$  content and higher ICV than clay minerals and tend to be higher in the weathering sequence of Goldich (1938). Microchemical approaches like those employing the Electron Probe Microanalyzer (EPMA) are well suited to be used for studying mudstone chemistry either as a natural occurring lithotype or as inclusion in a clay matrix of an experimental briquette or an ancient sherd. In the current research we collected eight samples of mudstones, five from the region of Aigialeia (Fig. 1a-d) and three from Feneos (Fig.2a-d). These samples and two samples from ancient ceramics

from the ancient city of Helike (Aigialeia, Greece) were examined by means of Electron Probe Microanalyzer (EPMA) at the Istituto Nazionale di Geofisica e Vulcanologia of Rome, Italy. CIA and ICV calculated using the molecular proportions and the weight percents, respectively. The very high content of CaO (in carbonatic rocks) was excluded from the CIA calculation, since it is not applicable. The average values from each sample were plotted on the binary diagram CIA index vs ICV index (Fig. 3). The preliminary results revealed that the mudstones identified into the ceramic paste are grouped with the mudstones from Aigialeia, indicating the same origin and consequently the local provenance of the ceramic sherds. About the mudstones from Feneos region the results showed a lower index of compositional variability compared to the Aigialeia samples, indicating the compositional maturity of the mudstones and the low content of nonclay silicates. Further research on the mudstone fragments, including mineralogical and bulk chemical analysis will complement the current research and is expected to provide relevant information to the study of mudstones as non-plastic inclusions in the ceramic paste, and shed light to provenance issues.

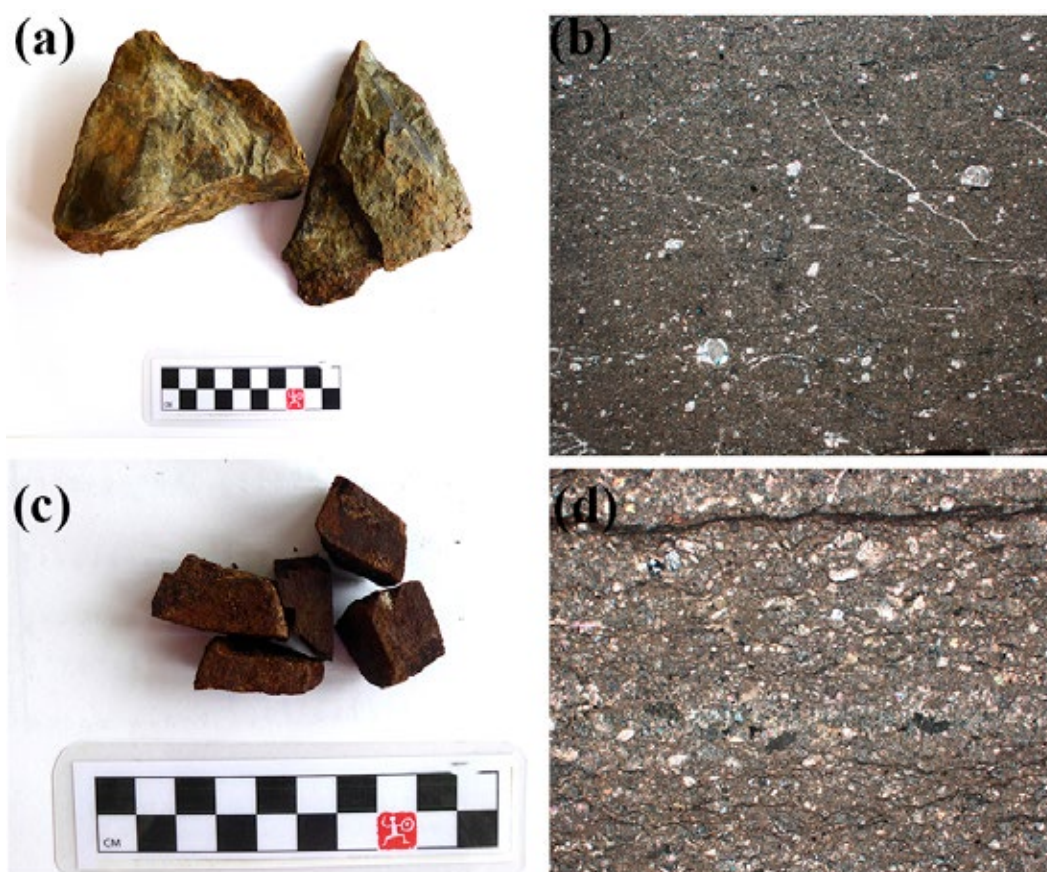


**Figure 1**  
Representative mudstones fragments of samples (a) MF1 and (c) MF5 and (b & d) microphotographs of the same samples respectively.

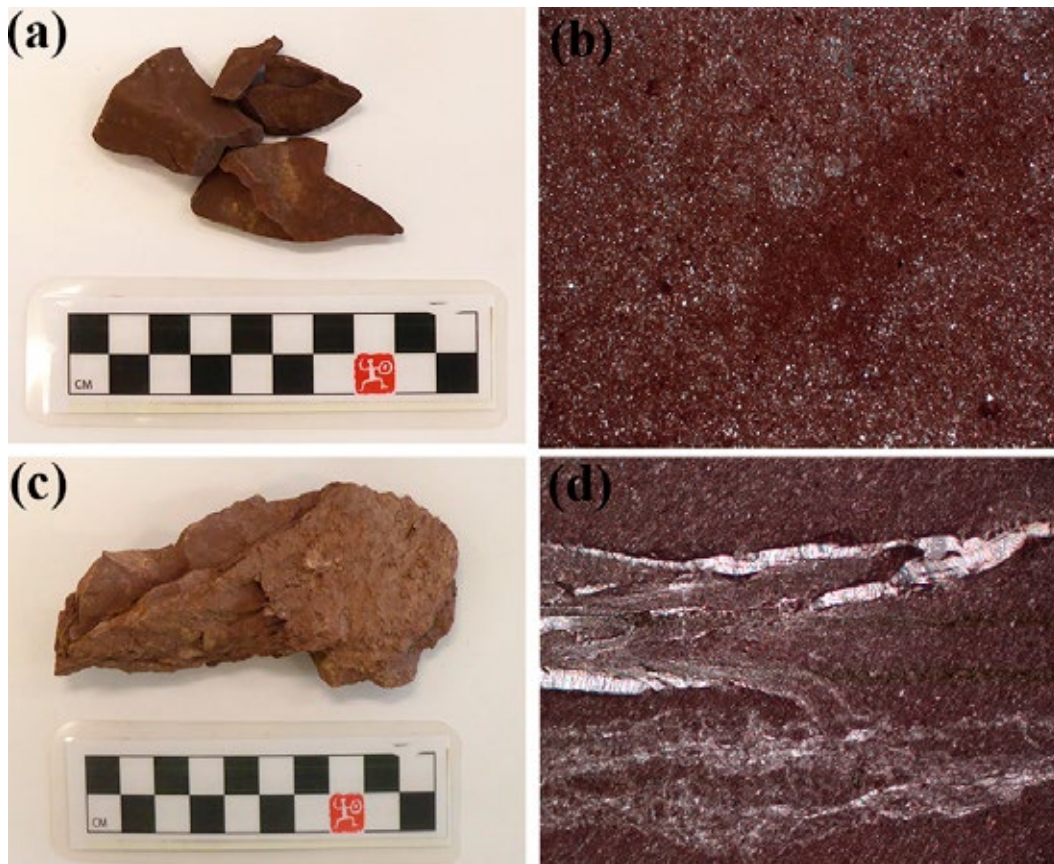


**Figure 2**  
Representative mudstones fragments of samples (a) AM2 and (c) AM4 and (b & d) microphotographs of the same samples respectively

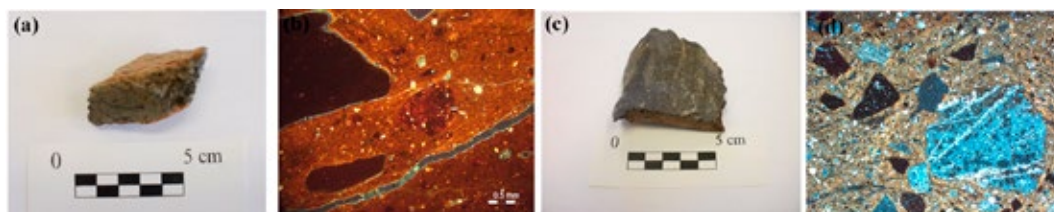


**Figure 3**  
Pottery samples (a) H08-02 and (c) H10-29 and (b & d) microphotographs of the same samples respectively

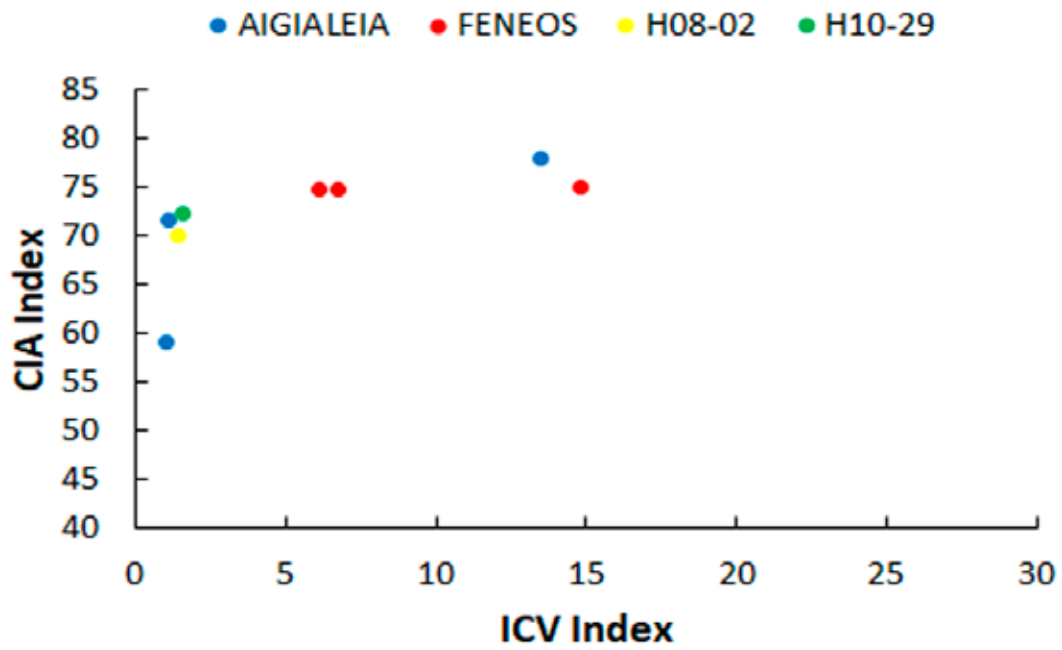


Figure 4  
 Plot of the average values of CIA index vs ICV index for all the studied samples. Aigialeia and Feneos: rock samples; H08-02 and H10-29: ceramic samples

# THE EFFECT OF THE MIXING TECHNIQUE ON THE MECHANICAL AND MICROSTRUCTURAL PROPERTIES OF A GEOPOLYMER-STABILIZED SOIL

Chami D., Cuccurullo A., Nazzari M., Gerard P.  
Excite TNA project ID: EXCITE\_C3\_2023\_06- MEGSS

Nowadays, geopolymer soil stabilization has become a focal point of interest for researchers due to its potential as an environmentally sustainable alternative to conventional chemical stabilization materials. Geopolymers are formed through a chemical reaction between a silica and alumina source and an activator. Geopolymer soil stabilization can be applied in two primary methods: one involves mixing the precursor with the soil before introducing the activator (technique 1), while the second consists of combining both geopolymer components before their addition to the soil (technique 2). It is worth noting that the choice of the mixing technique can significantly impact the progress of the reaction and subsequently influence the properties of the stabilized soil.

To investigate the effect of the mixing techniques, mechanical testing, such as unconfined compressive strength, has been conducted. The results of these tests showed that when the precursor content is relatively low, the choice of mixing technique has an important effect on the strength development of the stabilized soil. Conversely, with higher precursor content, the mechanical strength appears unaffected by the mixing technique.

To interpret these differences, scanning electron microscopy (SEM) analysis was carried out at INGV (Istituto Nazionale di Geofisica e Vulcanologia). When examining samples with lower precursor content prepared using technique 2, SEM images unveiled a less uniform structure and the presence of larger pores within the soil matrix. These structural irregularities directly correlate with the reduction in mechanical strength observed in these samples.

In contrast, when inspecting samples with higher precursor content, SEM images did not reveal any visual differences in the structural composition between the two mixing techniques. This explains the consistent mechanical strength observed in both cases, irrespective of the chosen mixing method.

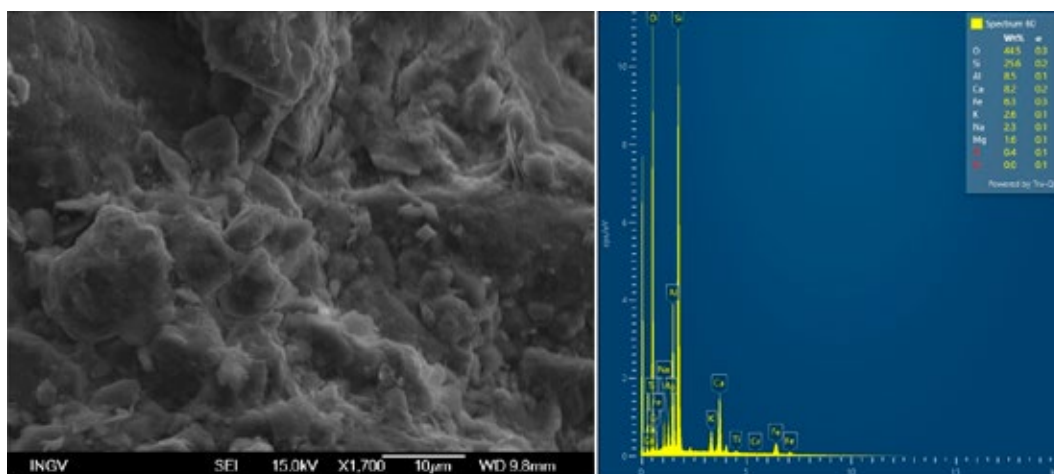


**Figure 1**  
SEM analysis showing for formation of the geopolymer phase ensuring the enhancement of the mechanical properties of the soil

## PETROCHEMICAL ANALYSES OF TEPHRA PRODUCTS FROM 2021 TAJOGAITE ERUPTION OF CUMBRE VIEJA (LA PALMA, CANARY ISLAND)

Rodriguez et al.

Excite TNA project ID: EXCITE\_C2\_2022\_77 – CUMBREVIEJACHEM\_2

The 2021 Tajogaite eruption of Cumbre Vieja volcano in La Palma, Canary Islands, has been described as an hybrid eruption given its complex description and classification, associated with multiple eruptive styles and multiple products. Multiple vents were formed throughout a ~1 km-long eruptive fissure, NW-SE oriented. Explosive activity, with almost continuous tephra emission, formed a complex pyroclastic cone and effusive activity, formed a wide lava flow field. This eruption has been considered as the most important in Europe during the last 75 years because of the significant amount of SO<sub>2</sub> released to the atmosphere and because of severe impact on the population and structures. This eruption has been also the longest of the historical eruptions on La Palma and caused the largest deposit footprint with 217.4 ± 6.6 million m<sup>3</sup> of lava flows and proximal fallout deposits over ~12 km<sup>2</sup> with ~20 million m<sup>3</sup> of tephra.

The main goal of this study was to obtain a comprehensive understanding of the eruptive activity and its implications for hazard assessment in the Canary Islands, as well as in other similar volcanic areas in the world. The previous TNA studies comprised component analysis by optical microscopy, morphological and textural analyses with the high-resolution Scanning Electron Microscopy (SEM) and the chemical composition of matrix glasses of the tephra samples analysed through the electron microprobe (EMP), the last two located at INGV-RM1.

From January 17 to 21, 2022, a INGV-INVOLCAN team carried out a field survey, aimed at mapping tephra deposits and collecting representative samples. Among more than 120 sections available, the stratigraphic section P72 with a total thickness of 184 cm, was chosen for its representativeness. Representative samples were collected at 11 different stratigraphic heights: from 0 to 26 cm, from 35 to 57 cm, from 57 to 62 cm, from 63 to 79 cm, from 79 to 80 cm, from 86 to 90 cm, from 90 to 95 cm, from 120 to 127 cm, from 143 to 144 cm, from 165 to 171 cm and from 171 to 178 cm. These samples were studied and compared with the control sites or tephra-collecting stations installed during all the period and picked up almost on a daily basis, in order to obtain a better picture of the evolution of the eruptive events.

The present TNA project was aimed at studying in detail the morphological and textural features of the different particles through the JEOL JSM-6500F (FEG-SEM), located at INGV-RM1, during 9 days of this Excite TNA access in May 2023. In synthesis, elongated, transparent and fluidal particles are characterised by elongated vesicles and a poor crystallinity, whereas blocky, shiny and opaque particles have rounded vesicles and abundant microlites. The detailed imaging work (Fig 1) carried on selected particles in the size range 8-16 μm from tephra samples from the main stratigraphic section of the eruption will allow us to determine particle and crystal size distributions which will allow to quantify crystallisation and magma fragmentation processes. These important constraints will be then integrated with data collected during previous TNA projects allowing to better interpret pre- to syn-eruptive processes. The larger and comprehensive study of petrochemical and textural analyses will be

crucial to understand and to reconstruct the stratigraphy of the deposits and establish the link between the physico-chemical evolution of the magmas that erupted and their physical behaviour during volcanic eruptions.

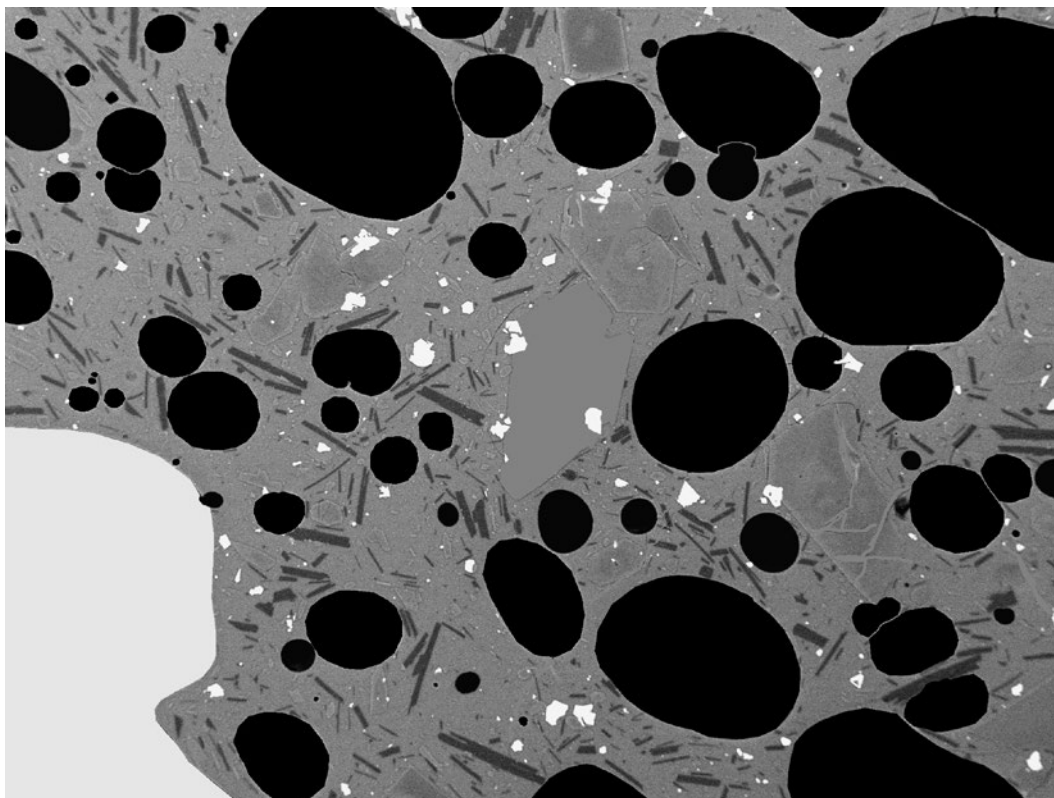


**Figure 1**  
Electronic image of the prepared sample from 57 to 62 cm height of the main stratigraphic section P72. Through the software ImageJ Fiji the image is prepared and left ready for analysis.

## 8.2 ROCK PHYSICS AND EARTHQUAKES

### FAULT CORE STRUCTURE AFFECTS FAULT SLIP DURING FLUID INJECTION: INSIGHTS FROM LABORATORY FRICTION EXPERIMENTS

Aretusini S., Cornelio C., Volpe G., Pozzi G., Spagnuolo E., Cocco M.

Natural faults when subjected to stimulation by fluid injection may result in slip acceleration because pore pressure (Pf) increases in the rock volumes inside and surrounding the fault zone leading to reduction of effective normal stress ( $\sigma_n'$ ). Slip mode ranges from aseismic creep to seismic ruptures defining a spectrum of fault-slip behavior. Fault stimulation experiments will be conducted in the Bedretto Underground Laboratory for Geosciences and Geoenergies (BULGG, Switzerland) to understand fault reactivation processes on a target well-identified fault zone, fully instrumented to monitor deformation and seismicity during both fluid injection and fault reactivation. This is envisioned in the ERC-Synergy FEAR (Fault Activation and Earthquake Rupture) project. In BULGG, the target fault zone has both a sub-centimetric fault core containing fault gouge and granite asperities in contact and other fractures in the surrounding rock volume. Therefore, it becomes important to define the frictional properties and slip mode of both gouges and bare rock surfaces taking advantage of a laboratory controlled experimental environment.

Fault stimulation by increasing Pf was simulated in laboratory following an injection protocol suitable for the BULGG fluid stimulation. Experiments were performed on the target fault gouge and on bare rock surfaces made of nearby Rotondo Granite. We employed a rotary shear apparatus (SHIVA) allowing the fluid injection under a controlled shear stress. First, we imposed the stresses measured at depth in the underground laboratory, halved due to apparatus limitations: 7.5 MPa  $\sigma_n'$ , 7.5 MPa confining pressure and 2.5 MPa Pf. Second, we imposed a slip rate of 10<sup>-5</sup> m/s for 0.01 m to have a reference texture. Third, we applied a shear stress so that an equivalent slip tendency of 0.35 (equal to the one measured in the target fault) is achieved (ca. 2.7 MPa) keeping it constant. We then increased stepwise the pore fluid pressure by 0.1 MPa every 150 s. After fault slip initiation, the maximum allowed slip velocity was 0.1 m/s. Between each of the experimental stages, permeability and transmissivity were measured with the gradient or Pf oscillations methods.

In Figure 1 we show that reactivation occurs at lower Pf in bare rock surfaces (4.7 MPa) with respect to MC fault gouge (6.5 MPa), suggesting that the effective coefficient of friction, the ratio of shear stress and  $\sigma_n'$ , is larger in gouge (0.58) than in bare rock surfaces (0.49). Moreover, upon the application of last Pf step, reactivation is slower in fault gouge (150 s delay) with respect to bare rock surfaces (10 s delay), consistently with the lower hydraulic transmissivity measured for target fault gouge with respect to bare rock surfaces (i.e., 10<sup>-19</sup> vs 10<sup>-17</sup> m<sup>3</sup>). Our experiments also show that creep and dilatancy precede reactivation in fault gouge, whereas reactivation is sudden and not preceded by dilatancy in bare rock surfaces.

We suggest that well-oriented and smooth bare rock surfaces might be easily reactivated similarly to what is observed for fault gouge during fluid stimulation. Our data and observations will contribute to shed light on the mechanics of faults and induced earthquakes by fluid stimulation experiments.

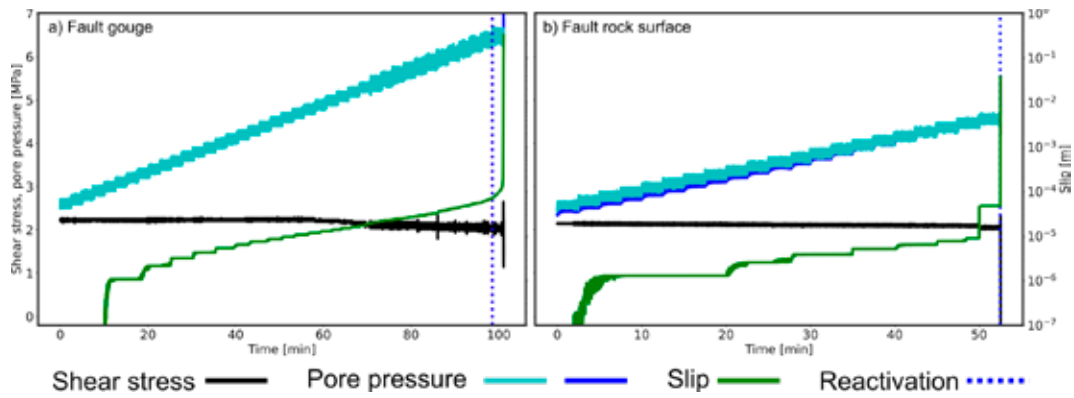


Figure 1

Injection stage of the experiments: from the first Pf step to the end of fast slip (reactivation, dotted blue line).

**a)** In fault gouge reactivation occurred at higher Pf (6.5 MPa) and is preceded by creep (i.e., progressive increase of slip with time). **b)** In fault rock surface reactivation occurred at lower Pf (4.7 MPa) and is not preceded by continuous creep, but occurs as a fast accelerating slip event.

## SEISMIC MIRROR-LIKE SURFACES IN BITUMINOUS DOLOSTONES (CENTRAL APENNINES, ITALY)

Chinello M., Schito A., Bowden S.A., Tesei T., Spagnuolo E., Aretusini S., Di Toro G.

Mirror-like Surfaces (MSs) are ultra-polished fault surfaces that reflect visible light, thanks to their nanometer-scale surface roughness. They are often found in seismogenic fault zones cutting limestones and dolostones. Both natural and experimentally-produced fault-related MSs have been described in spatial association with ultrafine matrix (grain size  $<10\mu\text{m}$ ), nanograins ( $<100\text{nm}$  in size), amorphous carbon, decomposition products of calcite/dolomite (i.e., portlandite, periclase), and larger but “truncated” clasts. However, the formation mechanism of MSs is still debated. Experiments show that MSs can develop both under seismic (slip rate  $\approx 1$  m/s) and sub-seismic (slip rate  $\approx 0.1\text{-}10$   $\mu\text{m/s}$ ) deformation conditions, involving various physical-chemical processes operating over a broad range of P-T conditions, strain, and strain rates.

To evaluate whether the MSs formed during the co-seismic (possibly associated with frictional heat pulses) or the inter-seismic (no heat pulses) phases where temperature might serve as a distinguishing factor, we assessed the thermal maturity of “bitumen” using biomarkers. We acquired data for natural and artificial MSs hosted within bituminous dolostones. We collected natural samples from faults with slip displacement from a few millimeters to a few meters, located in the Italian Central Apennines (Monte Camicia Thrust Zone, past burial depths up to  $\sim 3$  km). We obtained experimentally-produced MSs by deforming powdered bituminous dolostones in a rotary shear apparatus (SHIVA, INGV) at sub-seismic ( $V = 10^{-4}$  m/s) and seismic ( $V = 1\text{-}3$  m/s) slip rates for 1-2 m of slip, under room temperature and humidity conditions, and 20 MPa of normal stress.

We extracted solid bitumen of pre-oil window thermal maturity from the MSs and from the underlying slip zone of natural and artificial samples and we analyzed the bitumen using Gas Chromatography–Mass Spectrometry. We identified Steranes and other biomarkers based on relative retention time and measured peak heights to obtain thermal maturity parameters. By comparing different samples, changes in thermal maturity could be measured across slip zones bounded by the MS and possibly associated with frictional heat pulses during co-seismic slip.

Biomarker thermal maturity parameters are consistent with the immaturity of the host rock, which recorded a maximum ambient  $T < 100^\circ\text{C}$  during diagenesis. In the experimental MSs produced at seismic slip velocity, where frictional heat pulses reached  $T \sim 400^\circ\text{C}$ , thermal maturity of bitumen is higher than that of the entire slip zone and undeformed gouge. Higher thermal maturities were measured also in natural MSs but were not detected in the experimental MSs produced at sub-seismic slip velocity.

Microstructural analysis done previously revealed that these slip zones recorded the main phases of the seismic cycle, from rapid co-seismic slip to post/inter-seismic viscous flow and fault strength recovery. The results presented here (1) confirm this interpretation, (2) show that the frictional heat pulse associated with seismic slip can be recorded by biomarkers thermal maturity of bitumen trapped in the fault MSs, and (3) some natural MSs are associated with heat anomalies caused by seismic ruptures.

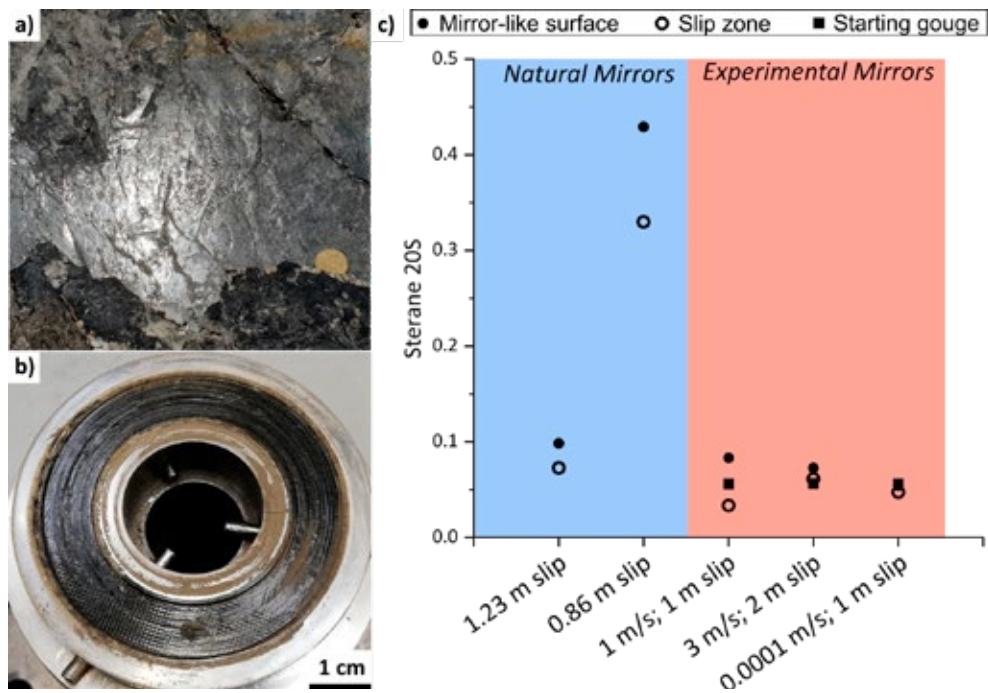


**Figure 1**

Natural and experimental Mirror-like Surfaces in bituminous dolostones and their thermal maturity. **a)** Natural Mirror-like Surface collected in the Monte Camicia Thrust Zone (Central Apennines, Italy), and **b)** experimental Mirror-like Surface obtained with SHIVA under room temperature and humidity conditions (1 m/s, 1 m of slip, 20 MPa normal stress). **c)** Thermal maturity of natural and experimental Mirror-like surfaces and associated slip zones, investigated with Sterane 20S biomarker.

## MIRROR-LIKE FAULT SURFACES IN CHERTS (ELBA ISLAND, ITALY)

Chinello M., Tesei T., Spagnuolo E., Pozzi G., Di Toro G.

Mirror-like surfaces (MSs) are ultra-polished fault surfaces that reflect visible light due to their low surface roughness (on the nm scale). Although common in nature across a wide variety of rock types (from carbonates to silicate rocks), their formation mechanism is still debated. Experiments in limestone gouges show that MSs can develop under both seismic and aseismic deformation conditions, involving various deformation mechanisms operating over a broad range of pressure-temperature (P-T) conditions, strain, and strain rates. MSs in quartz are often associated with nanoparticles, amorphous silica smeared on the fault surface, and melt patches.

We collected MS samples from normal and transtensive faults with measurable displacement (ranging from <1 mm to a few meters) hosted in Monte Alpe cherts on Elba Island (Italy), a geological formation mainly composed of microcrystalline quartz (80-90%) and clays (5-15%).

High-resolution microstructural investigations of MSs and the associated slip zones revealed that MSs are mainly composed of Fe and Ti-rich oxides and hydroxides, clay minerals, but also quartz. MSs from faults with about 1 m of displacement show different microstructures: in one case, the MS bounds a sintered-like slip zone made up of hundreds of nm-sized quartz clasts, and in another case, the MS is composed of euhedral quartz crystals (1-3  $\mu\text{m}$  in size) aligned in the slip direction and immersed in a clay matrix. At higher displacements (>1.5 m), the slip zone has multiple MSs associated with cataclastic layers, sometimes fragmented and boudinaged. All the slip zones are characterized by pervasive Fe-rich mineralizations, and sometimes MSs are opened and re-used by Fe-rich veins as discontinuities.

This study shows that these faults acted as a pathway for Fe-rich hydrothermal fluids associated with the Porto Azzurro pluton, and that the development of hydrothermal veins and MSs is intrinsically related. MSs present different features among each other and are made up of

(i) aligned euhedral crystals of quartz, or (ii) patches of Fe-oxides and -hydroxides embedded in a clay-rich matrix, and (iii) sintered-like quartz clasts. Higher displacement faults (>1 m) show sub-parallel MSs associated with cataclasites, suggesting multiple slip events recorded by these faults.

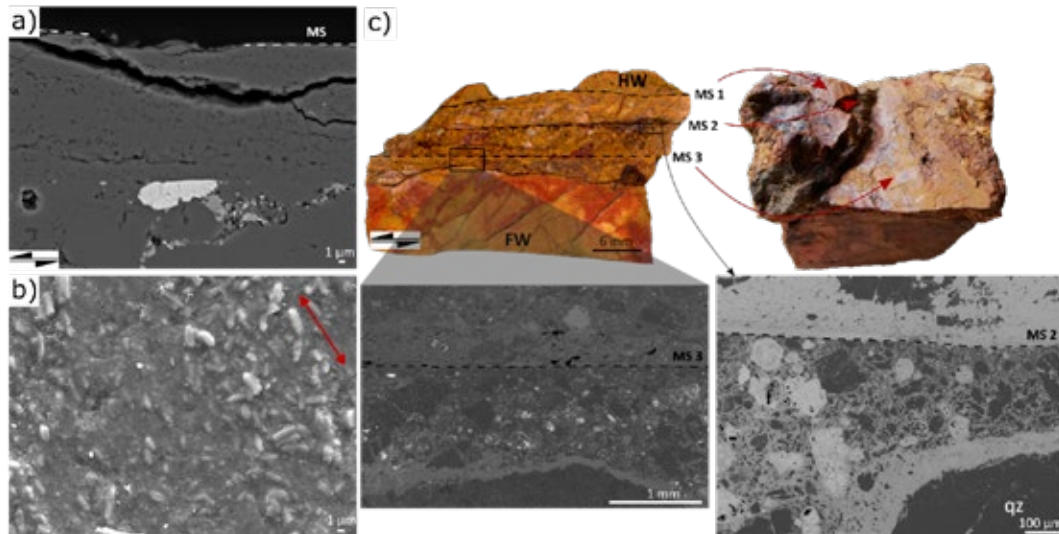


**Figure 1**

FESEM microstructures of slip zones and associated Mirror-like surface (MS) in cherts.

**a)** BSE image of a slip zone from a fault with ~1m of slip. The slip zone is made by sintered-like quartz clasts bounded by a MS. **b)** SE image of the MS from a fault with ~1m of slip composed by euhedral quartz crystals (1-3  $\mu\text{m}$  in size) aligned in the slip direction and immersed in a clay matrix. **c)** Thick section, hand sample, BSE and CL images of a slip zone and relative MS from a fault with 1.5-2 m of slip. In the slip zone there are multiple MSs also re-used as a discontinuity by an Fe-rich vein.

## DIFFERENCES IN BREAKDOWN WORK AND FRACTURE ENERGY IN SLIP WEAKENING CONSTITUTIVE LAWS)

Cornelio C., Murphy S., Spagnuolo E., Nielsen S., Cocco M.

Earthquakes are associated with the propagation of a dynamic rupture, which radiates elastic energy in the form of seismic waves. The generation of seismic radiation is related to the dynamic weakening of shear stress and stress drop. In modelling dynamic rupture, shear stress evolution is usually imposed by a constitutive law, such as the widely used slip weakening laws. According to these constitutive laws, shear stress evolves as a function of slip in each point of the rupturing fault, prescribing strength excess, stress drop and dynamic weakening.

Here, we compare two well-known slip weakening laws: namely, the classic Ida's (1972) and the Ohnaka's slip weakening laws. The former states that fault stress increases from the initial stress to the peak stress with zero slip and then decreases linearly from the peak value to a residual value over a slip distance  $D_c$  (dynamic weakening). The latter assumes that the initial stress hardening phase occurs over a non-negligible slip distance  $D_a$  and that the shear stress decrease from the peak value is non-linear. Ohnaka's law has been validated by numerous laboratory experiments. The evolution of shear stress with slip allows the estimation of the breakdown work  $W_b$ , i.e. the excess of work over a minimum stress level with slip from 0 to  $D_c$ .

We have collected data from high-velocity friction experiments to quantify yield, peak and residual stresses,  $D_a$  and  $D_c$  distances for bare-rock samples of Carrara Marble and Gabbro deformed under different experimental conditions (room humidity, vacuum, pressurized fluids) and normal stress (from 5 to 40 MPa) (Figure 1). The ratio  $D_a/D_c$  is much lower for Carrara Marble (0.015) than for Gabbro (0.12). We implemented Ohnaka's constitutive law in a 2D finite difference code for spontaneous dynamic ruptures characterized by a fault in a homogeneous elastic material. We perform simulations with the two different slip weakening laws. We kept  $D_c$  constant, and we compared the results of the simulations in terms of rupture style, rupture velocity, breakdown work, and cohesive zone size. As expected both laws produced crack-like ruptures. Moreover, compared to the linear slip weakening, the Ohnaka's law produces:

1. ~2 % higher rupture velocity;
2. breakdown work ( $W_b$ ) up to 60 % lower. Furthermore, dividing the breakdown work into the energy dissipated between the yield stress and the peak stress over the slip-distance  $D_a$  ( $W_{b\_a}$ ), we notice that  $W_{b\_a}$  can reach up to the 30% of the total  $W_b$  in case of Gabbro ( $D_a/D_c = 0.12$ ).
3. the size of the cohesive zone (defined as the portion of the fault in which the slip velocity is higher than zero and the stress is higher than its residual value) up to 50% larger.

Therefore, Ohnaka's law generates more energetic ruptures (i.e. faster rupture velocity and peak slip-rate) despite having a larger cohesive zone due to the lower breakdown energy dissipated during rupture propagation. We discuss our results in terms of the difference between breakdown highlighting the implications for dynamic rupture propagation and earthquake energy budget. We emphasize that common interpretations of the energy dissipated during rupture propagation are model-dependent.

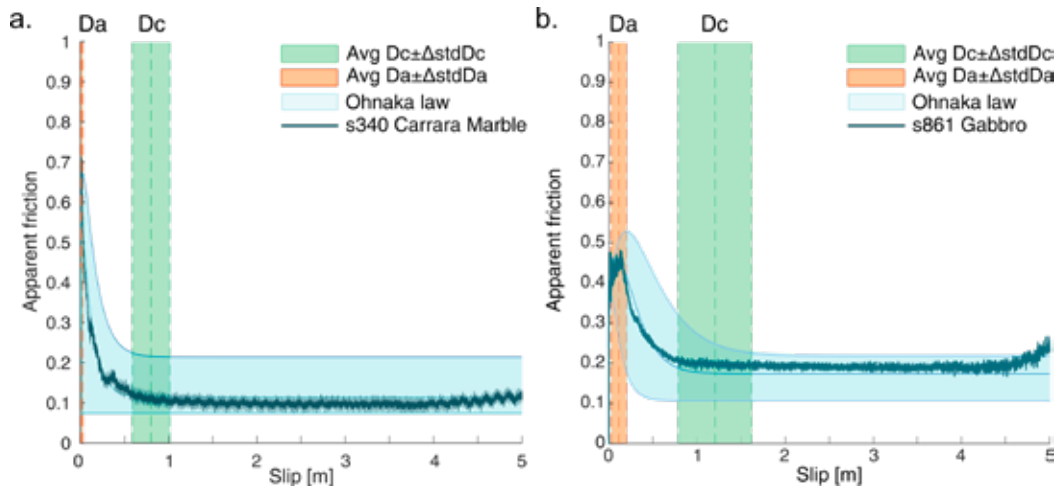


**Figure 1** Apparent friction versus slip with range of Ohnaka's friction law,  $D_a$  and  $D_c$  for **a)** Carrara marble **b)** Gabbro. The mean and standard deviation values of the parameters describing the Ohnaka's law ( $D_a$ ,  $D_c$  and peak friction and residual friction) are obtained by fitting 156 high velocity frictional experiments performed in SHIVA (97 on Carrara Marble and 59 on Gabbro). Experiments s340 (a) and s861 (b) are shown for comparison.

## MICROSTRUCTURAL ANALYSIS OF QUATERNARY FAULT CORES FROM NORTHERN CHILE

González Y., Pozzi G., González G., Spagnuolo E., Aretusini S., Nazzari M.  
Excite TNA project ID: EXCITE\_C3\_2023\_47- MAQF

In the northern Chilean forearc, the Atacama Fault System (AFS) evidences late Quaternary surface ruptures, qualifying as potentially active faults. However, the mechanical behavior of these Quaternary reactivations remains poorly understood. To solve this problem we collected samples from different faults cores and performed microstructural analysis on the recovered samples. Experiments performed at normal stress conditions from 10 to 125 MPa and slip velocities from 10  $\mu\text{m/s}$  to 1 m/s at the INGV - HPHT laboratory on the apparatuses BRAVA and SHIVA. The microstructural analysis was based on high-resolution Backscattered Electrons images obtained using the JSM-6500F Scanning Electron Microscope (SEM) located at INGV.

Sub-seismic velocity tests ( $v = 10 \mu\text{m/s}$ , Fig. 1a) indicate a close correlation between deformation styles and the mineralogical compositions and grain size of the fault gouges. Phyllosilicates-rich samples (>49%) predominantly revealed distributed deformation across the entire layer thickness and developed S-C fabric. This texture varied according to the phyllosilicate content and the grain size of the starting materials. Conversely, samples containing less than 38% of phyllosilicates, deformation is localized in principal slip zones (PSZs) with a thickness of a few tens of microns, characterized by an intense grain size reduction (Fig. 1c). These materials develop dominantly Y-B-P-R fabrics (Fig. 1a).

Samples deformed at seismic velocities ( $v = 1 \text{ m/s}$ , Fig. 1b) show localized deformation in PSZs with thickness of a few hundred microns, characterized by significant grain size reduction, low-angle foliation, and sub-rounded granular minerals (Fig. 1d). Deformation in samples with a higher percentage of fine materials tend to be more distributed than those with coarser grain sizes in the starting material (Fig. 1b).

Our analysis indicates combined operation of both ductile and brittle processes at low strain rates, such as cataclastic flow (Fig. 1c), kinking development, dilation cracks (Fig. 1c), boudinage development and foliation development (Fig 1c). Based on the velocity-strengthening behavior of the materials and the low frictional strength given by the complex composition of the fault gouges, typically rich in phyllosilicates, we propose viscous-frictional flow as the deformation mechanism operating during interseismic stages. However, during seismic slip, the microstructures can be overprinted at high strain rates by strain localisation in PSZs, intense grain size reduction, and development of intense phyllosilicate foliation. These results provide us with a clearer insight into the complexity of the reactivations occurring during the Quaternary in the AFS, and how their varied compositions and fabrics translate into different mechanical behaviors under various stress and slip velocity conditions controlled by the subduction seismic cycle.

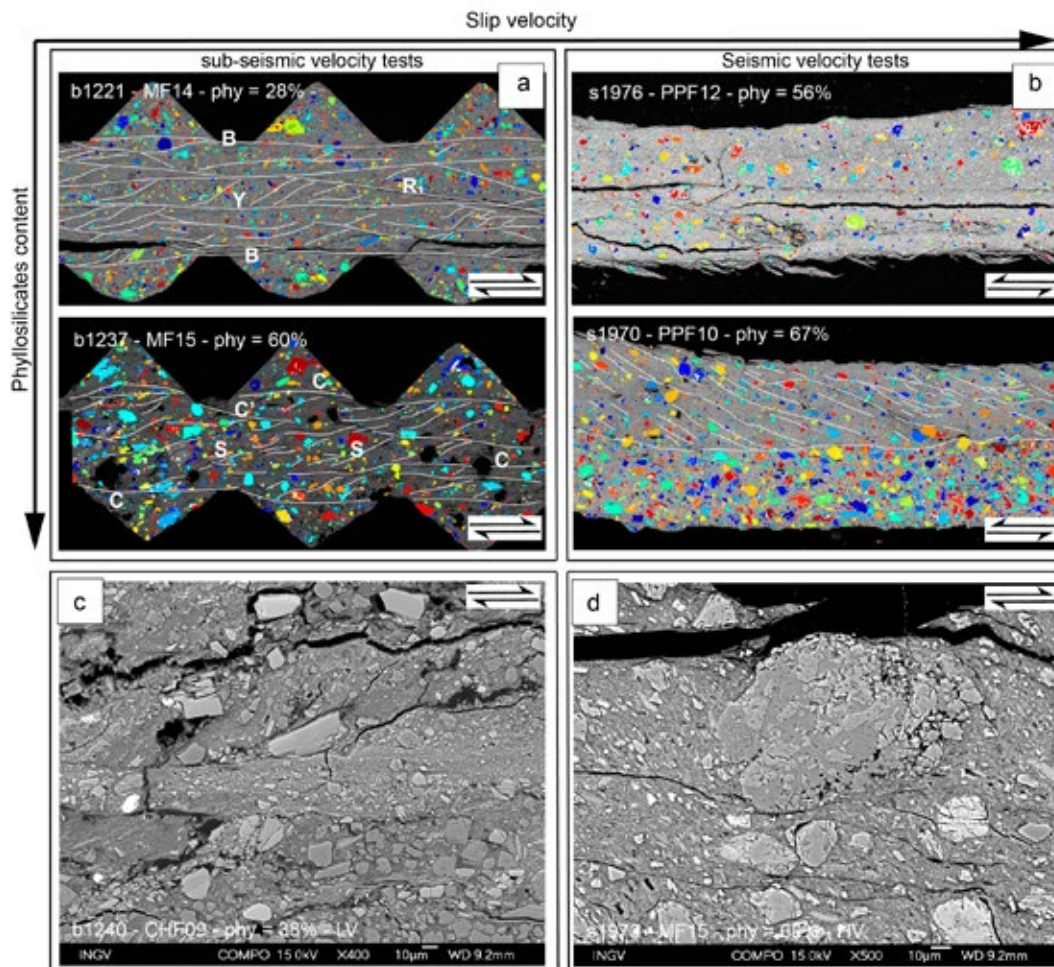


**Figure 1**

1a, b. Panoramic images of samples illustrating automated grain size analysis using MATLAB® to elucidate grain size and the porphyroclast/matrix relationship. (phy = phyllosilicate content, %).

**a)** Localized deformation observed in a granular-rich sample (top) and a phyllosilicate-rich sample exhibiting S-C texture (bottom). **b)** Partially homogeneous deformation observed across the entire layer in a matrix-rich sample (top) and localized deformation associated with significant grain size reduction (bottom). **c)** Intense grain size reduction accompanied by localized deformation, displaying Y and P fabrics. **d)** Coarse granular minerals with sub-rounded boundaries and phyllosilicates exhibiting low-angle foliation.

## **EXPLORING MICROSTRUCTURE AND PHYSICAL PROPERTIES OF ROCKS THROUGH TIME-RESOLVED (4D) X-RAY MICROTOMOGRAPHY IMAGING DURING IN-SITU EXPERIMENTS: APPLICATION TO THE CAMPI FLEGREI CALDERA**

Buono G., Pozzi G., Spagnuolo E., Pappalardo L.

Recent technological advances allow to characterize rocks in 3D and non-destructively in the digital rock physics framework. Rock samples are scanned by X-ray microtomography (micro-CT) to obtain digital rocks, then used to quantify microstructural parameters and estimate physical properties through numerical simulations. 3D imaging can be also performed during in-situ experiments to examine rock behaviour in 4D (Figure 1). Here we explored subsurface rocks of the Campi Flegrei caldera (CFc) extracted from 3-km-deep exploratory geothermal wells through an in-situ stage recently implemented at the X-ray micro-CT lab of the INGV-Vesuvius Observatory. The CFc is in an unrest phase since 2005, manifested by increasing ground uplift, seismicity and hydrothermal activity. The seismicity mainly involves the first 3 km below the hydrothermal site of Solfatara-Pisciarelli, where an intensifying heating and pressurization is inferred by gas geothermobarometers. Moreover, studies based on geodetic data inversion generally localize the deformation source in this sector of the caldera. In this frame, investigating the physical properties of these subsurface rocks can be valuable to define the source of the current and past unrest. In fact, they can largely affect local stress and strength, controlling volcano dynamics.

In this study we examined cores of caldera-filling rocks collected according to the most representative stratigraphic levels drilled from the CFc boreholes, dominated by tuffs alternating with minor lavas. Micro-CT investigations were combined with in-situ mechanical experiments (time resolved X-ray 4D imaging at room temperature and dry conditions) to characterize rock properties and link them with 3D microstructural changes. Particularly, an in-situ stage able to work up to 5 kN and 250 °C, under uniaxial compression or (direct/indirect) tension, and dry or partially/totally saturated conditions, was implemented at the X-ray micro-CT lab. Machine calibration was performed with both uniaxial compression and Brazilian tests using the Bi-Tri-Axial apparatus termed BRAVA and installed at INGV-Roma1. Samples have been selected from rocks having a wide range of transport and mechanical properties, and mainly on representative surface tuffs and lavas from CFc.

Our investigation of CFc well cores reveals a vertically heterogeneous layered crust characterized by rocks with different microstructure, physical properties and mechanical behaviour. Mineralogical assemblage of the well cores reflects different depth-dependent T-P conditions ranging from argillic alteration (150 °C) to thermometamorphism (350 °C). Combining preliminary data on elastic moduli obtained through Digital Image Correlation on micro-CT data with density values, P- and S-wave velocity was estimated. This data is in agreement with wave velocity variations measured using both P - and S- type piezoelectric crystals at the HT-HP lab and will be used to constrain 3D seismic tomographies at the crustal-scale in order to assemble a broader and clearer picture of the subvolcanic system at the CFc.

## Ongoing investigations: Crustal properties

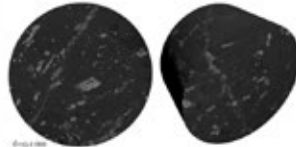
### 4D X-ray imaging during in-situ experiments



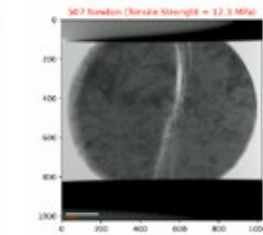
4D imaging during in-situ experiments at micro-CT lab of INGV-Vesuvius Observatory

- Force: up to 5 kN
- Mode: Compression and (direct/indirect) tension
- Motorspeed: 0.3 to 0.03 mm/min
- Temperature: up to +250°C
- Conditions: Dry and fully/partially saturated

#### In-situ indirect tensile test



0.04 mm



#### In-situ uniaxial compression test

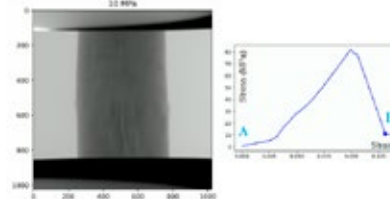
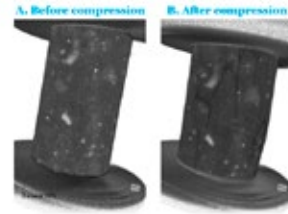
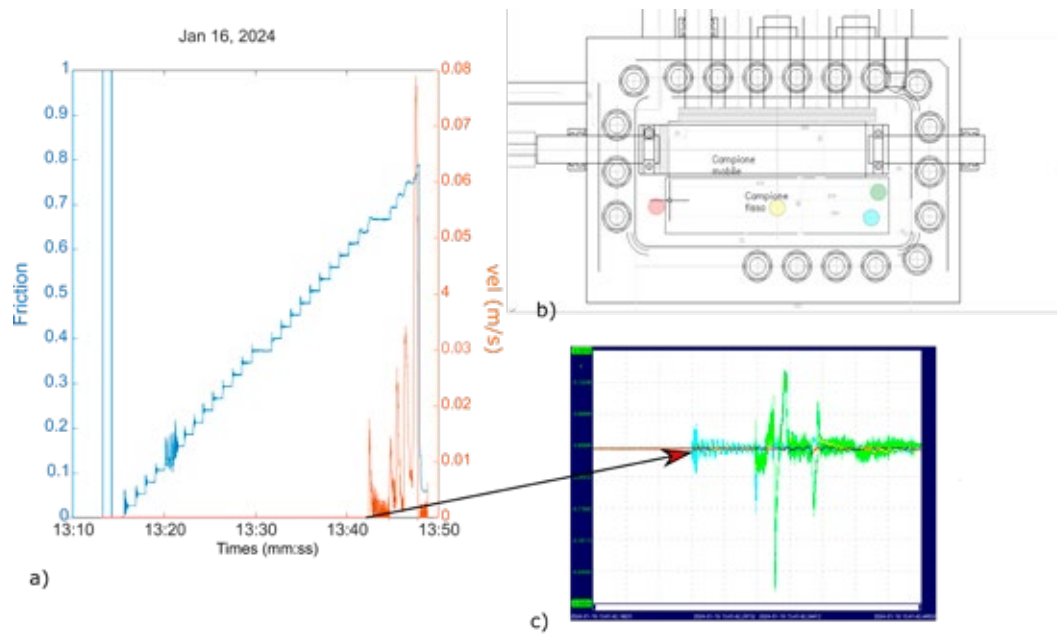


Figure 1 (left) Photograph of the 4D X-ray micro-CT scanner; (right) images of a sample tested under indirect tensile and uniaxial compression tests.

## A NOVEL APPARATUS TO STUDY THE MECHANO-CHEMICAL PROCESSES ACTIVE DURING THE NUCLEATION AND PROPAGATION OF EARTHQUAKES (MEERA).

Spagnuolo E., Cornelio C., Aretusini S., Pozzi G. , Cocco M., Selvadurai P., Di Stefano G.

We present a novel apparatus designed to investigate the mechanical and chemical processes active during the nucleation and the subsequent propagation of a seismic rupture. The earthquake is experimentally represented by the sudden frictional sliding of two blocks caused by either: i) the passage of a rupture front from a nearby seismogenic source at prescribed slip velocity, or ii) by the sudden release of strain energy accumulated during the slow (tectonic) loading stage preceding the nucleation of seismic rupture. M.E.E.R.A. (Mechanics of Earthquake and Extended Rupture Apparatus) is a biaxial horizontal machine installed at the laboratories of the Istituto Nazionale di Geofisica e Vulcanologia of Rome (Italy) thanks to a grant funded by the Italian Dipartimento di Protezione Civile. MEERA works on two blocks sized 320x80x50 mm<sup>3</sup> put in frictional contact under a normal load up to 30 MPa. Blocks can be either rocks or analogue materials. The normal load and the shear stress are supplied by 6 hydraulic piston cylinders. One piston applies the tangential force up to 150 kN and up to 40 mm/s of slip rate. The other 5 cylinders modulate the normal force on the 320 x 50 mm<sup>2</sup> contact surface. The 6 pistons are mounted on a rigid stainless-steel vessel that can be closed by a top built in plexiglass, which enables the environmental chamber for fluid confinement. MEERA is designed following the outline described in McLaskey and Yamashita (2017) and introduces three novelties: the control in displacement and displacement rate of the tangential piston up to 1kS/s; the environmental chamber; the rigid stainless-steel frame. MEERA is designed to study how the tectonic loading of a frictional interface composed of natural rocks determine the stress state and shear stress evolution governing seismogenic processes. To this end, we conducted a first series of experiments on cement, which is the closest analogous between previously tested PMME (plexiglass) and natural bare rocks. Calibration tests on cement reported  $V_p=3537$  m/s,  $V_s=2187$  m/s, whereas other elastic properties were available from @Geolite i.e. elastic modulus  $G=28$ GPa, Poisson coefficient  $\nu=0.2$ . Static models have been performed to study the initial distribution of forces along the fault surface and pressure films were used to map the initial real contact area. Figure 1 shows one friction test conducted on MEERA under shear-stress control with 7 MPa normal stress. Figure 1a shows the stepwise increase in shear stress resulting in an increase in friction (i.e. shear force / normal force, blue solid line) and the spontaneous evolution of slip rate (orange solid line). P-type broadband piezoelectric crystals (1 MHz) were installed on three out of eight faces of the stationary block (Figure 1b) to measure acoustic emissions. Acoustic emissions were recorded coeval to the increase in slip rate (Figure 1c, colors are referred to sensors colors in Figure 1b). All these measurements are used to constrain rupture nucleation processes and earthquake source parameters, including directivity and rupture velocity, the dynamics of seismic ruptures and the earthquake energy budget at different scales. We aim at comparing the laboratory observations and the signals collected by MEERA with those collected by the newly developed on-fault observatory of the ERC FEAR project in the Bedretto Underground Laboratory for Geosciences and Geoenergies (BULGG, Swiss Alps) to provide novel insights in earthquake mechanics.



**Figure 1**

Frictional tests in the horizontal biaxial machine MEERA: a) mechanical data showing the stepwise increase in shear stress resulting in an increase of friction (i.e. shear force / normal force, blue solid line) and the spontaneous evolution of slip rate (orange solid line) versus time. b) the sample assembly consisting of two blocks of cement put in frictional contact under a constant normal load and sheared. Colored circles represent the position of the four piezo crystals for acoustic sensing. c) one example of acoustic signals recorded at the four channels, color coded following the position of sensors in panel b).

## FRICIONAL INSTABILITIES IN CLAY ILLUMINATE THE ORIGIN OF SLOW EARTHQUAKES

Volpe G., Colletti C., Taddeucci J., Marone C., Pozzi G.

The shallowest regions of subduction megathrusts mainly deform aseismically, but they can sporadically host slow-slip events and tsunami earthquakes, thus representing a severe seismic hazard. However, the mechanisms behind these phenomena remain enigmatic because the frictional properties of shallow subduction zones, usually rich in clay, do not allow for earthquake slip according to standard friction theory. Here, we present new experimental data showing that clay-rich faults with bulk rate-strengthening behavior and null healing-rate, typically associated only with aseismic creep, can contemporaneously creep and nucleate slow-slip events. Our experiments document slow ruptures occurring within thin shear zones, driven by structural and stress heterogeneities developed on the experimental faults. We propose that bulk rate-strengthening frictional behavior promotes long-term aseismic creep whereas localized frictional shear allows slow rupture nucleation and quasi-dynamic propagation typical of rate-weakening behavior. Our results provide a new understanding of fault friction and illustrate the complex behavior of clay-rich faults, providing a new paradigm for interpretation of the spectrum of fault slip modes including slow-slip events and tsunami earthquakes.

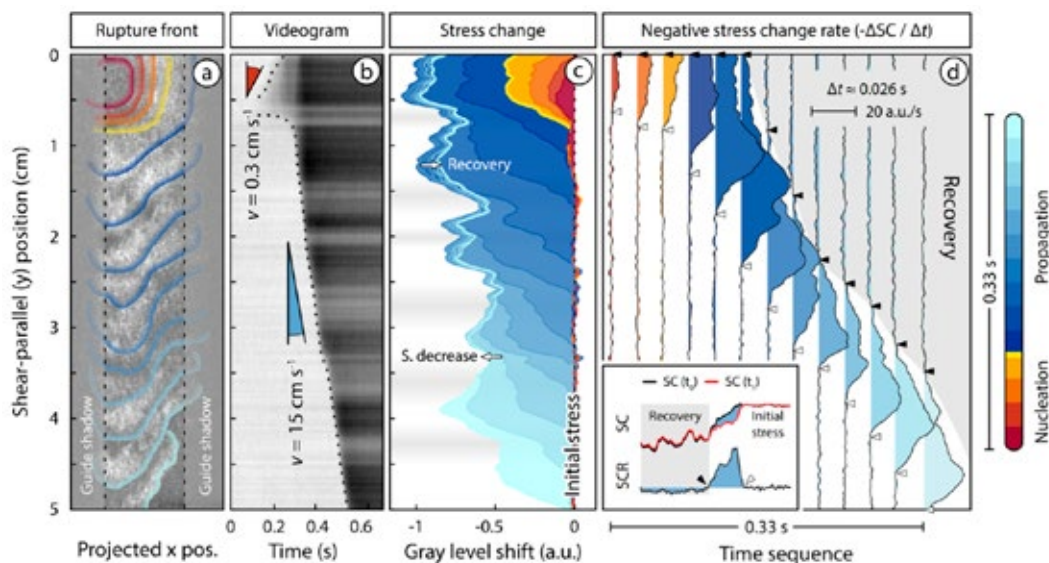


Figure 1

Spatial-temporal evolution of the rupture properties of a single stick-slip event imaged from video analysis: **a)** space-time evolution of the rupture front on the fault surface; **b)** space-time position of the rupture front within the vertical dashed lines in panel a; **c)** stress change and **d)** stress change rate during time highlighted by changes in reflectivity (grey level, arbitrary unit) proportional to the stress-field on fault. Inset of panel d) describes the evolution of stress change (SC) and stress change rate (SCR) along the fault for a time-window from  $t_0$  to  $t_1$ . The breakdown zone is restricted between the initial stress region (white arrow) and the recovery region (black arrow). Horizontal shades in panels b) and c) represent regions of the fault surface with stress heterogeneities caused by fault architecture.

## ALTERATION-CONTROLLED STRAIN LOCALIZATION AND STRUCTURAL SELF-SEALING IN THE CAPROCK OF A FOSSIL HYDROTHERMAL SYSTEM

Marchesini B., Pozzi G., Collettini C., Carminati E., Tesei T.

The mechanical and hydraulic behavior of faults in hydrothermal environments is strongly affected by fluid-rock interaction in the presence of hot and chemically aggressive fluids. This, in turn, affects our ability to model the properties of subsurface structures in reservoirs and caprocks to assess reservoir behavior and hazard during, for instance, geothermal exploitation. However, the combined effect of alteration on the mechanical and structural properties of faults in caprocks of geothermal reservoirs is severely underdocumented. We combined field structural observations (Fig. 1a) and friction experiments (Fig. 1b) in altered rocks from the caprock of a fossil hydrothermal system (Tolfa-Allumiere, Tuscany-Latium, Italy). We argue that fault weakening and strain localization is induced by mechanical comminution and hydrolytic alteration leading to enrichment in clay minerals along fault cores (Fig. a, FC3).

Argillic-altered rocks, rich in alunite and/or kaolinite, are much weaker (friction coefficient  $0.27 < \mu < 0.46$ , Fig. 1b) than the unaltered protolith (trachytes,  $\mu = 0.55$ , Fig. 1b) favoring the tectonic extension of the system. The enrichment and smearing of clays along fault cores also promote a 'combined conduit-barrier' fault behavior that may contribute to the efficiency of the caprock. This 'structural self-sealing' may guide the lateral flow of hydrothermal fluids, forcing the lateral migration of hydrolytic alteration, hence controlling the lateral growth of the caprock. Finally, the velocity-strengthening frictional behavior of alunite-kaolinite altered rocks may promote aseismic slip behavior of these faults. Our findings can be applied for the structural-mechanical characterization of faults in horizontal seals, which is crucial for geo-energies exploitation.

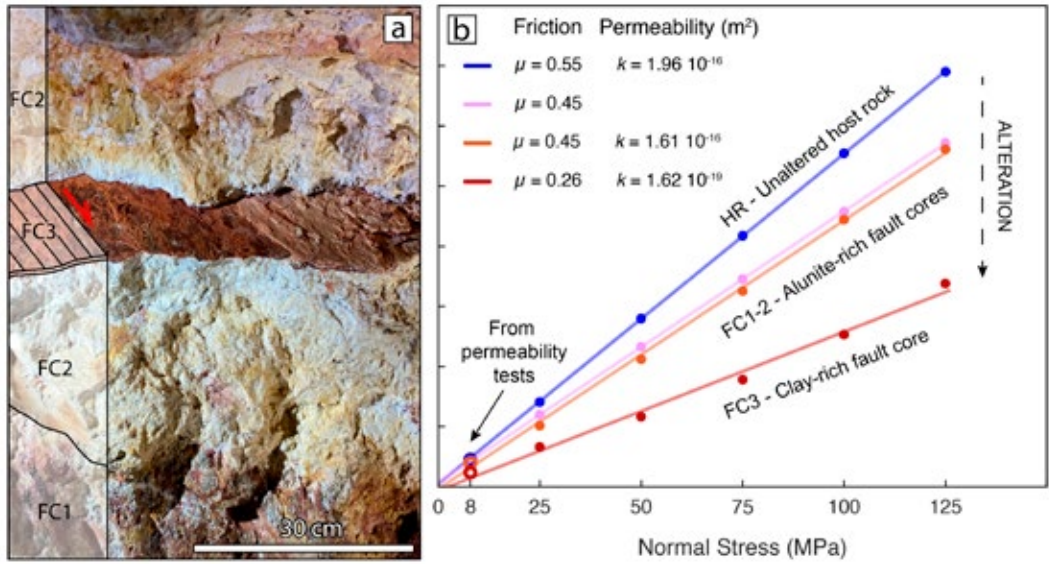


**Figure 1**  
 a) Example of fault core (red arrow indicates the shear sense) characterized by increasing alteration of the rocks from facies FC1 to FC2. b) Mechanical results of the friction (Mohr space) and permeability tests performed on selected rock samples.

## DEFORMATION STYLES IN MICA SINGLE CRYSTALS

Pozzi G., Tesei T., Collettini C.

Micas, a large group of phyllosilicate minerals characterized by a layered structure with perfect cleavage planes. Commonly found in both ductile (mylonites) and brittle (fault) shear zones, they play a pivotal role in controlling the rheology of crustal rocks due to their unique mechanical properties. Due to their frictional weakness and preferential alignment of the platelets during the formation of deformation fabrics, micas can dramatically decrease the shear resistance of faults and mylonites.

To better explore the mechanical properties of micas and associated deformation mechanisms, we have selected single large crystals (5x5 cm) devoid of inclusions, strained volumes, and cleaved planes to be tested with shear experiments at different normal stress (10, 30, 60, 120, and 240 MPa) and sliding velocities (0.1, 1, and 10  $\mu\text{m s}^{-1}$ ).

For each experiment, two trimmed crystals of average thickness 0.4 mm were placed on each flat side of a metal sample holder, assembled in double-direct shear configuration. The crystals were secured to the holder using epoxy resin on both sides to force deformation within the crystal and not the block-mica interface. The mounted holder was placed in the biaxial apparatus BRAVA (INGV, Rome), brought to the target normal stress (perpendicular to the shear plane), and moved to accommodate up to 4 mm of relative slip. We measured the evolution of shear stress with time, until the achievement of steady-state conditions. The steady-state shear stress is reported in function of the normal stress and slip velocity in a Mohr space (Fig. 1a).

The mechanical data shows that, at dry conditions, the shear strength of the mica crystals is always positively correlated with sliding velocity and presents a linear relationship with normal stress up to 60 MPa, which yields a friction coefficient  $\mu = 0.23-0.29$ . Above 120 MPa, the shear resistance of the crystals is no more dependent on normal stress. The mechanical results are matched by a change in deformation style. Below 60 MPa of normal stress, micas tend to delaminate and fold close to the sample boundary to produce a thin layer of gouge (Fig. 1b). At high normal stress (e.g., 240 MPa), deformation is distributed across the entire crystal thickness, and we do not observe the formation of cataclastic products (Fig.1d).

Supported by further SEM investigation, we infer that the principal deformation mechanism at all stresses is related to delamination of mica platelets and folding along cleavage planes, which produces work against the normal stress. During this process, if the local folding reaches a critical curvature radius before the delamination is propagated across the entire crystal, the lamellae buckle and break to form cataclastic products, which slide frictionally. If the folding is inhibited by the high normal stress, the fold propagates as a ripple, relieving the stored elastic strain at the fold edges by delamination and healing (ripplocation). This process is a function of the stress state at the ripple edges and correlates with the maximum adhesion and shear resistance of the mica, which are not normal-stress dependent.

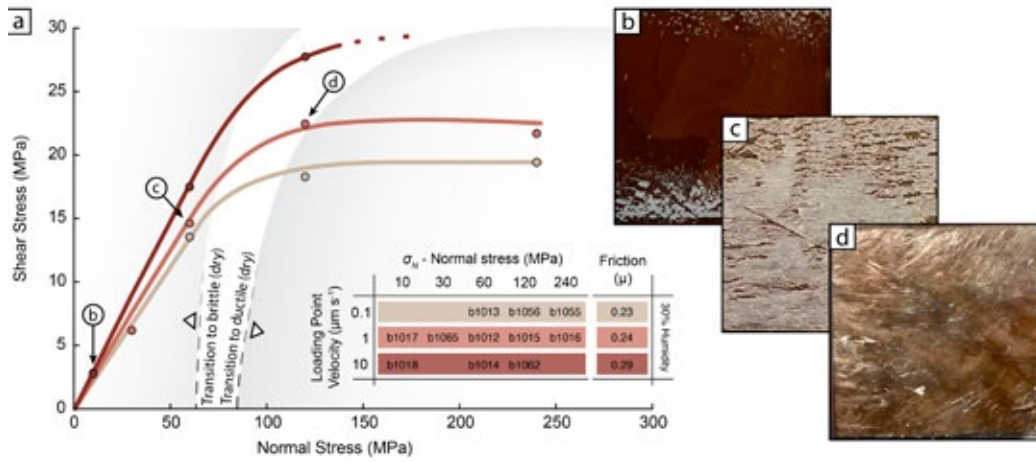


**Figure 1**  
 a) Mohr space showing the values of steady state shear stress as function of the normal stress, the lines indicate the inferred envelope at different sliding velocities. **b-d)** top view of the mica crystals after deformation, the sense of shear is top to the south.

## 8.3 TECHNOLOGY

### ASH SAMPLER

Vallocchia M., Di Stefano G., Iarocci A., Mari M., Spinelli G.

As part of the UNO Departmental project, the LNTS laboratory had the task of designing and developing the automatic ash sampler (fig. 1). The design and testing activity of the control and drive board (fig. 2a) was completed in the first half of 2023, which allowed the sampler to be installed on the island of Stromboli last July and the sampling activity to begin.

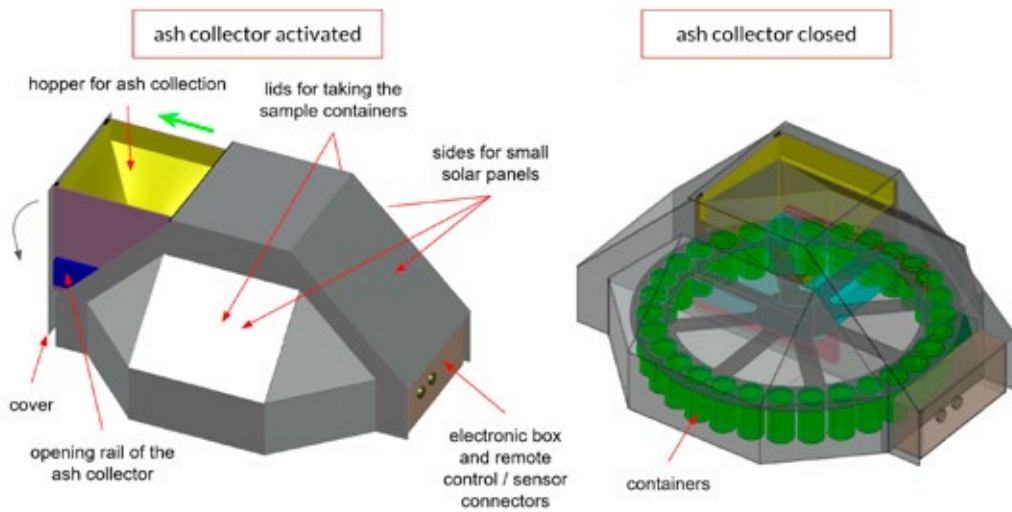


Figure 1  
The ash sampler sketch

The main components of the control and drive board are:

- Microcontroller board based on the Arduino platform;
- Stepper motor (12V, 0.31 A/phase, Holding Torque 0.518 Nm);
- Stepper Motor Driver;
- DC/DC converters (one generates 5V for the electronics, the other generates 6V for the motor).

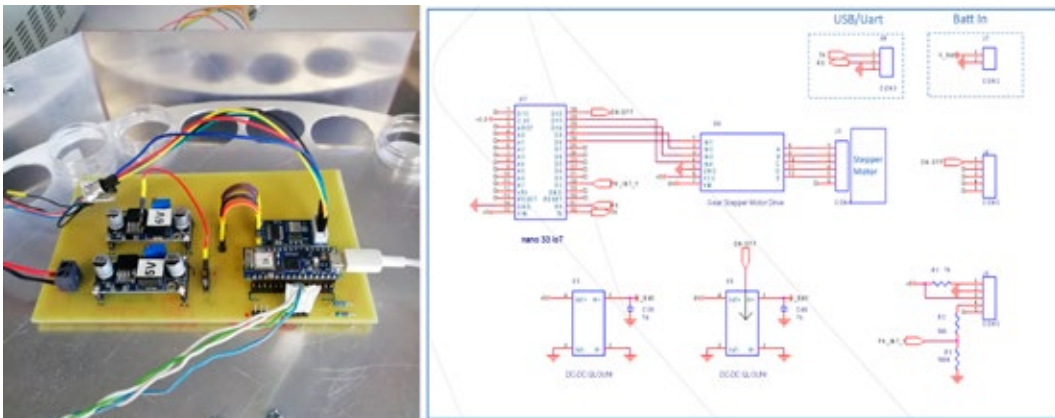


Figure 2  
The control & drive board

The board electrical diagram

The microcontroller board manages the following I/O:

- PhotoInterrupter (initialization); [I]
- On/Off 6V DC/DC converter (sleep mode); [O]
- UART/USB (PC connection); [I/O].

In order to limit absorption, the microcontroller sends a sleep mode command to the second DC/DC converter when the sampler is not rotating.

The following flowchart (fig. 3) illustrates the software architecture of the ash sampler.

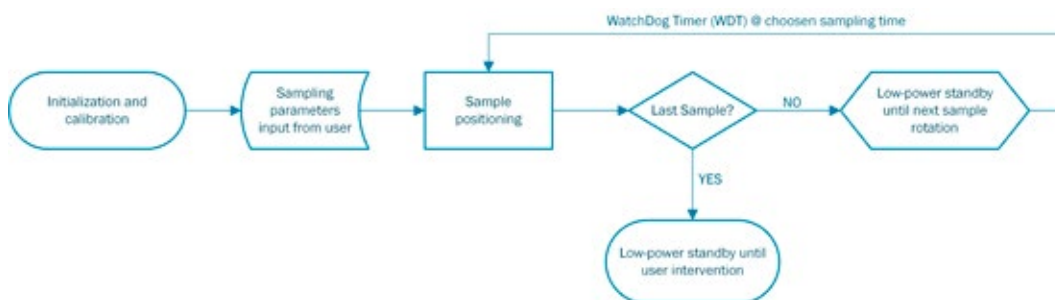


**Figure 3**  
The software architecture flowchart

When turned on, the sampler carries out the initialization procedure positioning the plate containing the tubes in a reference point, detected by a photo-switch in correspondence with a notch present on a concentric disk integral with the sampler plate.

The parameters required by the user to configure the sampler are listed below:

- Current time: set due to lack of time reference;
- Alarm time set: time of day at which the tube plate will rotate;
- Current sample: starting tube position n (default 1).

After the user confirms parameters via terminal using the USB/UART connection, the sampler places the chosen tube n under the funnel and switches to standby mode (low-power).

When alarm time occurs the sampler wakes up from standby mode and rotates the plate to the next tube position, unless it has already reached the last tube ( $n = 30$ ). Then, the next plate rotation will take place after 24 hours at the same time.

Each plate rotation will take place after 24 hours at the same time.

The future developments of the sampler will go in the direction of increasing energy autonomy (using solar panels), making the funnel tray automatic, and equipping it with a Wi-Fi connection.

The automatic funnel tray will allow to:

- Close it automatically in case of external parameters (e.g. rain, wind, etc.);
- Program the sampling duration less than 24h.
- The wifi connection will allow to have:
- Automatic time setting from the network (NTP);
- Simpler onsite programming;
- Periodic State Of Health (SOH) messages;
- Remote programming and SOH on demand;
- WEB page or Telegram BOT as user interface.

## SENSOR FOR THE DETECTION OF INFRASOUND GENERATED BY SEISMIC EVENTS

Sabatini D., Romeo G., Spinelli G., Pongetti F.

In order to increase his detecting capability, INGV decided to develop a sensor prototype for the detection and the measurement of atmospheric pressure waves in the infrasonic frequency band.

The aim is to include the sensor in the national seismic network so that pressure measurement produced by infrasound associated with seismic phenomena can be included among the observable quantities. Therefore, the implementation of such sensors would make the detection network a multi-parametric network and this is an objective of fundamental importance to allow a more accurate and in-depth study of natural geological events.

Davide Sabatini, student of Electronic Engineering at Roma Tre University, graduated in October 2023 arguing a thesis, in collaboration with INGV, focused on the realization of that sensor prototype.

The prototype is based on the measurement of the displacement, via an LVDT position sensor, of the membrane of a speaker, in particular a subwoofer since the frequency band considered goes from 0.001 to 20 Hz.

The LVDT, linear variable displacement transformer, is composed of three wire windings (one primary and two secondary) surrounding a core of magnetically permeable material. The variation in the position of the core with respect to the windings modifies the electromagnetic coupling or the mutual inductance that occurs between the windings and is transformed in an electric signal.

In order to carry out the displacement measurement, it is necessary for the LVDT core to physically follow the membrane's displacement. A possible solution to overcome this connection problem is the use of a cylindrical plastic "cap" that follows the profile of the central cap of the speaker membrane. This allows the core to be screwed into the center of the cap securely, figure 1 left.



Figure 1

The winding part of the LVDT is suspended via an aluminum frame constructed to suspend the hollow cylinder containing the windings above the cap, figure 1 right.

The signal produced by the LVDT cannot be used directly, but must be processed by an electronic signal conditioning board which provides a DC signal proportional to the displacement of the LVDT core.

The second board we introduce is an audio amplifier whose task is to drive the subwoofer that generates the pressure waves (simulating in this way the infrasonic seismic wave) used in the calibration of the prototype. At the input of this audio amplifier there is the output signal of a waveform generator.

To provide the different voltages that power the two previous boards, the sensor prototype is composed of two more boards: a mains voltage transformer and a double-half-wave diode bridge rectifier. The transformer has the task of decoupling the supply voltage, which has an RMS value of 220V and a frequency of 50Hz in Europe, from the mains and reducing its amplitude, while the double half-wave rectifier in addition to the leveling capacitors have the task of linearizing the alternating voltage making it an "almost continuous" voltage.

The four boards were placed inside a rack.

To obtain an infrasonic pressure wave generator we realized an acoustic chamber inserting the subwoofer inside the structure shown in the figure 2 with the rack containing the four boards.



Figure 2

Figure 3 shows the correspondence between the infrasonic signal (red) generated by the subwoofer membrane (with frequency from left to right: 1Hz, 2Hz, 0.5Hz) and the corresponding signal (blue) produced by the LVDT proportional to the displacement of the membrane.



Figure 3

## UPDATE FOR THE ACQUISITION OF A SIGNAL PRODUCED BY AN ACCELEROMETER

Romeo G., Spinelli G.

An accelerometer measures the linear acceleration along the three directions of space and, therefore, simultaneously generates 3 signals, each representing the acceleration according to the corresponding reference axis. We decided to update the filter created in 2022 for Roma Tre University to be able to study the acceleration along the x, y, z axes simultaneously,

The motherboard, shown in figure 1 with a single filter, can house three low-pass filters to simultaneously filter the three signals produced by the accelerometer and provide the complete filtered signal. The same picture shows how the three filters, which are identical, respond, apart from a gain factor to be adjusted appropriately, in an identical way to the same incoming square wave.



Figure 1

The motherboard was made in Eurocard format, a European standard format for printed circuit boards with modular height and depth. Our motherboard, 100 mm high and 160 mm deep, is placed in a standardized structure called a subrack. The subrack contains a series of rails, two per board positioned at the top and bottom, in which each board can slide and



Figure 2

remain upright, like a book on a shelf. Figure 2 gives us a top and a front image of the subrack.

There are 6 faceplates because, in order to improve the quality of the research, the researchers of Roma Tre University asked us to work simultaneously with five accelerometers. The faceplate on the left is the one related to the subrack power board and is not accessible from the outside. On each of the other five faceplates, there are six holes and an 8-pin circular connector. Through the holes we can adjust the trimmers, 2 per filter, which control the gain and offset for each x, y, z component of the accelerometer associated with the board. Through this 8-pin circular connector are transmitted the signals produced by the accelerometer before and after being processed by the filter, besides the power and the ground for the board.

To record fifteen signals, three for each card, we chose PicoLog 1216, a multi-channel data acquisition system which has 16 channels and a resolution of 12 bits; it is connected via terminal block to the DB25 connector fixed on the back of the subrack. Figure 3 also shows the representation of the acceleration on the three axes recorded by the second accelerometer. The representation on channels 4, 5 and 6 is active, while on the other channels it is deactivated. Obviously it is possible to activate all 15 channels at the same time to have a contemporary representation of the signals produced by the accelerometers.

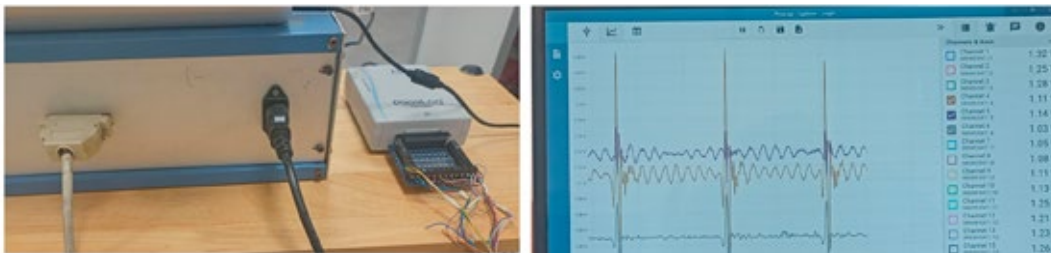


Figure 3

Experiment setup and experimental results are shown in the next figure.

The five accelerometers are positioned on a foam rubber wedge with an elastic angle of  $10^\circ$  resting on a plastic sheet. This wedge reproduces the elastic behavior of the upper plate in a subduction margin. At the contact between the wedge and the sheet, different materials are positioned to simulate a frictionally heterogeneous subduction interface (the so-called megathrust). Specifically, rice patches simulate the frictional behavior of seismic asperities, capable of generating earthquakes, surrounded by areas composed of frictionally stable sand. A pulley driven by a motor induces a constant displacement of the sheet: near the rice patches, the foam wedge is frictionally coupled, accumulating elastic stress during periods of interseismic loading. When the interface shear stress is exceeded, a frictional instability, i.e. a laboratory earthquake, is generated, releasing the accumulated elastic energy. The accelerations produced are recorded and represented as seen in figure 4.20. Such accelerations allow, for example, to localize laboratory earthquakes along the interface and trace their space-time evolution.

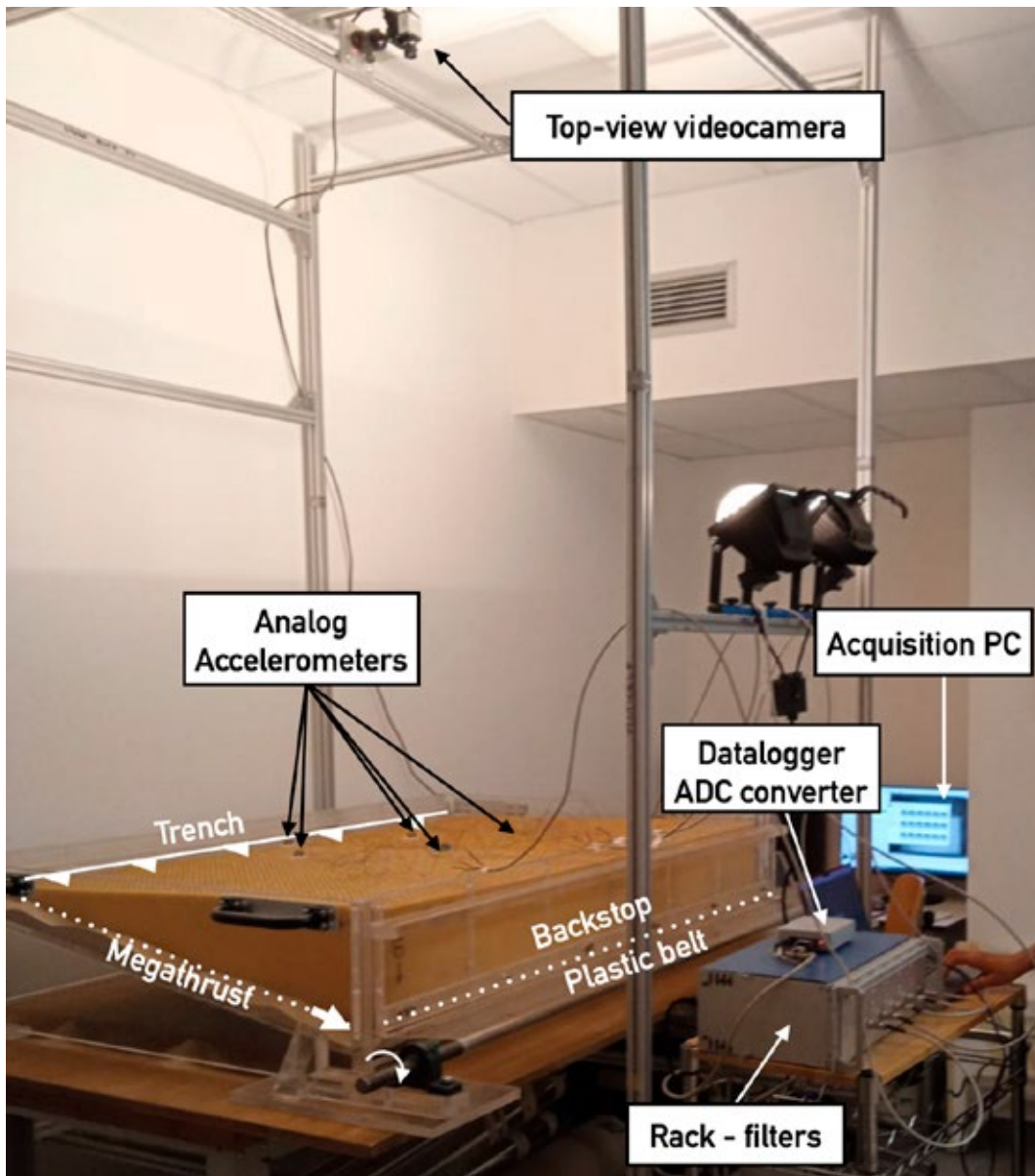


Figure 4

## DESIGN AND 3-D PRINT OF MECHANICAL PARTS IN ELECTRONIC LABORATORY

Pongetti F.

The wide availability on the market of three-dimensional printers and computer graphics design programs allows an electronics laboratory to carry out the design of simple mechanical parts used for the creation of prototypes. The main advantages (just a few) are that the necessary components can be made exactly as desired and produced in a short time; furthermore the cost is low and any modification can be made almost immediately. The limits are mainly due to the characteristics of the material, which in general is not very strong. Below are photographs of simple components designed and made for prototypes of electronic instruments or equipment, or even to create demonstrators for educational purposes at exhibitions or fairs. Another suggestive use is the possibility of creating molds for gaskets or other components, made starting from a liquid filler. The parts in pictures have been printed using a PRUSA I3, a very small and cheap printer (other models are available in LNTS lab.) that is fed by PLA wire material (some kind of plastic). Stronger feeding materials have been recently developed for more professional printers that enable designers to 3D print parts that are currently CNC machined.



**Figure 1**  
Simulator of a satellite orbiting around the earth for educational use; movement mechanism test.



**Figure 2**  
Support flanges for an aluminum bar used as a heat sink in a Peltier-cell thermal system

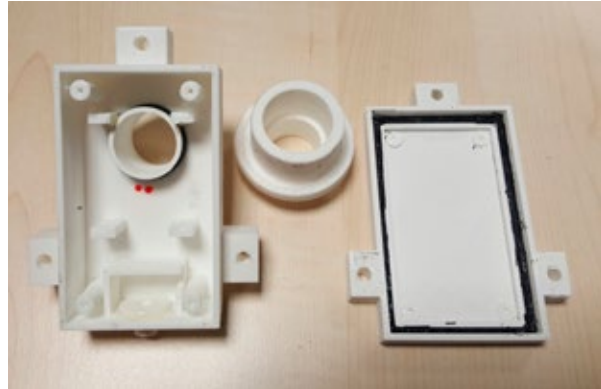


**Figure 3**  
Waterproof box to house an environmental sensor. Composed of various parts that can be assembled after printing. Silicone seals are extruded directly into grooves on the component.



**Figure 4**  
Extremely enlarged reproduction of a marine organism (foraminifera) for educational purposes.

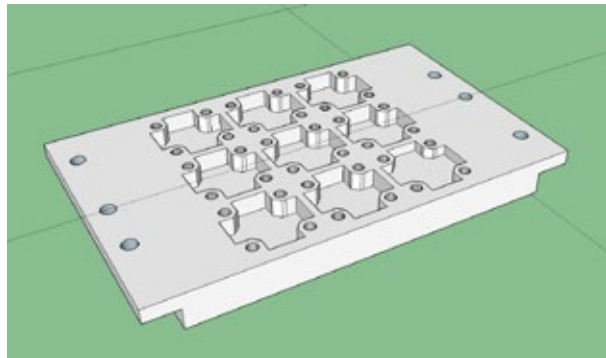


**Figure 5**  
CAD drawing of a mechanical support for small electronic sensors. Complex shapes are extremely labor-intensive for the machine shop, but not for the 3-d printer.

C H A P T E R N I N E

SEMINARS  
and TEACHING

## SEMINARS

Spagnuolo E. | **Strong or Weak? Achievements, limitations and perspectives on the study of frictional strength of sediments in experimental fault gouges** | ERC TECTONIC-FEAR, on line zoom meetings March 14th, 2023

Cocco E. | **Energy dissipation during earthquakes: spatial scale and model-dependent interpretations** | May 8 2023, ERC-TECTONIC-FEAR, online zoom meetings.

Spagnuolo E. | **Weak or strong? Slip behavior, stress and strength of the incoming sediments at the Sumatra subduction zone** | EarthFlows 2023, 14-15 June 2024, Oslo, Norvegia

Spina, L. | **Il vulcano in laboratorio: introduzione alla vulcanologia sperimentale e casi studio** Università di Catania, on line meeting on November 28th, 2023

## TRAINING

Catanese S. | **Stage | Analisi della sedimentazione di piroclasti (ceneri e lapilli fini) da immagini ad alta velocità** | Supervisors : Taddeucci J., INGV, Palladino D.M., Sapienza University of Rome

## THESIS

1. Amodio A. | **Master Thesis | Caratterizzazione delle proprietà dell'attrito delle serpentiniti ricche in Antigorite** | Supervisors : Collettini C., Sapienza University of Rome, Pozzi G., INGV
2. Califano E. | **Master Thesis | Experimental degassing of trace metals from a shoshonitic basalt eruption at Stromboli volcano** | Supervisors: Mollo. S. - Sapienza University of Rome; Moschini P. - INGV
3. Chiesurin A. | **Master Thesis | Mineralogical, geochemical and microstructural characterization of fault rocks from the Koyna deep drilling project (India)** | Supervisors: Di Toro G., Padua University; Spagnuolo E. INGV
4. Clivet F. | **Master Thesis | Friction of representative rocks hosting the seismicity of the Northern and Central Apennines** | Supervisors: Doglioni. C. - INGV, Sapienza University of Rome; Pozzi G. - INGV
5. Moltoni R. | **Master Thesis | Caratterizzazione di rocce di faglia sperimentali** | Supervisors: Collettini C. and Ruggieri R. - Sapienza University of Rome |
6. Zanella G. | **Master thesis internship - Institut de Physique du Globe de Paris | Imaging techniques for the parametrization and monitoring of volcanic eruptions** | Supervisors: Del Bello E., INGV

## PhD

1. Benà E. | **Tectonic control on enhanced geogenic radon as a first order factor in radon hazard assessment** | Padua University | Supervisors: Ciotoli G., Sassi R., CNR, Spagnuolo E., INGV
2. Biensan C. | **Linking styles of active magma degassing with fragmentation dynamics for mafic magmas: a multiparametric approach** | Sapienza University of Rome  
Supervisors: Palladino D. – Sapienza Università di Roma, Taddeucci J. - INGV
3. Califano E. | **Decoding the physico-chemical conditions of magmas triggering the 2022 eruption of Hunga Tonga–Hunga Ha’apai** | Supervisors: Brenna M. - University of Otago | Pontesilli A. - INGV | Mollo S. - Sapienza University of Rome
4. Chinello M. | **Formation of polished surfaces in natural rocks: experimental and field constraints.** | Supervisors Di Toro G. - Padua University; Spagnuolo E. - INGV; Oliver Plumper - Utrecht University
5. Feng W. | **Investigation of seismic slip in experimental faults under hydrothermal conditions. Chinese Government Scholarship.** | Supervisor: Di Toro G. - Padua University
6. Masoch S. | **Structure, evolution and deformation mechanisms of large displacement seismogenic faults in the continental crust.** | Supervisors: Di Toro G. and Pennacchioni G. Università di Padova; Cembrano J. - Universidad Ponteficia de Chile.
7. Schiavon B. | **Petrological monitoring of magma-mush dynamics at Stromboli: Insights on the transition from mild to violent eruptive styles** | Supervisors: Mollo S. - Sapienza University of Rome | Del Bello E. and Pontesilli A. - INGV.
8. Volpe G. | **Proprietà dell'attrito e permeabilità di faglie in basamento per una migliore caratterizzazione del loro potenziale sismogenico** | Supervisor: Collettini C. - Sapienza University of Rome | Pozzi G. - INGV.
9. Wu W.H. | **Experimental studies of fluid-rock interaction and seismic cycle in geothermal fields (Acronym EXPRESSO)** | European Union's Horizon 2020 research and innovation programme under the Marie Skłodowska-Curie grant agreement no 101034319 and from the European Union – NextGenerationEU. | Tutor: Di Toro G. - Padua University



C H A P T E R T E N

VISITING  
SCIENTISTS

Within the framework of the European project EXCITE (Electron and X-ray microscopy Community for structural and chemical Imaging Techniques for Earth materials, GA 101005611), a European infrastructure initiative for scientists working on Earth materials, Transnational access to research infrastructures using some of the world's best electron and X-ray imaging facilities is organized and coordinated by INGV-Rome. In 2023, 2 rounds of Trans-National Access (TNA) calls for proposals were organized and performed. This important initiative, financially supported by the EU, enables users from all countries (Eu and non-EU) to obtain excellence-driven, free access to the best Research Infrastructure in Europe to perform their research, enhancing scientific collaboration and innovation.

During the second TNA Round (access window 1 Nov 2022 - 30 April 2023), 3 projects were granted funded access at INGV-Rome HPHT lab EMPA/SEM facilities, whereas in the third Round (access window 1 May 2023 - 31 October 2023) 5 more projects were supported. In the following table we report the list of the 4 EXCITE TNA visiting scientists who successfully concluded their visits during 2023. The other projects were postponed to early 2024 and will be presented in the next Annual Report.

User Name	Affiliated institute	Project Title	Equipment	Access type	Access period	Access delivered
Fátima Rodríguez García	Instituto Volcanológico de Canarias (INVOLCAN), Spain	CUMBREVIEJACHEM_2 - Petrochemical analyses of tephra products from 2021 Tajogaite eruption of Cumbre Vieja (La Palma, Canary Islands)	JEOL JXA-8200 (EPMA)	Physical	2nd EXCITE TNA ROUND: 11-21/04/2023	9 days
Diana Chami	Université Libre de Bruxelles (ULB), Belgium	MEGSS - Chemo-mineralogical evolution and microstructural modifications of a geopolymer stabilized soil	JEOL JSM-6500F (FE-SEM)	Physical	3rd EXCITE TNA ROUND: 09-13/10/2023	5 days
Yerko Gonzalez	Universidad Catolica del Norte, (UCN), Chile	MAQF - Microstructural Analysis of Quaternary Fault Cores from Northern Chile	JEOL JSM-6500F (FEG-SEM)	Physical	3rd EXCITE TNA ROUND: 25/09-06/10/2023	10 days
Vayia Xanthopoulou	University of Patras, Greece	CERMUD - The analysis of mudstone in archaeometry	JEOL JXA-8200 (EMPA)	Remote	3rd EXCITE TNA ROUND: 01-15/12/2023	12 days
Yerko Gonzalez	Universidad Catolica del Norte, Antofagasta, Chile.	Frictional properties of Quaternary fault cores from the Atacama Fault System, northern Chilean forearc: Active faults or weakness zone of the upper plate?	SHIVA, BRAVA	Physical	Oct-Dec 2022	90 days
Chien Cheng Hung	Utrecht University, Utrecht, the Netherlands	Frictional behavior of sandstone-derived fault gouges during short seismic slip-pulse and its implications for induced seismicity in Groningen Gas Field	SHIVA	Physical	Feb 2022	
Kyungmin Kim	University of Alaska Fairbanks, Alaska, USA	Investigating the role of conduit permeable cap in generating seismic tremor and LP events through laboratory experiments	Analog Lab	Physical	Oct-Dec 2023	60 days
Tarsilo Girona	University of Alaska Fairbanks, Alaska, USA	Investigating the role of conduit permeable cap in generating seismic tremor and LP events: discussion and interpretation of performed experiments	Analog Lab	Physical	Dec 2023	10 days
Marco Brenna	University of Otago, Dunedin, New Zealand	Pinpointing the volatile driver for sudden large-scale volcanic eruptions. Natural and experimental investigation on the differentiation processes and eruption triggering mechanisms at Hunga Ha'apai volcano, Hunga Tonga	QUICK PRESS	Physical	Oct-Dec, 2023	30 days



C H A P T E R E L E V E N

MEETINGS,  
WORKSHOP  
and SYMPOSIA

## MEETINGS AND SESSIONS ORGANIZATION

### IUGG General Assembly 2023 (Berlin, Germany, July)

De Michieli Vitturi M., Andronico D., Pistolesi M., Van Eaton A., Fontijn K., Del Bello E.

**Session: V02 Modelling and Monitoring of Volcanic Ash Clouds**

## MEETINGS AND SESSIONS ATTENDANCE

### IAVCEI Scientific Assembly, Rotorua (New Zealand), 30 January – 3 February

Ricci T., R. Civico, Scarlato P., Andronico D., Cantarero M., De Beni E., Del Bello E., Kueppers U., Schmid M., Taddeucci J.

**Increased volcanic risk to nautical activities following morphological changes at Stromboli's crater terrace since 2019**

Andronico D., Del Bello E., Taddeucci J., Martín-Lorenzo A., Rodríguez F., Pontesilli A., Scarlato P., Civico R., Pennacchia F., Ricci T., Coldwell B., Melián G., Pankhurst M.J., D'Auria L., Hernandez P.A, Perez N.M.

**The explosive products erupted during the 2021 eruption at Cumbre Vieja volcano (La Palma, Canary Islands): distribution, stratigraphy, textural and petro-compositional variations**

Biensan C., Taddeucci J., Scarlato P., Andronico D., Ricci T., Del Bello E., D'Auria L., Asensio-Ramos M.

**In-flight fragmentation of pyroclasts during lava fountaining activity at Etna (Italy) and Cumbre Vieja (La Palma, Canary Islands) in 2021**

Civico R., Ricci T., Kueppers U., Schmid M., Scarlato P.

**UAS-based multitemporal remote sensing of the 2021 eruption of Tajogaite volcano (La Palma, Canary Islands, Spain)**

Davoli R., Engels K., Montanaro C., Ricci T., Sciarra A., Scheu B.

**Permeability and degassing of surficial Krafla lithologies: implications of the subsoil variability**

Del Bello E., Bagnato E., Tamburello G., Spina L., Ricci T., Taddeucci J., Scarlato P., Andronico D., Pennacchia F.

**Multidisciplinary characterization of the explosive degassing at Stromboli volcano from high-frequency UV, thermal, visual and acoustic time series**

Kueppers U., Jacobs B., Dingwell D.B., Houghton B.F., Johnson J., Krautblatter M., Ricci T., Ripepe M., Rosenblatt B., Schmid M., Taddeucci J., Scarlato P.

**Fast modulation of topography and eruptive activity**

Nave R., Ricci T., Davis M.S., Bellucci Sessa E.

**Comparing volcanic risk perception assessment after 10 years at Campi Flegrei active caldera (Italy)**

Pischiutta M., Puglia R., Ferrazzini V., Savage M., Duputel Z., Journeau C., Di Muro A., Peltier A., Paonita A., Ricci T.

**Temporal variations of ambient noise polarization on Piton de La Fournaise (La Réunion, France) and on Vulcano island (Italy)**

Proietti C., De Beni E., Cantarero M., Ricci T., Ganci G.

**Integration of multiplatform remote sensing techniques applied to the 2021 Etna lava flows: timely mapping and volcanological parameters quantification**

Scarlato P., Taddeucci J., Andronico D., Ricci T., Civico R., Del Bello E., Spina L., Biensan C., D'Auria L., Asensio-Ramos M., Calvo D., Padron E., Hernandez P.A., Perez N.M.

**Style Transitions and Physical Parameters of Explosive Activity During the 2021 Tajogaite Eruption (La Palma, Canary Islands)**

Sork A., Kennedy B., Fitzgerald R., Watson L., Dempsey D., Taddeucci J., Sellier M., Scarlato P., Andronico D., Ricci T., D'Auria L., Asensio-Ramos M.

**Deceleration as a drag proxy for irregularly-shaped volcanic bombs: Observations from high speed video at Stromboli and Cumbre Vieja**

Tournigand P.Y., Smets B., Ricci T., Civico R., Kueppers U., Kervyn M.

**Interdependence of source morphology and eruptive style at Stromboli volcano, Italy**

Vossen C.E.J., Cimarelli C., Bennett A.J., Schmid M., Kueppers U., Ricci T., Taddeucci J.

**The occurrence of volcanic lightning in basaltic explosive eruptions at Stromboli volcano, Italy**

#### **41° Convegno GNGTS, Bologna (Italy), 7-9 February**

Sapia V., Villani F., Fischanger F., Lupi M., Romano V., De Martini P.M., Ruggiero L., Sciarra A., Baccheschi P., Materni V., Maraio S., Smedile A., Pischiutta M., Rossi M., Civico R., Ricci T., Di Giulio G., Vassallo M., Brunori C.A., Improta L.

**3-D imaging strategies as an essential tool to investigate Quaternary tectonic basin internal structure and evolution. New insights from a 3-D deep electrical resistivity survey in the Campo Felice basin (central Italy)**

Villani F., Maraio S., Sapia V., Di Giulio G., Improta L., De Martini P.M., Materni V., Baccheschi P., Pischiutta M., Vassallo M., Bruno P.P., Brunori C.A., Civico R., Ricci T., Lovati S., Felicetta C., Lorenzetti A., Manganello P., D'Alessandro A., Scudero S.

**High-resolution geophysical investigations in the central Apennines seismic belt: preliminary results from the Campo Felice tectonic basin. 41**

Bruno P.P., Maraio S., Ricci T., De Martini P.M., Improta L., Materni V., Sapia V., Muccini F., Civico R., Rindinella A., Villani F., D&#39;Alessandro A., Pisciotta F., Sciarra A., Speciale S., Finizola A., Aquilina G., Giugliano N., Pucci S., Vitale G., Beltramone L., Pischiutta M., Scudero S., Bongiovanni S., Bagnato E., Di Vito M.A.

**Preliminary results of a high-resolution multidisciplinary investigation of the SW sector of Mt. Vesuvius**

### EGU General Assembly (Vienna, Austria, 24–28 Apr)

Schiavon B., Mollo S., Pontesilli A., Del Bello E., Scarlato P., Forni F., Tiepolo M.

**Plagioclase textural and compositional parameterization: A tool for tracking magma dynamics at Stromboli**

Petrone C.M., Mollo S., Gertisser R., Buret Y., Scarlato P., Del Bello E., Reagan M.

**Evolution of Stromboli basaltic plumbing system via magma recharges and mush rejuvenation**

Pontesilli A., Del Bello E., Scarlato P., Mollo S., Ellis B., Andronico D., Taddeucci J., Nazzari M.

**The efficacy of high frequency petrological investigation at open-conduit volcanoes: The case of**

**May 11 2019 explosions at southwestern and northeastern craters of Stromboli**

Giuliani G., Di Fiore F., Valdivia P., Mollo S., Romano C., Di Genova D., Vona A.

**The effect of CaO and CaO+MgO on the viscosity of a phonotephritic melt.**

Bini G., Chiodini G., Caliro S., Tassi F., Vaselli O., Rizzo A., Mollo S., Vougioukalakis G., Bachmann O.

**Tracking episodes of outgassing from upper crustal magma reservoirs through fumarole gas chemistry: the case of the Nisyros caldera (Aegean Arc, Greece)**

Cornelio C., Aretusini S., Spagnuolo E., Di Toro G., Cocco M.

**Frictional evolution of gouge-bearing faults during multiple seismic slip velocity pulses.**

Tinti E., Cocco M., Aretusini S., Cornelio C., Nielsen S., Spagnuolo E., Selvadurai P. Di Toro G.

**Fracture energy and breakdown work scaling with coseismic slip**

Aretusini S., Cornelio C., Volpe G., Pozzi G., Spagnuolo E., Di Toro G., Collettini C., Meier M., Cocco M.

**Fault reactivation by fluid injection: insights from laboratory friction experiments with multiple reactivation sequences**

Spagnuolo E., Cornelio C., Aretusini S., Pozzi G., Cocco M., Selvadurai P., Di Stefano G.

**A novel apparatus to study the mechano-chemical processes active during the nucleation and propagation of earthquakes (MEERA)**

Chinello M., Fondriest M., Tesei T., Spagnuolo E., Schito A., Bowden S., Germinario L., Mazzoli C., Cornelio C., Di Toro G.

**Mirror-like fault surfaces in bituminous dolostones (Central Apennines, Italy)**

Barat C., Savard G., Muñoz F., Stumpp D., Alparone S Ursino., A., Ricci T., Planes T., Pruiti L., Reyes Hardy M.P., Palano M., Sparacino F., Bonadonna C., Caricchi C., Ruch J., Lupi M.

**Deployment of dense nodal network during unrest: investigation of the Vulcano-Lipari System (Italy) with Local Earthquake Tomography**

Proietti C., De Beni E., Cantarero M., Ricci T.

**Timely mapping and quantification of volcanological parameters: the 2021-2022 Etna lava flows**

Sciarra A., Pizzino L., Ruggiero L., Galli G., Ricci T., Ciotoli G., Nave R., Graziani S., Beaubien S.E., Bigi S.

**Indoor Radon Measurements in public and private buildings in the Ciampino municipality and its risk perception assessment**

Ruggieri R., Pozzi G., Collettini C.

**Mineralogical control on fault friction and stability: a systematic study on quartz, calcite and muscovite ternary mixtures**

Volpe G., Locchi M. E., Pozzi G., Tinti E., Scuderi M., Marone M., Collettini C.

**Structural and frictional control on the transient deepening of the seismogenic zone following major earthquakes in Central Italy**

Pozzi G., Collettini C., Scuderi M., Tinti E., Tesei T., Viti C., Marone C., Amodio A., Cocco M.

**Slip velocity and fault stability in serpentine-rich experimental faults**

Buono G., Caliro S., Chiodini G., Giudicepietro F., Maccaferri F., Macedonio G., Pappalardo L., Pozzi G., Spagnuolo E., Tramelli A.

**The influence of physical properties of crustal rocks on volcanic unrest at Campi Flegrei caldera**

**XXI – INQUA, Sapienza University of Rome, July 14-20, Rome, Italy.**

Sunyé-Puchol I., Özsoy R., Aydar E., Miggins D., Bolós X., Mollo, S.

**Reassessing the volcanic hazards in the Central Anatolian Volcanic Province (CAVP), Turkey: Could a new tuff cone eruption trigger a third collapse in Acigöl caldera and produce a large ignimbrite forming eruption?**

Kaya S., Özsoy R., Sunyé-Puchol I., Aydar E., Nazzari M., Mollo S.

**Characterization of three large holocene pyroclastic deposits from Mt Erciyes Stratovolcano (Central Anatolia, Turkey): Karagüllü, Perikartın and Dikkartın**

Özsoy R., Sunyé-Puchol I., Aydar E., Pedrazzi D., Akkas E., Mollo S.

**Volcanic reconstruction of the Belbaşhanı Pumice eruption: a late Quaternary fallout deposit emitted in the Central Anatolian Volcanic Province (CAVP), Turkey. X**

**SIMP-SGI-SoGel-AIV, Potenza, Italy, 19-21 September**

Özsoy R., Sunyé-Puchol I., Pedrazzi D., Miggins D., Aydar E., Akkaş E., Tavazzani L., Mollo S.

**Reconstructing the recent eruptive history of Hasandağ volcano by tephrostratigraphic correlations along the Belbaşhanı Valley, Central Anatolia (Turkey). S**

Kaya S., Özsoy R., Sunyé-Puchol I., Aydar E., Nazzari M., Mollo S.

**Reconstructing the Holocene volcanic history of Erciyes stratovolcano, Central Anatolia (Turkey): the Karagüllü, Perikartin and Dikkartin explosive eruptions**

Schiavon B., Mollo S., Pontesilli A., Del Bello E., Scarlato P., Forni F., Petrone C., Nazzari M., Tiepolo M.

**Plagioclase textural and compositional parameterization: A tool for tracking magma dynamics at Stromboli.**

Misiti V., Di Laura F., Riposati D., Battelli P.

**Seismometer theft: discovering the guilty**

Bini G., Chiodini G., Ricci T., Sciarra A., Caliro S., Mortensen A., Martini M., Mitchell A., Santi A., Costa A.

**Soil CO<sub>2</sub> emission and stable isotopes ( $\delta^{13}C$ ,  $\delta^{18}O$ ) of CO<sub>2</sub> and calcites reveal the fluid origin and thermal energy in the supercritical geothermal system of Krafla, Iceland**

Capelli Ghioldi G., Tamburello G., Sciarra A., Rizzo A.L., Liuzzo M., Rouwet D., Tassi F., Coltorti M., Pesci A., Civico R., Ricci T.

**Estimation of natural methane release originating from a structurally controlled system**

Venturi S., Randazzo A., Cabassi J., Cinti D., Meloni F., Procesi M., Nisi B., Voltattorni N., Capecchiacci F., Ricci T., Vaselli O., Tassi F.

**Geochemical features of Volatile Organic Compounds (VOCs) in punctual and diffuse hydrothermal manifestations across the Sabatini Volcanic District (Latium, Italy)**

**AGU Fall Meeting, San Francisco (USA), December**

Marchesini B., Pozzi G., Collettini C., Carminati E., Tesei T.

**Alteration-controlled strain localization in a fossil hydrothermal system**

Pozzi G., Achtziger-Zupančič P., Aldega L., Ceccato A., Collettini C., Escallon D., Hertrich M., Ma X., Meier M., Osten J., Shakas A., Spagnuolo E., Volpe G., Zappone A., Amann F., Cocco M., Giardini D., Wiemer S.

**The candidate fault for fluid-induced earthquake rupture experiments in the Rotondo granite.**

Spina L., Taddeucci J., Pennacchia F., Morgavi D., Peña Fernández P.P., Sesterhenn J., La Spina G., Scarlato P.

**Laboratory Volcanic Jets: the Effect of Conduit Roughness on Subsonic to Supersonic Jet Dynamics and Related Seismo-acoustic Signals (V13A-07)**

Schiavon B., Mollo S., Pontesilli A., Del Bello E., Scarlato P., Forni F., Petrone C.M., Nazzari M., Tiepolo M.

**Magma-mush dynamics driving violent explosions at Stromboli: Insights from plagioclase growth kinetics and zoning patterns**

Sielfeld G., Cronin S.J., Montanaro C., Brooks-Clarke I., Scheu B., Ricci T., Tamburello G., Civico R., Cecili A.

**Is the Shallow Fault-Fracture Network Key to Understanding Hydrothermal Eruptions?**

Sapia V., Villani F., Maraio S., Improta L., Fischanger F., Lupi M., Di Giulio G., De Martini P.M., Baccheschi P., Pischiutta M., Vassallo M., Materni V., Sciarra A., Ruggiero L., Romano V., Rossi M., Smedile A., Nicolosi I., D'ajello Caracciolo F., Minelli L., Carluccio R., Brunori C.A., Civico R., Ricci T., D'Alessandro A., Felicetta C., Lovati S., Bruno P.P., Scudero S.

**Multiparametric and Multiscale 2D and 3D Mapping as a Tool to Shed Light on Tectonic Basins Structure and Evolution**

Tesei T., Felli G., Pozzi G., Harbord C., Collettini C., Nielsen S. B., De Paola N.

**Roughness-controlled weakness and instability of experimental fault surfaces.**

Volpe G., Pozzi G., Locchi M. E., Tinti E., Scuderi M. M., Marone C., Collettini C.

**Seismicity Distribution within a Rheologically Heterogeneous Deformation zone: Insights from the Central Apennines**

Volpe G., Pozzi G., Taddeucci J., Marone C., Collettini C.

**Frictional Instabilities in Clay and Implications for Shallow Slow Slips.**



C H A P T E R T W E L V E

# PUBLICATIONS

Aretusini S., Mitterpergher S., Remitti F., Arletti R., Polisi M., De Paola N., Tesei T.

**Heterogeneity-driven localization and weakening in scaly clays from a fossil accretionary prism**

Journal of Geophysical Research: Solid Earth, 128, e2023JB027332

<https://doi.org/10.1029/2023JB027332>

Benà E., Spagnuolo E., Piersanti A. et al.

**Rock deformation vs. radon emission: some constraints from shear stress-controlled experiments**

Sci Rep 13, 16399. <https://doi.org/10.1038/s41598-023-43374-6>

Bigaroni N., Scuderi M.M., Guglielmi Y., Nussbaum C., Aldega L., Pozz, G., Collettini C.

**Frictional properties of Opalinus Clay: influence of humidity, normal stress and grain size on frictional stability**

Geophysical Journal International, 233, 211–228.

Cocco, M., Aretusini, S., Cornelio C., Nielsen S.B., Spagnuolo E., Tinti E., Di Toro G.,

**Fracture energy and breakdown work during earthquakes**

Annual Review of Earth and Planetary Sciences 51, 2023 <https://doi.org/10.1130/G50810.1>

Colle F., Masotta M., Costa S., Mollo S., Landi P., Pontesilli A., Peres S., Mancini L.

**Effect of undercooling on clinopyroxene crystallization in a high K basalt: Implications for magma dynamics at Stromboli volcano**

Lithos 456–457, 107327. <https://doi.org/10.1016/j.lithos.2023.107327>

Del Gaudio P., Misiti V., Cantucci B., Liotta M., Ventura G., Ricci T., Sciarra A., Di Naccio D., Amoroso S., Monaco P.

**Multidisciplinary study of mud emissions following the 2016 Norcia earthquake**

Applied Sciences, <https://doi.org/10.3390/app13126968>

Di Fiore F., Vona A., Mollo S., Nazzari M., Giordano G., Romano C.

**Experimental insights on the shear-induced crystallization of a phonotephrite magma**

Chemical Geology 637, 121682. <https://doi.org/10.1016/j.chemgeo.2023.121682>

Gomila R., Fondriest M., Jensen E., Spagnuolo E., Masoch S., Mitchell T., Magarini G., Bistacchi A., Mitterpergher S., Faulkner D. and others

**Data set for: Frictional melting in fluid-rich faults: Field and experimental evidence from the Bolfin Fault Zone (Chile)**

Research Data Unipd

Lazari F., Castagna A., Nielsen S., Griffith A., Pennacchioni, G., Gomila R., Resor P., Cornelio C., Di Toro G.

**Frictional power dissipation in a seismic ancient fault**

Earth and Planetary Science Letters, 607, 2023, 118057

<https://doi.org/10.1016/j.epsl.2023.118057>

Lustrino M., Luciani N., Stagno V., Narzisi S. Masotta M., Scarlato P.

**Experimental evidence on the origin of Ca-rich carbonated melts formed by interaction between sedimentary limestones and mantle-derived ultrabasic magmas**

Geology, 50, <https://doi.org/10.1130/G49621.1>

MacDonald A., Ubide T., Mollo S., Pontesilli A., Masotta M.

**The Influence of Undercooling and Sector Zoning on Clinopyroxene–Melt Equilibrium and Thermobarometry**

Journal of Petrology 64, 1-18. <https://doi.org/10.1093/petrology/egad074>

Magnarini G., Aretusini S., Mitchell T.M., Pennacchioni G., Di Toro G., Schmitt H.H.

**Friction experiments on lunar analog gouges and implications for the mechanism of the Apollo 17 long runout landslide**

Journal of Geophysical Research: Planets, 128, e2022JE007520.

<https://doi.org/10.1029/2022JE007520>

Mollo S., Moschini P., Ubide T., MacDonald A., Vetere F., Nazzari M., Misiti V., Miyajima M., Melai C., Di Genova D., Vona A., Di Fiore F., Romano C.

**Kinetic partitioning of trace cations between zoned clinopyroxene and a variably cooled-decompressed alkali basalt: Thermodynamic considerations on lattice strain and electrostatic energies of substitution**

Geochimica et Cosmochimica Acta 361. 40–66. <https://doi.org/10.1016/j.gca.2023.10.012>

Moschini P., Mollo S., Pontesilli A., Nazzari M., Petrone C.M., Fanara S., Vona A., Gaeta M., Romano C., Scarlato P.

**A review of plagioclase growth rate and compositional evolution in mafic alkaline magmas: Guidelines for thermometry, hygrometry, and timescales of magma dynamics at Stromboli and Mt. Etna**

Earth-Science Reviews 240, 104399. <https://doi.org/10.1016/j.earscirev.2023.104399>

Pontesilli A., Del Bello E., Scarlato P., Mollo S., Ellis B., Andronico D., Taddeucci J., Nazzari M.

**The efficacy of high frequency petrological investigation at open-conduit volcanoes: The case of May 11 2019 explosions at southwestern and northeastern craters of Stromboli**

Lithos, 107255, <https://doi.org/10.1016/j.lithos.2023.107255>

Pozzi G., Collettini C., Scuderi M.M., Tesei T., Marone C., Amodio A., Cocco M.

**Fabric controls fault stability in serpentinite gouges**

Geophysical Journal International, 235(2), 1778–1797. <https://doi.org/10.1093/gji/ggad322>

Proietti C., De Beni E., Cantarero M., Ricci T., Ganci G.

**Rapid provision of maps and volcanological parameters: quantification of the 2021 Etna volcano lava flows through the integration of multiple remote sensing techniques. Bulletin of Volcanology**

<https://doi.org/10.1007/s00445-023-01673-w>

Revil A., Finizola A., Johnson T., Ricci T., Gresse M., Delcher E., Barde-Cabusson S., Duveillard P.A., Ripepe M.

**The thermal plumbing system of Stromboli volcano, Aeolian Islands (Italy) inferred from electrical conductivity and induced polarization tomography**

Journal of Geophysical Research – Solid Earth, <https://doi.org/10.1029/2023JB026475>

Schiavon B., Mollo S., Pontesilli A., Del Bello E., Nazzari M., Scarlato, P.

**Plagioclase crystal size distribution parameterization: A tool for tracking magma dynamics at Stromboli**

<https://doi.org/10.1016/j.lithos.2023.107143>

Spina L., Taddeucci J., Pennacchia F., Morgavi D., Peña Fernández J.J., Sesterhenn J., La Spin, G., Scarlato P.

**The Effect of Conduit Walls Roughness on Volcanic Jets and Their Seismo-Acoustic Radiation: An Experimental Investigation**

Geophysical Research Letters, 50(19), e2023GL104717.

Taddeucci J., Scarlato P., Andronico D., Ricci T., Civico R., Del Bello E., Spina L., D'Auria L., Asensio-Ramos M., Calvo D., Padrón E., Hernández PA., Pérez N.M.

**The Explosive Activity of the 2021 Tajogaite Eruption (La Palma, Canary Islands, Spain)**

Geochemistry, Geophysics, Geosystems, 24(6), e2023GC010946.

<https://doi.org/10.1029/2023GC010946>

Venturi S., Randazzo A., Cabassi J., Cinti D., Meloni F., Procesi M., Nisi B., Voltattorni N., Capecchiacci F., Ricci T., Vaselli O., Tassi F.

**Volatile organic compounds (VOCs) from diffuse degassing areas: interstitial soil gases as message bearers from deep hydrothermal reservoirs**

Science of the Total Environment, <https://doi.org/10.1016/j.scitotenv.2023.169047>

Villani F., Maraio S., Improta L., Sapia V., Di Giulio G., Baccheschi P., Pischiutta M., Vassallo M., Materni V., Bruno P.P., Brunori C.A., Civico R., D'Alessandro A., Felicetta C., Lovati S., Ricci T., Scudero S., De Martini P.M.

**High-resolution geophysical investigations in the central Apennines seismic belt (Italy): results from the Campo Felice tectonic basin**

Tectonophysics, <https://doi.org/10.1016/j.tecto.2023.230170>

Volpe G., Pozzi G., Collettini C., Spagnuolo E., Achtziger-Zupančič P., Zappone A., Aldega, L., Meier M.A., Giardini D., Cocco M.

**Laboratory simulation of fault reactivation by fluid injection and implications for induced seismicity at the BedrettoLab, Swiss Alps**

Tectonophysics, 862(July), <https://doi.org/10.1016/j.tecto.2023.229987>

Volpe G., Pozzi G., Locchi M.E., Tinti E., Scuderi M.M., Marone C., Collettini C.

**Rheological heterogeneities at the roots of the seismogenic zone**

Geology <https://doi.org/10.1130/G51432.1>

Wang H. Li H.B., Di Toro G., Kuo L.W., Spagnuolo E., Aretusini S., Si J.L., Song S.R.

**Melting of fault gouge at shallow depth during the 2008 MW 7.9 Wenchuan earthquake, China**

Geology 51(4), 345-350, 2023 <https://doi.org/10.1130/G50810.1>



Design by Laboratorio Grafica e Immagini INGV

Editing by Valeria Misiti

Rome, April 2023

## **DISCLAIMER CLAUSE**

This report contains data and information property of Istituto Nazionale di Geofisica e Vulcanologia in Rome (Italy). The information contained in this report don't imply the responsibility of the Istituto Nazionale di Geofisica e Vulcanologia.

Our purpose is to supply reliable scientific information to the members of the national and international scientific community and to whoever could be interested in them. Istituto Nazionale di Geofisica e Vulcanologia does not engage any responsibility for the content. This material is constituted by information of general character, result of specific researches, or data coming from the laboratory activity. Copy and the dissemination of this report are authorized only under licence of HP-HT Laboratory people.